Optical Properties of Coupled Quantum Wells and Their Use As Electro-Absorptive Modulators.

A thesis by

David Atkinson

submitted to the University of London for the degree of Ph.D.

Department of Electronic and Electrical Engineering

University College London

December 1990

Abstract

This thesis describes some of the ways in which the coupling between closely spaced quantum wells may be used to enhance the performance of quantum well optical modulators. These are identified as having a useful role as electro-optic modulators for which operating voltage and contrast ratios are two crucial parameters.

The background to Airy function solutions of Schrödinger's equation using a matrix matching technique is outlined and absorption spectra calculated at various applied electric fields for a range of quantum well structures. Through a consideration of coupling effects, the width of the barrier separating a pair of wells is optimised for optical modulation at room temperature and this is confirmed from photocurrent measurements. The electric field changes required are shown to be smaller than comparable multiple quantum well devices. Based upon this and an experimental determination of the absorption coefficient an asymmetric Fabry Perot reflection modulator employing coupled quantum wells is designed and fabricated. This exhibits the expected zero field reflectivity and similar devices should operate at low voltages giving good contrast ratios.

A p-i-n diode with the wells in the intrinsic region is used to apply bias to these well structures. The diode has a built in voltage and for any low electric field device this can degrade performance. Allowance was made for this in the design of the device above by the use of an extra layer between the p and n regions. As a possible alternative, the use of a particular asymmetric well structure is investigated.

Finally, the use of barriers narrower than normal in multiple quantum wells is modelled taking coupling into account. Modelling and photocurrent results show that a reduction in operating voltage through a reduction in barrier width is possible without coupling worsening the optical modulation.

Table of Contents

List of Figures

List of Tables

Notation, constants, useful relations and abbreviations

A	variable used in §2.2 algebra and separately in chapter 5
AFPM	asymmetric Fabry Perot reflection modulator
Ai	Airy function (see figure 2.2)
AlGaAs	Aluminium Gallium Arsenide
α	absorption coefficient
α_{e-h}	absorption coefficient due to electron-hole pair $e-h$
Å	Angstrom (10^{-10}m)
B	variable in Fabry Perot calculations
B_{e-h}	exciton binding energy for the electron hole pair $e-h$
Bi	Airy function (see figure 2.2)
C	coefficient in wavefunction expression
CCD	charge coupled device
CDC	control data corporation
CDQW	coupled double quantum well
Cr:Au	chrome gold (contacts to p-type region)
CV	capacitance voltage
d	thickness of absorber, or atomic nuclei separation (in chapter 1)
D	coefficient in wavefunction expression
δ	total optical phase shift after a cavity roundtrip
dB	decibel = $10\mathrm{LOG}_{10}(\mathrm{Power}_{\mathrm{in}}/\mathrm{Power}_{\mathrm{out}})$
DOS	density of states
e_1	first electron energy level
E	carrier energy
E_1	SQW energy level
ΔE_2	separation of levels in a two well structure
$\mathrm{e}_1\mathrm{hh}_1$	transition between first electron and heavy hole energy levels
E_b	barrier material band gap
E_{BE}	binding energy of the exciton
E_c	depth of well in the conduction band
ECL	emitter coupled logic
E_e	electron energy with respect to GaAs conduction band
E_{e-h}	spectral transition energy for electron hole pair $e-h$
E_g , E_{gap}	energy gap
E_h	hole energy with respect to GaAs valence band
E_p	carrier energy at Breit Wigner resonance
η	diode quantum efficiency
E_v	depth of well in the valence band
E_w	well material band gap
ϵ_0	dielectric constant ($8.85419 \times 10^{-12}\mathrm{Fm}^{-1}$)

ϵ_r	relative dielectric constant
f	photon frequency
F	electric field [10KV/cm=1V/micron=0.1meV/Å] also used in Fabry Perot calculations in chapter 5
F_T	transition field
FWHM	full width at half maximum
GaAs	Gallium Arsenide
$g(\omega)$	density of states at angular frequency ω
γ	variable in Airy function approximation
Γ	FWHM of absorption peak Lorentzian
Γ_p	FWHM of DOS Lorentzian at Breit-Wigner resonance
h	Planck's constant (6.626176×10^{-34} Js)
H''_{mn}	matrix element between energy levels m and n
$\hbar$	$h/2\pi$ ($1.054588664 \times 10^{-34}$ JS)
hh	heavy hole
I	photocurrent
κ	used in trigonometric and exponential arguments
L	box limits or Lorentzian function
$\mathbf{L}$	2×2 matrix at left side of material layer
λ	wavelength [nm]=1239852/energy[meV]
L_c	length of Fabry Perot cavity
lh	light hole
L_i	length of intrinsic region
L_z	well width
m^*	effective mass (in kg not units of m_e)
m^*_{hh}	heavy-hole effective mass (in z direction)
m^*_{lh}	light-hole effective mass (in z direction)
$m^*(z_L)$	effective mass in material to left of interface
$m^*(z_R)$	effective mass in material to right of interface
m_e	electron mass (9.109534×10^{-31} kg)
M_{e-h}	square of overlap integral for electron-hole pair $e-h$
$\mathbf{M_T}$	transfer matrix across whole structure
MBE	molecular beam epitaxy
meV	milli electron volt (10^{-3} q [Joules])
micron	10^{-6} m
MLS	multilayer stack
MOCVD	metal organic chemical vapour deposition
MOS	metal oxide semiconductor
MOVPE	metal organic vapour phase epitaxy
MQW	multiple quantum well
μ	symbol for 10^{-6} or reduced effective mass

n	number of states (chapter 2), number of wells (chapter 6)
N	number of layer pairs in a MLS
n_c	cavity refractive index
N_i	impurity concentration
n_p	number of coupled well units
OEIC	optoelectronic integrated circuit
OMA	optical multichannel analyser
ω	angular frequency $= 2\pi f$
p	MQW period
P	optical power
ϕ	phase shift
π	3.141592654
PL	photoluminescence
PLE	photoluminescence excitation
ps	picosecond (10^{-12} s)
ψ	carrier wavefunction
ψ_L	wavefunction to left of interface
ψ_R	wavefunction to right of interface
q	carrier charge ($1.6021892 \times 10^{-19}$ C) (negative for electrons)
r_{e-h}	ratio of exciton area to level of continuum
R	intensity reflectivity
$\mathbf{R}$	2×2 matrix at right side of material
R_α	used in Fabry Perot equations
R_b	back reflectivity
RC	resistance capacitance time constant
R_f	front reflectivity
R_y	Rydberg
ρ	density of states
ρ_q	charge density
SEED	self electro optic device
SERC	Science and Engineering Research Council
SLM	spatial light modulator
Sn:Au	Tin gold (n-type contact)
SQW	single quantum well
t	matrix elements
T	intensity transmission, or temperature
TMA	trimethyl aluminium
TMG	trimethyl gallium
TTL	transistor-transistor logic (0-5V)
$U(z, F)$	overall potential experienced by carriers
V	bias voltage

$V'(z)$	reflected potential $\equiv V(-z)$
$V(z)$	zero field one dimensional well/barrier potential
V_0	potential energy of semi-infinite barriers at zero field
V_{ap}	applied voltage
V_q	potential due to charges
W_{abs}	rate of photon absorption
y	Airy function argument
x	mole fraction of aluminium in $Al_xGa_{1-x}As$
ξ	variable in density of states calculation
z	growth direction
z_1	lower limit of overlap integral
z_2	upper limit of overlap integral

Preface

This thesis will be concerned with the study of quantum well devices as electronically controlled optical modulators. Prior to a more detailed description I will summarise in this preface some of the motivating factors behind this research.

There is a desire for electronically controlled optical modulators that can act as the interface between electronics and optics. A major application for these devices is in the coding of optical signals from electronic data for telecommunications purposes where the trunk telecommunication medium is the fibre optic cable. The current and future requirements for high volume, high bit rate communications [Cochrane 1989, O'Mahony] are likely to enhance the need for electro-optic modulators, especially those showing low voltage operation for compatibility with electronic logic, and good optical modulation.

Arrays of modulators formed into a spatial light modulator (SLM) can be used to switch parallel optical signals. In telecommunications this could be used to control the routing of data if a high contrast, high speed SLM could be fabricated. The control of this SLM by electronic logic could bring benefits over attempts to use all optical control [Midwinter 1987].

In addition to data communication this optical switching could be used in computers employing optics for parallel processing. Within these computers SLMs again can be used [McAulay 1987], this time as processing elements, for example in matrix multiplication, or as logic elements, a specific example using quantum well modulators being highlighted later in this preface.

Hence there are a number of roles for the electro-optic modulator of which quantum well devices are one type. These are semiconductor devices and as such are applicable to optoelectronic integrated circuits (OEICs) in which optical and electronic devices are integrated onto one chip, hopefully yielding cost and size benefits (see Yariv (1984), Hutcheson (1986) and Miller D A B (Jan 1989b) for more information). This thesis will be concerned with the quantum well devices themselves and improvements in operating voltage and contrast ratio rather than their integration or application. However, many applications have already been reported and these are mentioned below.

In connection with fibre optic communications Wood *et al* (1986) demonstrated bidirectional fibre optic transmission using quantum wells as both modulator and detector achieving speeds up to 600Mbit/s . For OEICs, work is underway to exploit the benefits of both the optical properties of GaAs quantum wells and the electrical properties of silicon by integration of the two materials, see for example Barnes *et al* (1989) or Goossen *et al* (1989). As well as electro-optic modulators other devices useful for optoelectronics can be fabricated from quantum well material, for example semiconductor lasers, field effect transistors and optical gate switches [Ajisawa *et al*, Wada *et al* (1989)]. The construction of these from a common multiple quantum well structure on one chip is an attractive route to integration.

For SLM applications a number of groups have reported results from arrays of quantum well modulators and Hsu *et al* (1988) produced a range of conceptual designs. In the InP/InGaAs material system Rejman-Greene *et al* (1990) have fabricated a 2x2 array of multiple quantum well modulators (MQWs). McIlvaney *et al* (1990) have demonstrated a 4x4 SLM array using matrix addressing of GaAs/AlGaAs quantum wells with matrix address lines allowing array elements to be selected line by line. Alternatively the addressing of multiple quantum well arrays by charge coupled device (CCD) can be used and considered by Goodhue *et al* (1986) and Singh *et al* (1988) and demonstrated by Nichols *et al.* In terms of speed Wood *et al* (1987) have produced a 2x2 quantum well SLM with rise and fall times of roughly 400ps, short rise and fall times being desirable for high bit rate communications.

In addition to these results the self-electro-optic-effect device (SEED), first proposed by Miller D A B *et al* (Jul. 1984), has received a large amount of attention. In the original SEED devices the MQWs were in series with a resistor. When the MQWs absorb light a photocurrent is generated, by placing the devices in series with a resistor the photocurrent changes the bias across the MQW region which alters its absorption and can lead to positive feedback and optical bistability. Various other configurations have been demonstrated, for example Wheatley *et al* (1987) placed the MQW region in series with a phototransistor to give optical gain (but not bistability). Another configuration which can give bistability is the symmetric SEED (s-SEED) [Lentine *et al* (1988)], here two identical SEEDs are placed in series each forming the load of the other. The pair and connections can be fabricated from one MQW structure and so the device is useful for integration as well as being able to function as a logic gate or optical memory element. To my knowledge this is the only configuration in commercial production and is available as a 64x32 array [Lentine *et al* 1990].

More recently this group has described a prototype all-optical switching network employing s-SEEDs [Cloonan *et al*], this arrangement of devices has potential applications in the interconnection networks envisaged as a part of future telecommunications systems or in optical computers. Although these devices are 'all-optical' in the sense that optical signals control optical output they are dependent upon the quantum well modulator's current generating and electro absorption characteristics.

There is clearly an internationally recognised role for quantum well optical modulator devices. My PhD project was to develop a computer model to calculate the absorption spectrum of these devices at various electric fields. The parameters in the model would then be used to predict absorption spectra for devices that had not previously been studied and either optimise design or investigate new effects. The actual model developed drew upon and extended the most suitable aspects of other published calculations. It was applied to a wide range of structures with particular emphasis on coupling effects between quantum wells. It is principally this application of the model to structures useful for optical modulators that forms the novel aspect of this work.

Chapter 1 Introduction to optical modulators and the quantum well modulator

§1.1 Optical Modulators

Intensity modulation of an optical beam can be achieved directly through changes in the absorption or reflection coefficient of a device. Alternatively a phase change can be introduced into one portion of the optical signal, upon recombination with the unaltered portion of the signal in a Mach Zender arrangement, interference results in intensity modulation [see for example Hecht and Zajac]. Direct intensity modulation is generally simpler to implement and it is this that is used in the quantum well devices considered in this thesis. To predict performance of both transmission and reflection devices it is necessary to calculate electroabsorption spectra, the reflection modulators discussed in chapter 5 fundamentally operate through changes in absorption within the device.

The "performance" parameters used to describe modulators are listed below. In order to achieve some change of absorption within a device a drive voltage, or bias, must be applied. This operating voltage should ideally be compatible with the electronic drive circuitry for ease of integration and generally low to decrease the power required as all devices contain capacitance and the charging of this capacitance requires a power proportional to the voltage squared. Transistor to transistor logic (TTL) operates between 0V and 5V, CMOS between 0V and 3V to 18V and the higher speed emitter coupled logic (ECL) between ≈ -0.9V and ≈ -1.8V for the logic levels [Sedra and Smith]. Reduction of operating voltages from over 5V forms a major part of this work.

The capacitance of the device affects the power dissipation and speed of operation, capacitance is a function of device size and is largely beyond the scope of this thesis. Boyd *et al* (1989) reported a 5.5GHz multiple quantum well reflection modulator, the speed of the device is limited by the *RC* time constant, which in this case was 29ps, and it is generally *RC* time constants that limit the speed of quantum well modulators. The range of wavelengths or optical bandwidth over which a given modulation occurs is also an important parameter. Finally, in a transmission or reflection device the modulation between the two biased states is described either in absolute percentage terms or by contrast ratio and insertion loss. Low insertion loss and high contrast ratios are desirable although there is often a trade off between the two, the exact balance acceptable depends upon the system requirement.

To set the quantum well modulator in context, some of the other modulation mechanisms available are summarised first. Waveguide devices require the optical signal to be guided usually by refractive index changes between a core and cladding, the modulation takes place in the guiding region where the interaction length may be long.

Liquid Crystal : These are widely used for display purposes and exhibit high contrast ratios but are slow due to their reliance on reorientation of molecules. The common nematic liquid crystals have switching times of the order of 1ms. Faster

performances of the order 10^{-6}s have been reported [Crossland *et al* 1990] but this is still slow in comparison with the quantum well modulator mentioned above.

Lithium Niobate : An electric field changes the refractive index giving a phase modulator, intensity modulation being achieved using a Mach Zender interferometer. Devices must be long (≈1cm) and are restricted to a waveguiding geometry. Dolfi *et al* fabricated an intensity modulator operating at speeds up to 40GHz with a 7.5V operating voltage and a 3.5dB optical insertion loss. There are commercially available devices.

Direct modulation of semiconductor lasers : This is the process currently used to provide coded optical signals. The UK fibre network's highest bit rate is 565 Mbit/s at present, but 2.4Gbit/s is of interest [O'Mahony]. (For comparison a standard telephone operates at 64kbit/s and a video phone might need 70Mbit/s [Kao].) However the range of distances over which the signal can be successfully transmitted is reduced at higher bit rates (≈ 1Gbit/s) because direct modulation of the semiconductor laser injection current results in changes of refractive index within the laser cavity. These changes alter the laser's mode frequency and hence broaden the spectral line, limiting bit rate [Linke 1984] and the distance the pulse can travel due to dispersion spreading the pulses. External intensity modulation of the lasers output, for example by quantum wells, would eliminate this source of 'chirp'. Although an intensity modulator operating through changes in absorption results in some phase modulation due to the Kramers-Kronig relation and so inducing chirp, if a suitable waveform is used the effects can be minimised and benefits over direct laser modulation achieved [Koyama 1985, Okiyama 1988].

Bulk semiconductor modulators : These suffer from low absorption coefficients and small changes of absorption upon application of an electric field (443 cm^{-1} for the maximum change of absorption coefficient in GaAs compared with changes of the order 10000 cm^{-1} for 100Å wide quantum wells [Jelley *et al* 1989]). In normal incidence (not a waveguide) Wight *et al* (1985) demonstrated a GaAs device showing a contrast ratio of 1.1dB , an insertion loss of 8.2 dB when operating at 5V.

Deformable Mirror Devices: These are thin reflective films on silicon MOS transistors, they are suitable for formulating into arrays and are addressable by TTL circuitry. Switching times are of the order of microseconds. Devices give phase modulation, hence lenses are required for intensity modulation [see McAulay and references therein].

For comparison, GaAs based quantum well modulator performances in the literature around the time of the start of this project (October 87) were; 131ps modulation [Wood *et al* 1985], for an applied voltage of approximately 8V, the insertion loss was low (1.2dB) but the contrast ratio was poor (≈ 1.7:1). Improved contrast ratios were achieved by using waveguide geometries, for example Wood *et al* (Aug 1985) who achieved 10:1 .(A review of quantum wells in waveguide modulators was written by Wood (1988) .) In 1988 Hsu *et al* achieved approximately a 10:1 contrast ratio in a transmission modulator (not a waveguide). They used a 4 micron thick MQW modulator (thicknesses are usually 0.5 to 1 microns), however, the price was a high operating

voltage of 20V and high insertion loss of 13dB. It was not until Whitehead *et al* (1989) used quantum wells within a Fabry-Perot cavity that contrast ratios increased dramatically to greater than 100:1 for non waveguide devices. Throughout this time operating voltages remained generally in excess of 5V.

From the applications described in the preface and the description of quantum well and other modulators above it is clear that the quantum well modulator has a useful role to play. Liquid crystal devices show high contrast but are too slow for many applications, lithium niobate can only be used in a waveguide geometry, the modulation of semiconductor lasers could benefit from external modulation, bulk semiconductor devices show poor modulation and deformable mirror devices result in phase, rather than intensity modulation. Quantum well modulators have recently shown high contrast, they are suitable for array configurations and can operate at high speed.

The next section introduces the modulator device structure and the operation of the device.

§1.2 The quantum well modulator.

Quantum well modulators are fabricated from layers of different band gap semiconductor materials grown epitaxially. The materials GaAs and $Al_xGa_{1-x}As$ have the same lattice constant and the system is not strained, for $x < 0.45$ they are both 'direct band gap' so the potential experienced by an electron in the direction normal to the plane of the layers, usually z the growth direction, varies from one layer to the next as in figure 1.1 .

In this thesis I will be concerned with GaAs and AlGaAs devices because of the greater availability of data and material. These devices operate at $\approx$0.86 microns which is suitable for local area networks but is not suitable for long haul fibre optic communications where wavelengths in the 1.3 to 1.55 micron region are used for minimum signal loss or dispersion. The modelling work in this thesis should be readily applicable to the InP/InGaAs system which does operate in this wavelength range.

Growth of these material layers is typically by molecular beam epitaxy (MBE) or metal organic vapour phase epitaxy (MOVPE), otherwise known as 'metal organic chemical vapour deposition' (MOCVD) [for review papers on MBE see Gossard (1986) and for MOCVD Stringfellow (1985), more recent reviews appear in Stradling and Klipstein]. The relationship between waveguide and 'transmission' modes to the quantum well layers is shown in figure 1.2.

In order to obtain an electric field across the wells the quantum well layers are grown in the intrinsic region of a p-i-n diode, see figure 1.3. Contacting to the p and n layers permits an electric field to be applied to the wells, the field strength being given approximately by V_{ap}/L_i where V_{ap} is the applied voltage and L_i is the length of the intrinsic region. (The voltage appears only across the intrinsic region because the p and n layers have a relatively high conductivity.)

Potential wells and barriers are formed by the different band gap layers. These

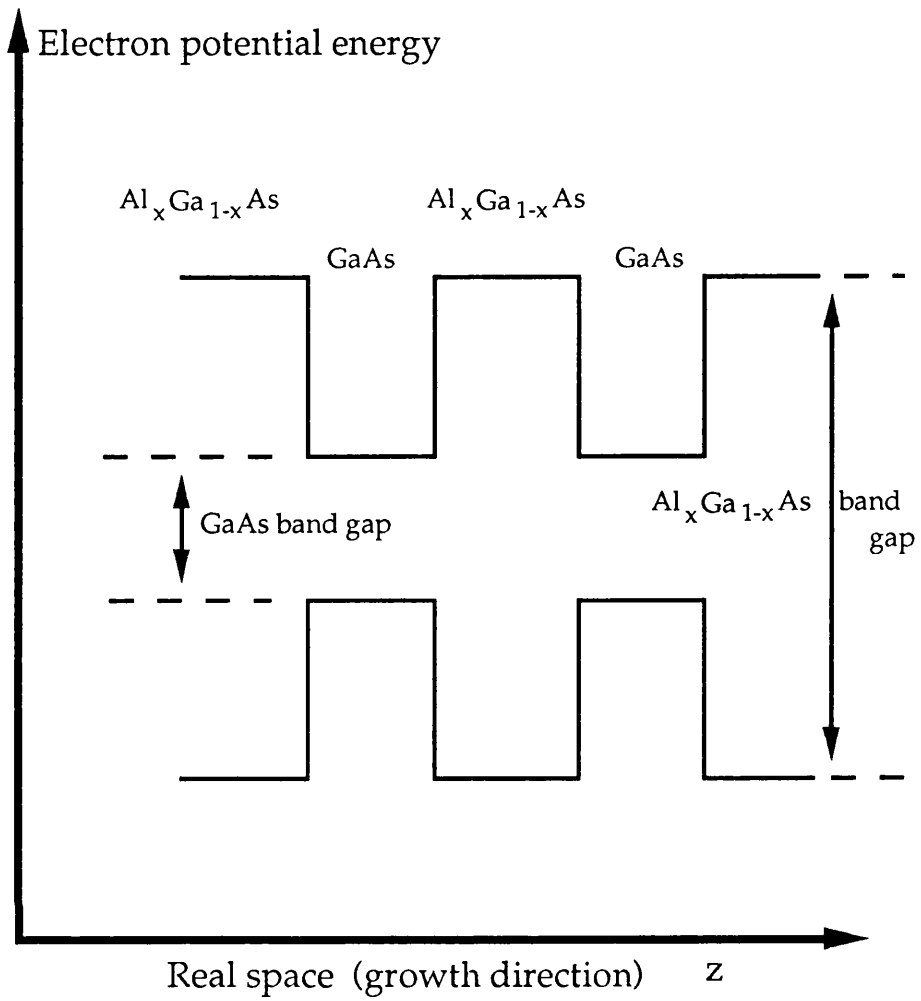

Figure 1.1 Relation of material layers to well/barrier potential. Successive material layers are deposited in the growth direction. $Al_xGa_{1-x}As$ material has the larger band gap and forms the barrier material between GaAs wells.

potential wells are sufficiently thin such that quantum mechanics apply and Schrödinger's equation can be used to find the energy levels and wavefunctions of the carriers (electrons, heavy-holes and light-holes). This is discussed more fully in chapter 2.

The thickness of the barrier material layers determines some of the properties of quantum well devices, the terminology used is clarified here. For multiple quantum well structures (figure 1.4a) the wells are assumed to be sufficiently separate as to be independent, the potential term in Schrödinger's equation need only contain one well and its adjacent barriers. Each well has its own carrier energy levels and wavefunctions. These wavefunctions are largely localised within the well material but do penetrate into the barrier material. If the barrier between two wells is made thin as in figure 1.4b there is an interaction between the carrier wavefunctions of wells separated by

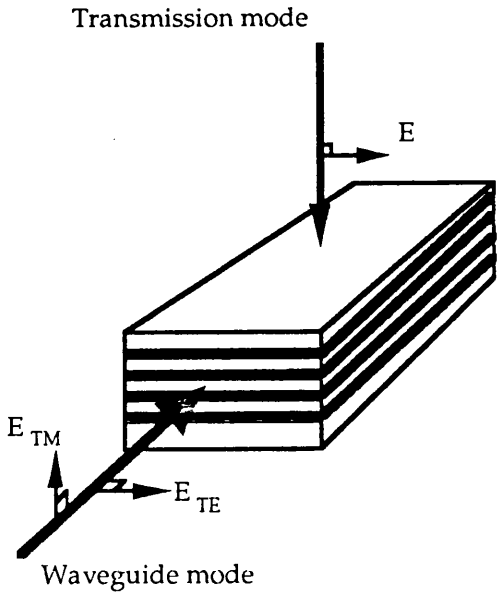

Figure 1.2 showing schematically the relation between the direction of incident light and the quantum well layers. Short arrows denote the polarization of the light's electric field. In transmission mode this polarization can only be parallel to the layers.

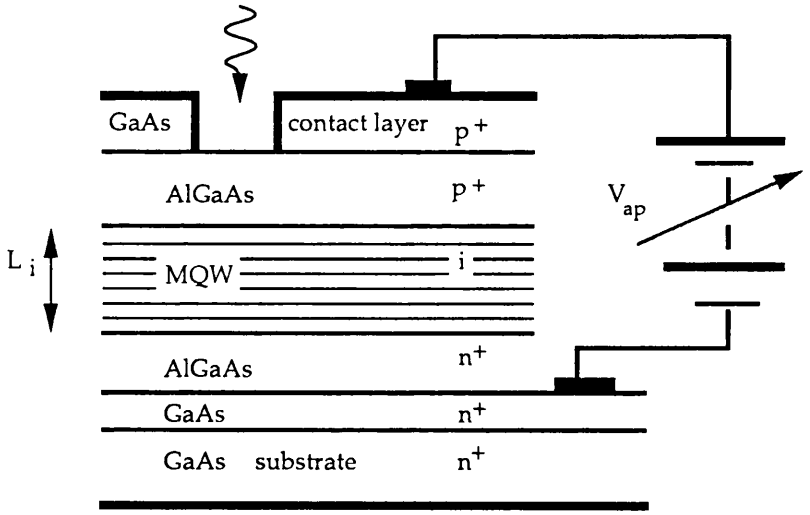

Figure 1.3. Schematic representation of the basic diode structure. This is suitable for photocurrent measurements, a hole must be etched in the substrate to make a transmission device.

Figure 1.4 Schematic representations of,

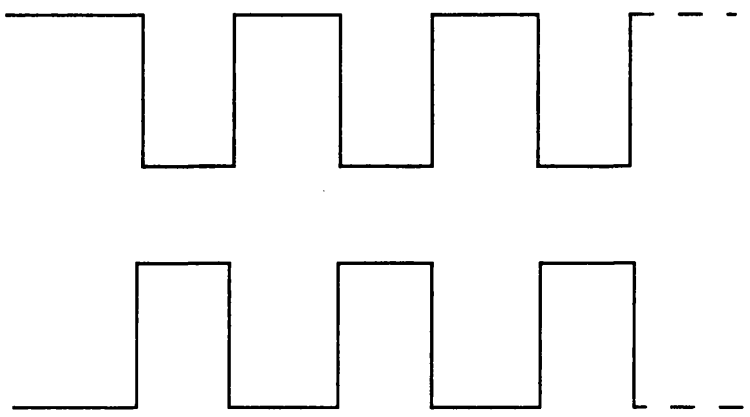

a Multiple Quantum Wells

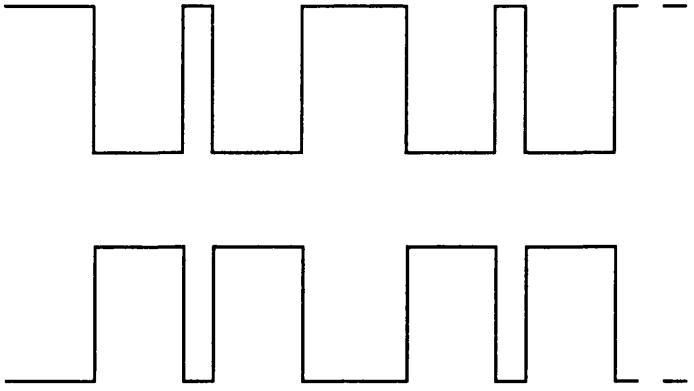

b Coupled Double Quantum Wells

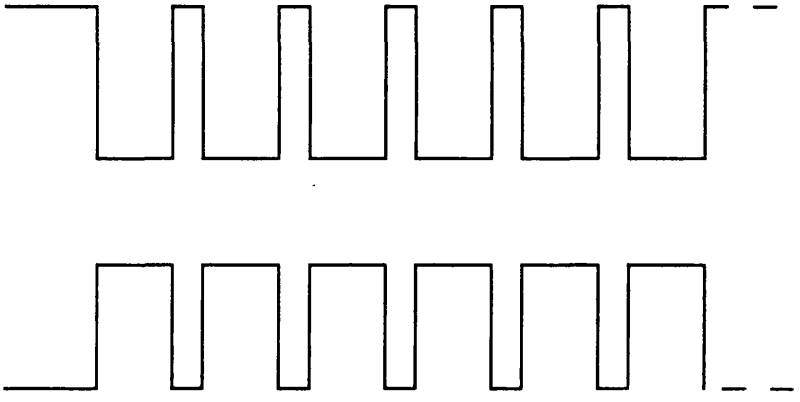

c Superlattice

a narrow barrier - coupling is said to have taken place and we have a coupled double quantum well (CDQW). Provided the barriers between the pairs are large, a series of CDQWs can be modelled by just considering one pair. For narrow barriers separating all wells (figure 1.4c) a superlattice is formed. Here the carriers' energies form bands in a manner analogous to the energy levels in a bulk semiconductor lattice.

The z-momenta of carriers in MQW and CDQW structures at zero field are quantised into energy levels. I label the energy levels e_1, e_2 etc as in figure 1.5 which shows some of the other notation used later and gives approximate magnitudes of some quantities.

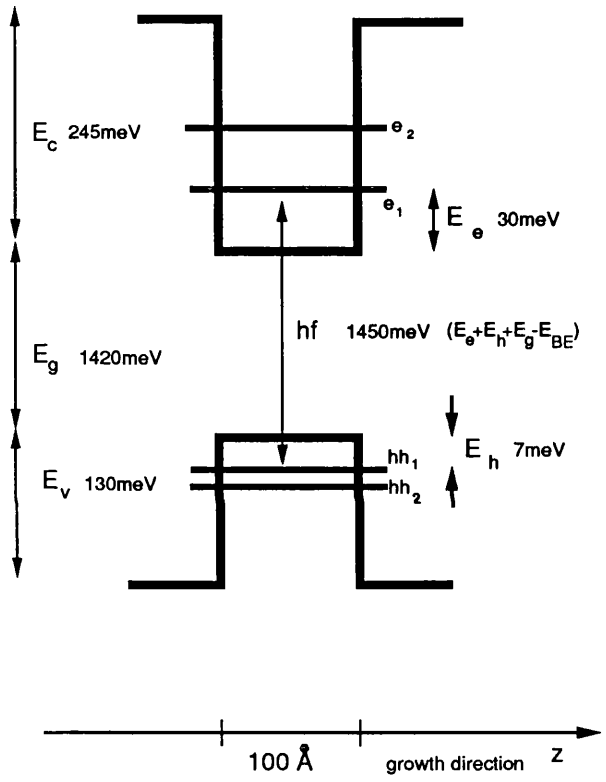

Figure 1.5 showing some of the notation used and approximate values of some quantities for a GaAs well with $Al_{0.3}Ga_{0.7}As$ barriers.

Absorption of a photon incident upon the quantum well material may take place if the photon has the correct energy. This energy is approximately the GaAs band gap energy E_g plus the energies E_h and E_e of the hole and electron energy levels. In figure 1.5 E_e corresponds to the energy of the level labelled e_1. This results in an electron in the conduction band and a positively charged hole in the valence band. In MQWs this electron and hole pair are confined spatially to the well layer and hence are attracted by the Coulomb interaction, they bind together to form an exciton pair. (This is called an interband transition and is labelled by the electron and hole energy levels eg e_1hh_1, promotion of, say, an electron from the ground state to a higher excited electron state

is termed an intersubband transition and typically occurs at wavelengths of the order of 10 microns [eg Harwit *et al* (1987)].)

The confinement of carriers in one dimension to distances of the order of 100Å by the well/barrier potential ensures that the electron and hole forming the photogenerated pair are located spatially close together in the z direction. Specifically they are closer than the Bohr diameter of the exciton in bulk GaAs (≈300Å). The consequence of this is that the absorption due to the quantum well exciton is greater than an exciton in bulk material (especially at room temperature where excitonic absorption in bulk material is weak [Sturge 1962]) , furthermore, the exciton is still observed when an electric field is applied to the quantum well structure, unlike in bulk material where it rapidly vanishes [Miller *et al* (Nov 1984)]. The binding energy E_{BE} of the quantum well exciton (ie the difference in potential energy between a free and a bound electron hole pair) is about 7meV.

The details of the interaction of light with matter is beyond the scope of this thesis and the reader is asked to accept that this absorption can take place and that the photon energy necessary need only be $E_g + E_e + E_h - E_{BE}$ despite the implication that the photon knows about all the processes to come and 'borrows' energy before promoting an electron from the valence to conduction band and then forming a bound exciton. (If it is of any help, absorption and emission must occur at the same energy and if there are no energy sources or sinks it is relatively easy to visualise emission (due to recombination of electron and hole) at an energy of $E_g + E_e + E_h - E_{BE}$.)

Calculation of the absorption coefficient is explained in more detail in section 2.3, for now note that the absorption spectrum is the sum of the absorption from the creation of each possible electron and hole pair. The contribution from each pair has two components, a peak from the bound pair or excitonic contribution and a continuum from the unbound, free particle contribution. The spectral energy, hf, at which the peak occurs is given by $E_g + E_e + E_h - E_{BE}$, the different peaks having different E_e and/or E_h. The height of the peak is related to the overlap integral of the electron and hole wavefunctions. These wavefunctions are found by solving Schrödinger's equation for the well and barrier potential.

A constant electric field applied to the well and barrier potential causes the wavefunctions to localise, the energy levels to shift and the wavefunction overlaps to change. This shifts the heights and spectral energies of the peaks in the absorption spectrum as depicted schematically in figure 1.6. This is the so-called 'quantum confined Stark effect' (QCSE) because the well confinement ensures that the exciton is still observed after the application of an electric field but its spectral energy has changed, or Stark shifted.

Hence we have the basis of an electroabsorption modulator. The absorption spectrum changes when the electric field changes, there is no delay associated with molecular reorientation or carrier dynamics. From an engineering point of view we have to make these changes in absorption large and change the electric field rapidly and

easily. The purpose of this being to achieve good optical modulation at low operating voltages, preferably compatible with high speed logic circuits.

§1.3 Outline for the PhD project

The original direction for this PhD was to undertake theoretical modelling to optimise the properties of GaAs/AlGaAs multiple quantum well optical modulators [SERC proposal]. At the outset (October 1987) results had been published on different well shapes, obtainable by varying the aluminium concentration, specifically parabolic wells [Miller R C *et al* (March 1984)] and graded gap quantum wells [Hiroshima *et al* (1987), Nishi *et al* (1987) and Hong *et al* (June 1987)], the latter group also considered wells with asymmetric barrier heights on either side of the well. However, few attempts had been made to study systematically how the structure of the MQW system could be optimised to give the best possible performance (although Newson *et al* (1987) had considered the effect of residual doping in the intrinsic region on the number of wells to include in a multiple quantum well.) The flexibility available in design, ie number of wells, well width, barrier width, composition of wells and barriers and electric field effects provided a good incentive to model theoretically the performance of these devices so that the parameters listed above might be optimised. A model was developed to calculate absorption spectra but I chose to focus upon the possible benefits of coupling between wells rather than an optimisation of complete MQW structures. This choice was made because I found it more interesting and there was the hope of using coupling to give large improvements in device performance rather than the smaller improvements likely to come from optimisation. During the course of my work a number of papers were published on MQW optimisation and these are listed next. Experimentally measured absorption coefficients for different well widths and for various electric fields were made by the Siemens research group [Jelley *et al* (1988), Jelley *et al* (1989) and Lengyel *et al* (1990)], the latter paper demonstrating how optimum values of some parameters may be chosen. A theoretical comparison between a selection of structures with different combinations of well widths, barrier widths and aluminium concentrations in the barriers was made by Cho *et al* (1989). Nojima *et al* (1988) optimized well widths and band gaps in the InGaAsP/ZnP and InGaAlAs/InAlAs material systems to achieve the largest ratio of the change in absorption coefficient to its zero field value. Stevens *et al* (1989) investigated the limits to normal incidence electroabsorption in GaAs based multiple quantum wells with particular reference to telecommunications.

In the previous paragraph I mentioned that coupling might be used to give large improvements in device performance, this is outlined below and discussed more fully in chapter 4.

If two quantum wells are formed in close proximity as in figure 1.4b the carrier wavefunctions are solutions to Schrödinger's equation for the whole, two well system. For certain barrier widths separating these coupled wells, when an electric field is applied the changes in energy levels and wavefunction localisation occur more rapidly than in comparable single quantum wells. From figure 1.3 one can see that if the

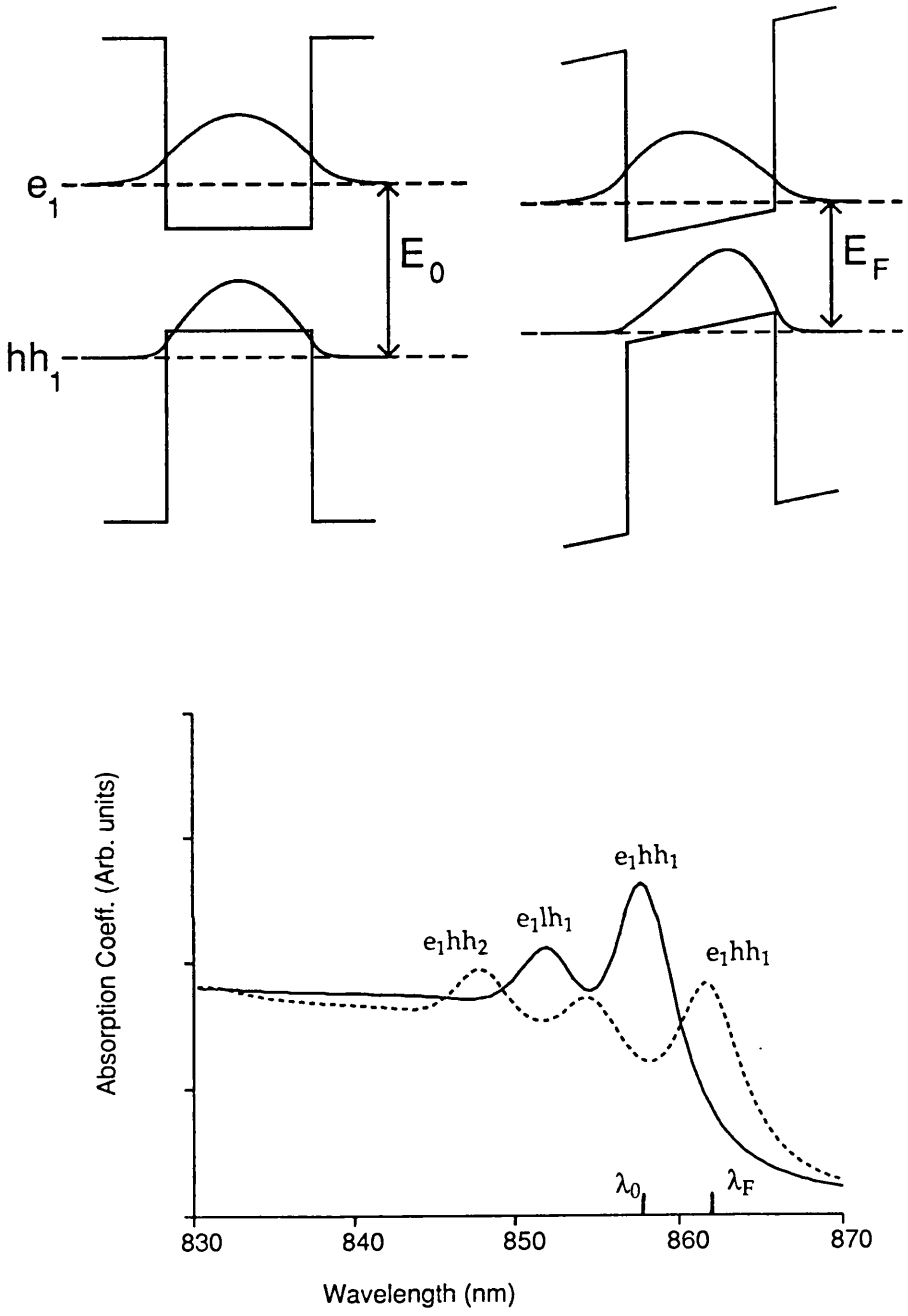

Figure 1.6 showing: top, the calculated lowest electron and hole wavefunctions (e_1 and hh_1) at 0kV/cm and 40kV/cm overlaid upon the potential of a 115Å wide GaAs well; bottom, the calculated absorption spectra for this structure, solid line 0kV/cm, dashed 40kV/cm. The electric field tilts the potential and the wavefunctions polarise towards opposite corners of the well. The energy separation of the levels decrease from E_0 to E_F ('Stark shift') resulting in a shift of the e_1hh_1 absorption peak from λ_0 to λ_F. The polarisation of e_1 and hh_1 wavefunctions with field reduces their overlap and the e_1hh_1 absorption peak height falls. The other features in the spectrum are from light holes (e_1lh_1) and the next heavy hole energy level (hh_2).

field required for a given absorption change is lower in coupled double wells than multiple quantum wells with similar lengths of intrinsic region, L_i, then the operating voltage V_{ap} can be reduced. In uncoupled MQW structures the barrier material is not absorbing yet it contributes to the intrinsic region length L_i. Reducing the barrier width to a minimum and hence reducing L_i would enable operating voltages to be reduced without affecting absorption.

In summary, I set out to develop a model of the quantum well electroabsorption to cope with a wide range of quantum well structures, the purpose being to improve theoretically the performance of these modulators. When it became clear that the study of coupling could yield useful results I focussed my work in this direction, the aim being to model electroabsorption for coupled well structures, in particular to look for trends as, say, barrier width is changed. Thus the emphasis was on developing and using a model to predict useful device structures rather than an exact modelling of the complete absorption spectrum.

Chapter 2
Modelling the electroabsorption spectrum

In order to assess modulator performance I need to be able to model absorption spectra for a range of coupled and uncoupled structures both with and without electric field applied. To do this the calculations can be broken into two distinct areas - the evaluation of carrier energies and wavefunctions, and, the calculation from these of the absorption spectrum.

§2.1 Introduction and literature review

§2.1.1 Evaluation of carrier energy levels and wavefunctions

Materials with different band gaps grown epitaxially cause carriers to experience a potential energy of wells and barriers, $V(z)$, varying in the one dimensional growth direction (z), see figures 2.1 and 1.1.

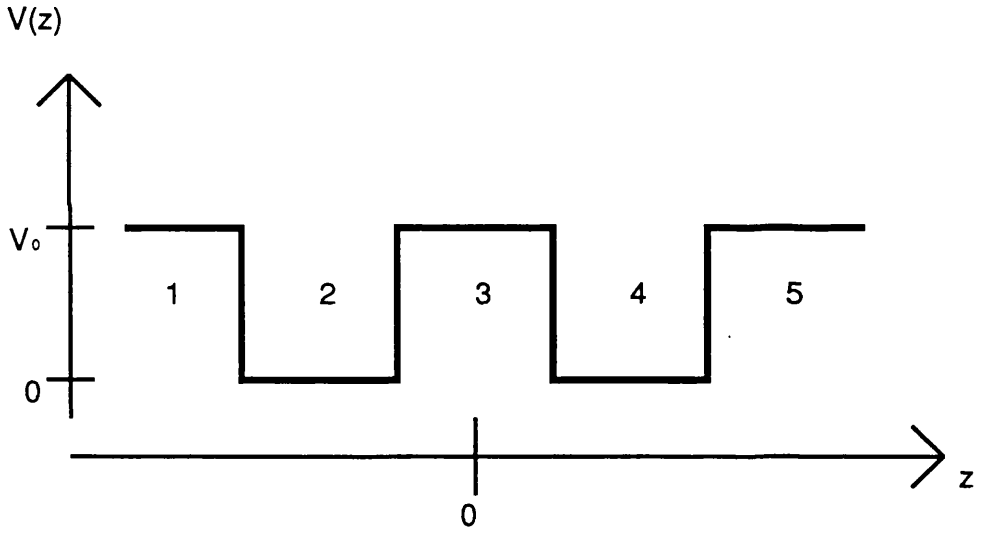

Figure 2.1 depicts the function $V(z)$ for a coupled double quantum well. The origin of z is at the centre of the structure, the origin of $V(z)$ is at the bottom of the GaAs wells. Numeric labels are used in the text to explain the calculations.

With electric field (F) applied across the structure in the growth direction, this one dimensional potential tilts to slope linearly with distance as in figure 1.6 . The overall carrier potential energy is given by $U(z,F) = V(z) - qFz$ where q is the charge of the carrier. Evaluation of energy levels and wavefunctions is based upon the solution of the time independent, one dimensional, Schrödinger's equation using the potential $U(z,F)$.

$$\frac{-\hbar^2}{2m^*(z)}\frac{d^2\psi(z,E,F)}{dz^2} + U(z,F)\ \psi(z,E,F) = E\ \psi(z,E,F) \qquad (2.1)$$

where $m^*(z)$ is the effective mass in the well or barrier and $\psi(z, E, F)$ is the carrier wavefunction at the energy E.

Many solutions have been reported in the literature and some of those applicable to quantum wells are summarised here. One should bear in mind that the solution technique adopted here should be able to cope with coupled wells both with and without electric field.

a) Perturbation theory.

(i) Variational calculations eg Bastard *et al* (1983). A functional form for the carrier wavefunction is assumed. This functional form should contain at least one variational parameter which when varied changes the shape of the wavefunction. The best guess to the exact wavefunction and energy level occurs when the variational parameter is such that the expectation value of the Hamiltonian is at a minimum with respect to the variational parameter. The method relies for its accuracy upon a good guess at the functional form of the wavefunction. This is difficult to extend from the relatively simple ground state energy levels (e_1, hh_1 and lh_1) of a single quantum well to coupled wells and to states other than the ground state because the shape of the wavefunction for coupled wells and non-groundstate energy levels is complicated. Furthermore, the technique is inaccurate at high electric fields [see Austin *et al* (1985)].

(ii) Lengyel *et al* (1990) express perturbed wavefunctions (due to the electric field perturbation) as a sum of unperturbed wavefunctions and find coefficients numerically. They perform the calculation only for ground states. It is likely that extension to coupled wells and high energy levels would be complex because of the complicated shape of the wavefunctions and rapid changes in shape of coupled well wavefunctions with field (described later).

b) Approximation of the potential $U(z, F)$ in a 'piecewise-constant' manner. With field applied $U(z, F)$ slopes with distance, in this technique the sloping potential is divided into many flat steps, for example Harwit *et al* (1986), Stevens *et al* (1988) and Ghatak *et al* (1988). Calculation of tunnelling resonance peaks may then be used to give energy levels. This method is computationally simple to implement as it involves only exponential, sine and cosine functions to describe the wavefunction, can be used for arbitrary potential shapes, and is accurate if the potential is broken onto a sufficient number of steps. It has the disadvantage that a matrix multiplication must be undertaken at each of the many step edges resulting in slow computation times.

c) Exact solutions. The zero electric field solution is fairly simple and described for a single well in many undergraduate texts eg Rae chapter 2. A more general solution for an arbitrary number of wells is described later in §2.2.

With constant field applied, the qFz term in $U(z, F)$ gives potentials that slope linearly with distance. By transforming variables, Schrödinger's equation can be expressed as a differential equation with Airy function solutions, eg Austin *et al* (1986). This is not an approximation and to find the solution requires a matrix matching only

at the well and barrier interfaces lending itself to many-well calculations. This is the method I chose to adopt and is described in more detail in §2.2. Similar matrix matching techniques involving Airy functions have been published, see for example Brennan *et al* (1987), Hutchings (1989), McIlroy (1986) and Campi *et al* (1989). There are differences between the last 4 methods in determining the exact positions of energy levels. This will be addressed in §2.2. The exact Airy functions also form the basis of Chiba *et al*'s work.

Airy function solutions are valid only for linearly sloping potentials. If the well shape $V(z)$ is, for example, parabolic or the electric field is not constant over a well then a hybrid approach may be taken. In this case the well potential is divided into many steps of linearly varying potentials eg Tan *et al* (1990).

d) Numerical solutions to the Schrödinger differential equation. A Monte Carlo approach, eg Singh (1986) and Singh *et al* (1986), this has the advantage of being readily applicable to any potential profile, can include the Coulomb interaction between the electron and hole and the final solution is independent of a trial wavefunction. However Monte Carlo techniques are notoriously slow due to the large number of iterations needed (of the order 10^4 here) to achieve convergence of the solution.

A finite element method has been used for a two-dimensional quantum-confined structure [Kojima *et al* 1989] which the authors state is also applicable to a one dimensional potential. Bloss (1989) has developed the methods of 'shooting' and 'relaxing' which use, respectively, the Runge Kutta method and a form of finite difference to solve Schrödinger's equation. These were applied to a coupled well structure [Bloss (1990)] but the wavefunction boundary conditions need careful consideration (see Bloss (1989) and mentioned in §2.2).

e) Analogies with optical waveguide theory. The mathematics of optical waveguide theory is directly analogous to quantum wells; the optical amplitude being the carrier wavefunction and the refractive index the potential experienced by the carrier. Chuang *et al* 1987 use a strong coupling of modes approach for coupled quantum wells drawing direct analogies with coupled optical waveguides. Kim *et al* (1990) use the beam propagation method although this requires fast Fourier transform algorithms. Yariv *et al* (1985) draw analogies from optical directional couplers and use a linear combination of well wavefunctions calculating wavefunctions for coupled quantum wells. These analogies with optical waveguide theory tend to consider only zero electric field situations (an electric field would be represented by a 'waveguide' with a continuously varying refractive index).

f) Analogies with semiconductor theory. Bleuse *et al* (Jan 1988) apply tight-binding theory to calculations of energy levels in superlattices. Variations on the Kronig Penney model have been applied to the calculation of superlattice bands [Bastard (1981) or Yuh *et al* (Dec 1988)]. Marsh *et al* (1986) have used a scattering matrix approach (which is not restricted to periodic structures). Fiorentini (1990) has published a self-consistent density functional theory but this does not lend itself to simple

absorption spectrum calculations. These techniques generally tend to be applicable more to superlattices as these are composed of repeated potential wells (like a bulk semiconductor but on a different scale).

It is generally assumed that these solutions of the *time independent* Schrödinger equation are valid provided the measurement time is shorter than the tunnelling time.

I have listed above some of the techniques that have been employed in the solution of Schrödinger's equation. All have their advantages and disadvantages but as far as I was concerned, the perturbation theory approaches could not be used because of their complexity for coupled structures and non-groundstate energy levels; numerical solutions would probably be too slow or complex; the analogies with optical waveguide theory and semiconductor theory do not easily address the problem of electric field or small numbers of coupled wells respectively, the 'piecewise-constant' approximation requires many matrix multiplications especially for coupled well structures but was otherwise an attractive option. Exact solutions can be obtained very quickly on a computer system with Airy function algorithms, for many different forms of $V(z)$. I use the Numerical Algorithms Group routines running on a CDC Cyber 960 computer at Imperial College, London.

§2.1.2 Evaluation of the absorption spectrum

The second half of the absorption spectrum calculation is discussed next. All the methods described below require prior determination of energy levels and wavefunctions by one of the techniques above and some assumption as to the lineshape of the excitonic absorption and broadening.

Stevens *et al* (1988) calculate absorption peak wavelengths from energy levels, exciton binding energy and assumed strain shifts. The absorption spectrum is composed of Lorentzian peaks with heights proportional to the square of the electron-hole wavefunction overlap integral and of a continuum contribution representing the unbound electron-hole pairs. This is the method used in this thesis and is described in more detail in §2.3 . Lee *et al* (1989) use a similar technique but with a more complete treatment of excitons.

Klipstein *et al* (1986) also use a similar method of Lorentzians and continua but show in more detail the physics behind this ie. indicating how absorption can be calculated from polarisability which can be determined from Maxwell's equations. They do not, however, include the change of overlap integral with applied field in their model.

Masselink *et al* (1985), Hong *et al* (Dec 1987), Ahn (1989) and others have calculated absolute quantum well absorption coefficients by including explicitly the interaction of the optical radiation with the electron hole dipole and by including the Bloch states in the wavefunction overlap. I do not do this because I believed it would be more fruitful to devote my time to studying changes in the absorption spectra rather than the exact values of the absorption coefficient. The calculations in this thesis give scaled absorption coefficients proportional to their absolute value. The scaling constant is dependent upon the factors mentioned above and I fit the value from experimental

data. (My work does account for the different momentum matrix elements for heavy and light holes).

In summary, I adopt a method similar to Stevens *et al* (1988) for calculating absorption spectra given the energy levels and wavefunctions because this is relatively simple to implement yet shows the changes in absorption coefficient necessary for optical modulation. The wavelengths of interest for optical modulation are those close ($\approx \pm 30$nm) to the absorption edge of the material at which application of an electric field can result in large absolute and percentage changes in absorption.

§2.2 Details of the energy level and wavefunction calculation

Schrödinger's equation (2.1) must be solved. The chosen method in the previous section was that of exact solutions. The effective mass $m^*(z)$ is independent of energy E if band non-parabolicities are neglected. Stevens *et al* (1988) show that the inclusion of band non-parabolicity gives a small shift of absorption peaks, for ground state levels in a single quantum well, of the order of 1meV. I decided to neglect band non-parabolicity initially but make the effective mass a value returned by a function in my programs so that I left myself the option of including this effect later if necessary by making the mass energy dependent. I also neglected light and heavy hole mixing because there is usually a reasonable separation between the major heavy and light hole exciton peaks at the wavelengths of interest for optical modulation in chapters 4 and 5. Furthermore, Andrews *et al* (1989) suggest that band mixing in a similar structure to that in chapters 4 and 5 results in little change of exciton transition energies but the exciton linewidths are affected at 5K. All modelling in this thesis of optical modulators is for room temperature where thermal broadening dominates. The wavefunctions and energy levels found in this section are for free electrons and holes - the Coulomb attraction has been omitted. In the absorption coefficient calculations of §2.3 allowance is made for these excitonic effects.

Equation (2.1) has the zero field solutions below.

In regions where $E < V(z)$

$$\psi(z,E) = C(E)\exp[-\kappa(E,z)z] + D(E)\exp[\kappa(E,z)z] \tag{2.2}$$

the argument F of $\psi(z,e,F)$ and of the coefficients $C(E,F)$ and $D(E,F)$, is dropped when I am considering only one particular field, and, in regions where $E > V(z)$

$$\psi(z,E) = C(E)\sin[\kappa(E,z)z] + D(E)\cos[\kappa(E,z)z] \tag{2.3}$$

where

$$\kappa(E,z) = \sqrt{\frac{2m^*(z)\ |(V(z)-E)|}{\hbar^2}} \tag{2.4}$$

The z dependence of $m^*(z)$ and $V(z)$ is through the composition of the well material. At each interface we must have continuity of wavefunction and particle flux (for example Schiff 1981). Wavefunction continuity requires

$$\psi_L(z_{int},E,F) = \psi_R(z_{int},E,F) \tag{2.5}$$

ψ_L is the wavefunction to the left of the interface at z_{int} and ψ_R is the wavefunction to the right. Particle flux conservation and wavefunction continuity lead to the following condition on the wavefunction derivative:

$$\frac{1}{m^*(z_L)}\frac{d\psi_L(z_{int},E,F)}{dz} = \frac{1}{m^*(z_R)}\frac{d\psi_R(z_{int},E,F)}{dz} \tag{2.6}$$

where $m^*(z_L)$ is the effective mass of the carrier in material to the left of the interface and $m^*(z_R)$ is to the right [verified for GaAs/AlGaAs by Galbraith *et al* (1988)]. In regions where $E < V(z)$ we have from equation (2.2)

$$\begin{pmatrix} \psi \\ \frac{1}{m^*(z)}\frac{d\psi}{dz} \end{pmatrix} = \begin{pmatrix} \exp[-\kappa\, z] & \exp[\kappa\, z] \\ -\frac{\kappa}{m^*}\exp[-\kappa\, z] & \frac{\kappa}{m^*}\exp[\kappa\, z] \end{pmatrix} \begin{pmatrix} C(E) \\ D(E) \end{pmatrix} \tag{2.7}$$

(dropping the arguments for clarity) and where $E > V(z)$ from equation (2.3)

$$\begin{pmatrix} \psi \\ \frac{1}{m^*(z)}\frac{d\psi}{dz} \end{pmatrix} = \begin{pmatrix} \sin(\kappa z) & \cos(\kappa z) \\ \frac{\kappa}{m^*}\cos(\kappa\, z) & -\frac{\kappa}{m^*}\sin(\kappa\, z) \end{pmatrix} \begin{pmatrix} C(E) \\ D(E) \end{pmatrix} \tag{2.8}$$

Equations (2.5) and (2.6) can be used to match the matrices in (2.7) and (2.8). For example at the interface between materials 1 and 2 (see figure 2.1) we write

$$\mathbf{R_1}(E)\begin{pmatrix} C_1(E) \\ D_1(E) \end{pmatrix} = \mathbf{L_2}(E)\begin{pmatrix} C_2(E) \\ D_2(E) \end{pmatrix} \tag{2.9}$$

where $\mathbf{R_1}$ denotes the relevant 2×2 matrix from equation (2.7) or (2.8) for the right hand side of material 1, with z being the value of the interface between 1 and 2 and $m^*(z)$ evaluated for material 1. Similarly $\mathbf{L_2}$ denotes the relevant matrix for the left hand side of material 2. Likewise at the boundary between 2 and 3 the matrix equation is

$$\mathbf{R_2}(E)\begin{pmatrix} C_2(E) \\ D_2(E) \end{pmatrix} = \mathbf{L_3}(E)\begin{pmatrix} C_3(E) \\ D_3(E) \end{pmatrix} \tag{2.10}$$

hence

$$\begin{pmatrix} C_1(E) \\ D_1(E) \end{pmatrix} = \mathbf{R_1}^{-1}(E)\,\mathbf{L_2}(E)\,\mathbf{R_2}^{-1}(E)\,\mathbf{L_3}(E)\begin{pmatrix} C_3(E) \\ D_3(E) \end{pmatrix} \tag{2.11}$$

and over the whole structure of figure 2.1

$$\begin{pmatrix} C_1(E) \\ D_1(E) \end{pmatrix} = \mathbf{R_1}^{-1}(E)\,\mathbf{L_2}(E)\,\mathbf{R_2}^{-1}(E)$$
$$\mathbf{L_3}(E)\,\mathbf{R_3}^{-1}(E)\,\mathbf{L_4}(E)\,\mathbf{R_4}^{-1}(E)\,\mathbf{L_5}(E)\begin{pmatrix} C_5(E) \\ D_5(E) \end{pmatrix} \tag{2.12}$$

where the multiplied matrices can be expressed as one matrix $\mathbf{M_T}(E)$ and

$$\mathbf{M_T}(E) = \begin{pmatrix} t_{11}(E) & t_{12}(E) \\ t_{21}(E) & t_{22}(E) \end{pmatrix} \tag{2.13}$$

This is readily extendible to a large number of interfaces and applies to structures containing layers of $Al_xGa_{1-x}As$ with differing values of x.

At zero field the solutions are bound, that is to say, $\psi(z,E) \rightarrow 0$ as $z \rightarrow \pm\infty$ hence $C_1(E) = 0$ and $D_5(E) = 0$. In order that this is true $t_{11}(E)$ must be zero. This occurs only at the energies E which are valid solutions.

Hence by varying E I can locate the roots of $t_{11}(E) = 0$ giving the zero field energy levels. From these all the coefficients $C(E)$ and $D(E)$ can be calculated and hence the wavefunctions.

I will now turn to the with field case. With electric field (F) applied the qFz term in Schrödinger's equation is non zero and the equation is transformed into a differential equation with Airy function solutions.

The substituted variable y (Austin *et al* 1985) is,

$$y(z,E,F) = \left(\frac{2Fm^*(z)q}{\hbar^2}\right)^{1/3}\left[-z + \frac{V(z)-E}{qF}\right] \tag{2.14}$$

As z is varied, $V(z)$ and $m^*(z)$ are both constant throughout a material until an interface is reached. At each interface the conditions of continuity of wavefunction and particle flux must be applied and hence in the differentiation of y with respect to z , $V(z)$ and $m^*(z)$ can be treated as constants. From equation (2.14),

$$\frac{dy}{dz} = -\left(\frac{2Fm^*q}{\hbar^2}\right)^{1/3} \tag{2.15}$$

By the chain rule,

$$\frac{d\psi}{dz} = \frac{dy}{dz}\frac{d\psi}{dy} \tag{2.16}$$

Hence,

$$\frac{d^2\psi}{dz^2} = \frac{d^2y}{dz^2}\frac{d\psi}{dy} + \frac{dy}{dz}\frac{d}{dz}\left(\frac{d\psi}{dy}\right) \tag{2.17}$$

Using equation (2.15) ,

$$\frac{d^2\psi}{dz^2} = +\left(\frac{2Fm^*q}{\hbar^2}\right)^{2/3}\frac{d^2\psi}{dy^2} \tag{2.18}$$

Now, from equation (2.14),

$$z = -y\left(\frac{2Fm^*q}{\hbar^2}\right)^{-1/3} + \frac{V-E}{qF} \tag{2.19}$$

and by substituting this and equation (2.18) into Schrödinger's equation,

$$-\frac{\hbar^2}{2m^*}\frac{d^2\psi}{dz^2} + (V - qFz - E)\psi = 0 \tag{2.20}$$

the differential equation below results.

$$\frac{d^2\psi}{dy^2} - y = 0 \tag{2.21}$$

This is the standard differential equation with Airy function solutions:

$$\psi = C\ Ai(y) + D\ Bi(y) \tag{2.22}$$

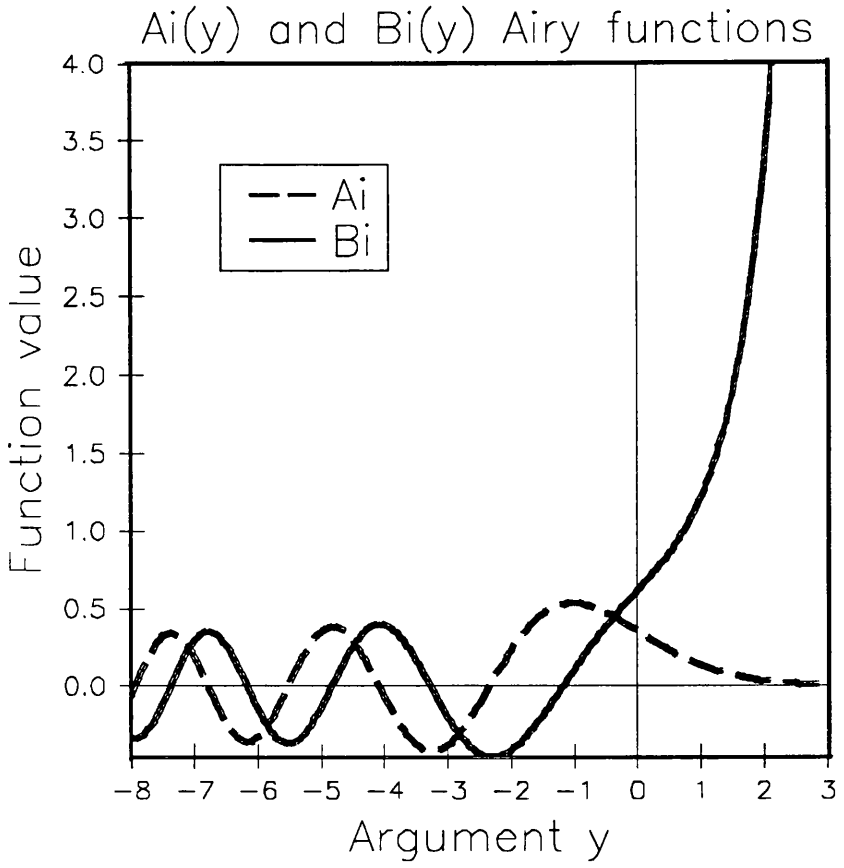

Figure 2.2 The Airy functions.

where Ai and Bi are Airy functions (see figure 2.2) and the omitted dependencies are, $\psi = \psi(z, E, F)$, $C = C(E, F)$, $D = D(E, F)$ and $y = y(z, E, F)$.

The asymptotic Airy functions for large $|y|$ are:

$$Ai(y) \approx \frac{1}{2\sqrt{\pi}} y^{-1/4} \exp\left[-\frac{2}{3}y^{3/2}\right] \tag{2.23}$$

$$Bi(y) \approx \frac{1}{\sqrt{\pi}} y^{-1/4} \exp\left[\frac{2}{3}y^{3/2}\right] \tag{2.24}$$

$$Ai(-y) \approx \frac{1}{\sqrt{\pi}} y^{-1/4} \sin\gamma \tag{2.25}$$

$$Bi(-y) \approx \frac{1}{\sqrt{\pi}} y^{-1/4} \cos\gamma \tag{2.26}$$

where

$$\gamma = \frac{2}{3}y^{3/2} + \frac{\pi}{4} \tag{2.27}$$

derived from Abramowitz and Stegun, chapter 10.

The general solution to Schrödinger's equation with a linearly varying potential is equation (2.22). With no wells present ie $V(z) \equiv 0$ equation (2.22) is the solution to Schrödinger's equation for all z. Hence in this case $D \equiv 0$ in order that $Bi(y)$ does

not become very large as $z \to -\infty$ $(y \to +\infty)$. At large positive z (large negative y), the wavefunction behaves like equation (2.25).

$$\psi \propto \frac{1}{\sqrt{\pi}} y^{-1/4} \sin\gamma \tag{2.28}$$

To determine energy levels the phase shift of the wavefunction between solutions for a linearly varying potential, qFz, and the true potential $V(z) - qFz$ is required. For the true potential the same continuity conditions apply as the zero field case and similar matrix matching equations can be formed. With a positive field applied, positively charged holes move in the direction of positive z, so for $z \to -\infty$ $(y \to +\infty)$ the Bi coefficient must be zero. Hence $D_1 = 0$ and I set $C_1 = 1$, the normalisation of the wavefunction takes care of an arbitrary factor.

At the positive z side of a double well structure, such as that shown in figure 2.1,

$$\psi_5 = C_5 Ai(y) + D_5 Bi(y) \ . \tag{2.29}$$

Here y is large and negative and ψ_5 can be written

$$\psi_5 = \frac{1}{\sqrt{\pi}} y^{-1/4} \left(C_5 \sin\gamma + D_5 \cos\gamma\right) \tag{2.30}$$

writing ψ_5 as

$$\psi_5 = \frac{1}{\sqrt{\pi}} y^{-1/4} A \sin(\gamma + \phi) \tag{2.31}$$

so that ϕ is a phase shift representing the difference in phase of the wavefunction at large z between the potential inserted case and the no wells case (equations 2.31 and 2.28 respectively).

Hence,

$$\psi_5 = \frac{1}{\sqrt{\pi}} y^{-1/4} A(\sin\gamma\cos\phi + \cos\gamma\sin\phi) \tag{2.32}$$

Equating coefficients of $\sin\gamma$ gives

$$A\cos\phi = C_5 \tag{2.33}$$

$$A\sin\phi = D_5 \tag{2.34}$$

therefore,

$$\tan\phi(E) = \frac{D_5(E)}{C_5(E)} \tag{2.35}$$

putting in the E dependencies.

In order to determine the density of states (DOS), box limits on the wavefunction are imposed. If the potential structure is inserted in a large 1D box extending from $z = -L$ to $z = +L$ the wavefunction at $-L$ is negligible due to the exp $\left[-\frac{2}{3}y^{3/2}\right]$ factor in $Ai(y)$. Equation (2.31) is used to set the wavefunction to zero at $z = L$, in this case $\gamma_{(z=L)} + \phi$ must be an integral number of π, ie,

$$\gamma_{(z=L)} + \phi = n\pi \tag{2.36}$$

where n is an integer and is equivalent to the number of energy levels at energy E in the large box between $-L$ and $+L$. Hence the density of states $\rho(E)$ can be determined:

$$\rho(E) = \frac{dn}{dE} \tag{2.37}$$

$$\rho(E) = \frac{2}{\pi}\frac{d\gamma_{(z=L)}}{dE} + \frac{2}{\pi}\frac{d\phi}{dE} \tag{2.38}$$

inserting a factor 2 for spin degeneracy. Using (2.14), the expression for y, and (2.27), the expression for γ gives,

$$\gamma_{(z=+L)} = \frac{2}{3}\left[\xi\left(-L + \frac{V-E}{qF}\right)\right]^{3/2} + \frac{\pi}{4} \tag{2.39}$$

(setting $\xi = (2Fm^*q/\hbar^2)^{1/3}$). Therefore,

$$\frac{d\gamma_{(z=L)}}{dE} = -\frac{1}{qF}\xi\left[\xi\left(-L + \frac{V-E}{qF}\right)\right]^{1/2} + \frac{\pi}{4} \tag{2.40}$$

At $z = +L$, z is a long way into the barrier material so $V = V_0$ (see figure 2.1) and $d\gamma_{(z=L)}/dE$ does not depend on E if

$$L \gg \frac{V_0 - E}{qF} \tag{2.41},$$

a condition I ensure. Hence the energies at which there are peaks in $\rho(E)$ are given by the maxima in $\Delta\rho(E)$ where

$$\Delta\rho(E) = \frac{2}{\pi}\frac{d\phi(E)}{dE} \tag{2.42}$$

For very highly confined levels (ie low electric fields and/or energy levels deep in the well) the energy levels, or resonances (a term from scattering theory) are extremely narrow in energy and become difficult to handle computationally. This and other problems are elaborated upon in chapter 3. For example, for a 100Å wide single quantum well of $GaAs/Al_{0.3}Ga_{0.7}As$ the lowest-energy heavy-hole level has a width of 10^{-116}meV at a field of 5kV/cm (assumed data is: valence band well depth 225meV, heavy hole mass in the well $0.34m_e$ and in the barrier $0.46m_e$). In comparison, the lowest heavy hole state of $In_{0.53}Ga_{0.47}As/InP$ occurs with a width of 10^{-110}meV at a field as large as 35kV/cm (assumed data is: valence band well depth 300meV, well mass $0.5m_e$ and barrier mass $0.56m_e$). To determine these widths a Breit-Wigner parameterisation was applied to the phase shift. Close to a narrow energy level E_p, Callaway (1976) writes

$$\tan\phi_p(E) = \frac{\Gamma_p}{2(E_p - E)} \tag{2.43}$$

Using this expression to give $\phi(E)$ and substituting into equation 2.42 gives

$$\Delta\rho(E) = \left(\frac{\Gamma_p}{\pi}\right)\left[\frac{1}{(E-E_p)^2 + \Gamma_p^2/4}\right] \tag{2.44}$$

where Γ_p is the width of the resonance. This has its basis in scattering theory, see Callaway (1976) and Newton for more details.

Hence there are two methods used for finding energy levels. At moderate and high electric fields the DOS can be plotted using equations (2.42) and (2.35), and, the energy levels found by locating the peaks in DOS and their widths by measuring the Full Width Half Maximum (FWHM). At low electric fields the Breit-Wigner parameterisation is applied when the phase shift increases by $\pi/2$ as the energy E goes through E_p from below. Densities of states are calculated at energies on either side of the peak and the Lorentzian of equation (2.44) is fitted. I have compared the values calculated from the two methods at an intermediate field and there is good agreement.

In these methods energy levels are taken to be at the maxima in the density of states which appears to be a physically reasonable thing to do. Some authors have taken energy levels to be at the maxima in the tunnelling resonance coefficient - see for example Stevens *et al* (1988), Hutchings (1989) and Miller et al (1985) (Appendix C). There appears to be little difference between the results of the two methods [Trzeciakowski *et al* (1989) and Pandey *et al* (1990)]. Computationally both methods require peak finding routines and neither appears easier than the other.

The physical basis for these calculations arises because if the well or coupled wells are assumed to exist in an infinite extent of barrier material, then with field applied, there is always a part of the structure at a lower potential energy than a carrier in the well. Hence carriers in the well have a finite probability of tunnelling out of the well - there are no truly bound (discrete) solutions, as there are in the zero field case, and all energies are valid solutions to Schrödinger's equation. (The energy levels are broadened, the width of the levels being inversely related to the tunnelling time.) Because there are no discrete solutions a peak in the DOS must be found, this is computationally harder than the simple root finding problem at zero field.

One alternative is to force there to be bound solutions by assuming the wells are infinitely deep. This is applied to a single quantum well [Miller D A B *et al* (May 1986) and one of the options used by Miller D A B *et al* (July 1985)], the energy levels are correct only if the well width is changed to an 'effective well width'. I find this boundary condition unphysical and it could not be applied to a coupled well structure where the whole point is that there is coupling through a finite barrier. Another trick is to put the well/barrier potential structure inside an infinitely deep box with walls judiciously placed away from the true structure such that energy levels are not significantly affected [eg Bloss (1989), Lee *et al*]. Care must be taken to ensure that the box walls do not affect the true structure's energy levels and also that the states of the artificial box do not interact with the true states [Bloss (1989)]. Alternatively, McIlroy (1986) set the potentials to be constant at some distance from the structure. This latter method provides bound solutions for all energies lower than the lower of the constant potentials, one must be careful not to apply too great an electric field.

The Airy function method gives exact wavefunctions which must be normalised to

a length. Calculation of the electron-hole overlap integral also requires length limits. The overlap limits were chosen such that they do not go beyond the z values where electron or hole wavefunctions become insignificant. For example, with a positive electric field applied, holes become free at large positive z and their wavefunctions are oscillatory; at large negative z their wavefunction decays (conversely for electrons) - see figure 2.3 . The chosen limit for evaluation of the overlap integral in the positive z direction, in this case, would be z_2 where the electron wavefunction has become insignificant and in the negative z direction z_1 where the hole wavefunction has become insignificant. The normalisation limits for the individual hole wavefunctions are where the wavefunction has decayed to an insignificant amount in the negative z direction and also in the positive z direction unless the oscillatory portion of the wavefunction commences close to the wells. In this case the chosen limit is where the wavefunction first crosses zero beyond the positive z side of the structure. Conversely for electrons - see figure 2.3 . Hence this somewhat arbitrary fixing of normalisation limit can introduce a small error in the wavefunction normalisation, and consequently the overlap integral. This is only the case in energy levels that are less well bound ie those close to the top of the well. These levels are involved in spectral transitions at energies above and away from the absorption edge, furthermore their overlap integral with the other carrier wavefunction is generally small in comparison with the transitions close to the absorption edge. Hence this approximation can lead to small errors in the spectrum at energies well above the absorption edge. (The errors in wavefunction normalisation relevant to the situations considered in chapters 4 and 5 for optical modulators, are less than 1% because the applied fields are so low).

§2.3 Calculation Of Optical Absorption Spectra

A photon incident upon the structure can be absorbed by promoting an electron from the valence to conduction band, creating an electron-hole pair. This pair can be bound together - an exciton, or unbound in free-particle states. There is only significant probability of creating a carrier pair where their density of states are high (Fermi's Golden Rule) i.e. at the energy levels.

Optical absorption was modelled as the sum of absorption from the creation of different electron-hole pairs. With field applied, all the energy levels were considered that arise from states originally within the well at zero field. In this way all the observable electron-hole pairs were considered both with and without applied electric field. Hence this work accounts for all so-called 'forbidden transitions'. The absorption from all electron-hole pairs was summed to give the final absorption spectrum at a given field [Stevens *et al* (1988)].

$$\alpha_{total}(hf,F) = \sum_{i,j} \alpha_{e_i - hh_j}(hf,F) + \frac{1}{3}\sum_{i,l} \alpha_{e_i - lh_l}(hf,F) \qquad (2.45)$$

where α is proportional to the absorption coefficient, hf is the spectral energy, e_i denotes the ith electron energy level, hh_j denotes the jth heavy-hole level and lh_l

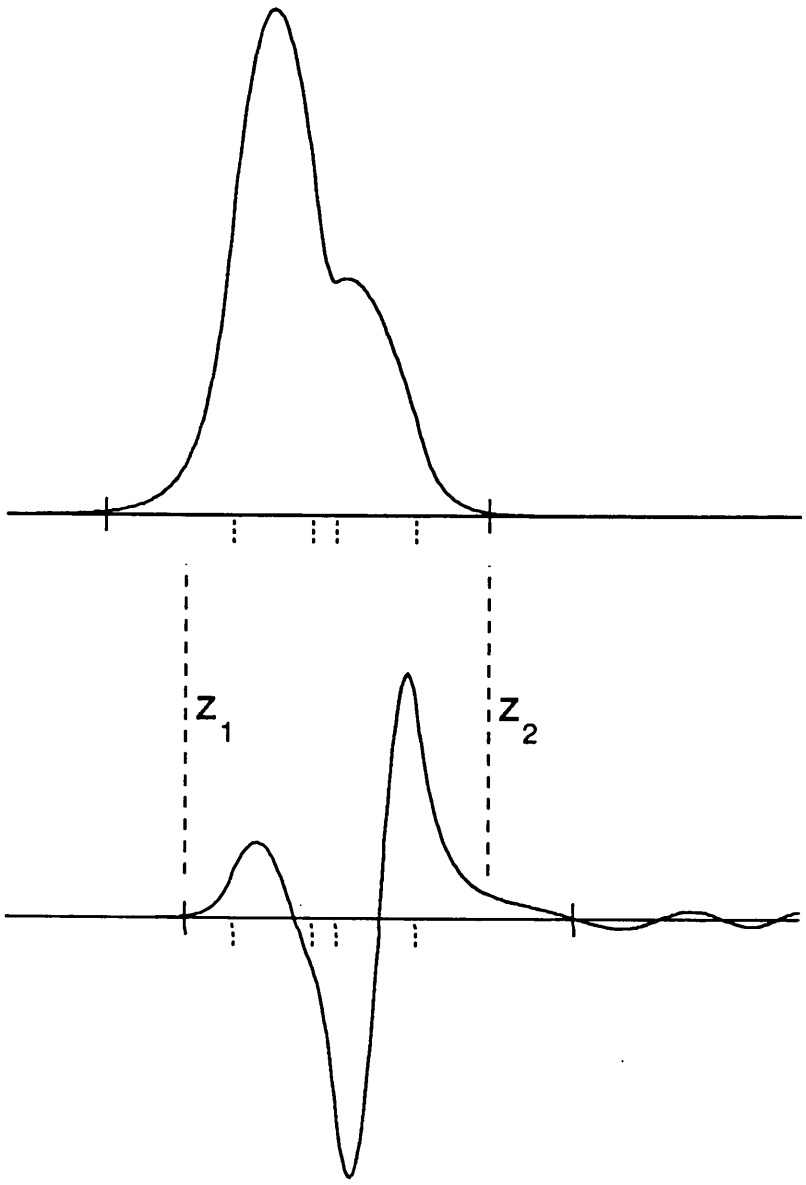

Figure 2.3 Wavefunctions against z for e_1 (upper) and hh_3 (lower) carriers demonstrating normalisation limits (short vertical solid lines), and, overlap limits z_1 and z_2. Short dashed lines indicate the material interfaces. The electric field is 50kV/cm applied across a 50Å GaAs /15Å $Al_{0.3}Ga_{0.7}As$ /50Å GaAs CDQW. Note the hh_3 wavefunction oscillates close to the CDQW.

denotes the lth light-hole level. The calculated absorption coefficient is proportional to its true value as mentioned in §2.1.2 . The constant of proportionality is determined once by experimental fit.

An optical beam is considered incident normal to the plane of the layers (polarization parallel to these layers) as in the transmission mode of figure 1.2. In this configuration the different angular momentum components of the heavy and light hole

bands result in the heavy hole to conduction band transition being three times more probable than the light hole transition between the subband edges [Yamanishi *et al* 1984]. Hence the factor 1/3 before the light hole contribution in equation (2.45). This is only strictly true at the spectral energy of each subband transition [Yamanishi *et al* 1984], at higher energies the heavy hole transition probability decreases with respect to the light hole, although this is ignored here. I have also neglected the decrease of the Sommerfeld factor [Shinada *et al* 1966] with higher spectral energy. Both these factors vary on a scale of tens of meV from each subband transition ie a few tens of nm in wavelength. This will have little effect upon calculated spectra near the absorption edge but may lead to my calculations giving too high an absorption at high spectral energies.

For MQWs, phonon broadening is a significant broadening mechanism, especially at low fields [Stevens *et al* 1988]. This homogeneous phonon broadening was accounted for by expressing the bound excitonic contribution as a Lorentzian and the unbound states as an integral of Lorentzians. The bound electron-hole pair exists in quantised levels analogous to the hydrogen atom. I have only considered the 1S exciton because the oscillator strength falls off rapidly with higher bound states [Klipstein *et al* 1986]. The 2S exciton is only observed in very good quality material at low temperatures eg. Dawson *et al* 1986 .

With the wells in the intrinsic region of a p-i-n diode structure (figure 1.3) , unintentional background doping of the intrinsic region results in an electric field variation across this region. Here I have considered only a single well or a single pair of coupled wells and so the field variation across the one well or pair is very small. For transverse (non-waveguide) devices there are many, isolated, wells or pairs of coupled wells in the intrinsic region. This work is readily extendible to include electric field variations across the intrinsic region and variations in well width and barrier width. These will increase the amount of broadening observed. In reality broadening is also dependent upon material quality and growth. Here, all broadening was quantified by the FWHM of the Lorentzian and was taken to be constant with the applied field and the structure considered. The room temperature value of FWHM chosen was 8.5 meV taken from experimental data on 100Å wide MQWs (Stevens *et al* 1988). This value is in agreement with data in Jelley *et al* (1989) and is shown by them to be valid for well widths from $\approx$ 75Å to $\approx$ 200Å. This broadening is predominantly due to phonon interactions which I have assumed to be of a similar value in coupled and uncoupled quantum wells. Fluctuations in the width of the coupling barriers are considered in chapter 4. The absorption expression used for the creation of each electron-hole pair was from Stevens *et al* (1988):

$$\alpha_{e-h}(hf,F) = M_{e-h}(F) \times L\left[hf,(E_{e-h}(F) - B_{e-h})\right] + \frac{1}{r_{e-h}R_y} M_{e-h}(F) \int_{E_{e-h}(F)}^{\infty} L(hf,E')\, dE' \quad (2.46)$$

where

$$M_{e-h}(F) = \left| \int_{z_1}^{z_2} \psi_e^*(z, E_e, F)\ \psi_h(z, E_h, F)\ dz \right|^2 \tag{2.47}$$

z_1 and z_2 are the limits of wavefunction normalisation discussed earlier; ψ are normalised wavefunctions; r_{e-h} is the ratio of exciton area to the level of the continuum [Klipstein *et al* 1986]; $E_{e-h}(F) = E_e(F) + E_h(F) + E_{gap}$, $E_e(F)$ is the electron subband energy, $E_h(F)$ is the hole subband energy and E_{gap} is the band gap of GaAs; R_y is the Rydberg and is given by,

$$R_y = \frac{q^2 \mu}{8\epsilon_0^2 \epsilon_r^2 h^2} \tag{2.48}$$

where μ is the reduced mass calculated as in Stevens *et al* (1988), ϵ_r is the relative dielectric constant, ϵ_0 is the dielectric constant and ;

$$L(hf, E') = \frac{\Gamma}{2\pi \left[(hf - E')^2 + \Gamma^2/4 \right]} \tag{2.49}$$

where Γ is the FWHM of the Lorentzian $L(hf, E')$, B_{e-h} is the exciton binding energy and E' is a dummy variable.

The integral over E' is comparatively large at spectral energies, hf, above the band edge and small below it giving the absorption edge contribution. The first term in equation (2.46) is a single Lorentzian superimposing a peak upon the free particle spectrum calculated in the second term. The binding energy of the exciton B_{e-h} shifts the centre of the Lorentzian with respect to the absorption edge.

In summary, Schrödinger's equation is solved to give energy levels. The carrier wavefunctions at these energies are then calculated and hence the overlap integrals are determined. The height of the exciton peak is directly related to the overlap integral. The complete absorption spectrum is the addition of all exciton peaks and the continuum contributions (figure 2.4).

The carrier effective masses in the wells and the barriers were calculated for the stated aluminium concentration, x, using the following linear interpolations; electron $0.0667 + 0.0835x$, heavy-hole $0.34 + 0.412x$ and light-hole $0.094 + 0.066x$ [Miller R C *et al* (June 1984)] in units of the real electron mass. The conduction:valence band offset ratio was taken to be 65:35 (=1.857) [Duggan *et al* (1985)] . The values of the band gap energies in eV were calculated from $1.424 + 1.247x$ (Adachi 1985). The rate of change with temperature of the $Al_xGa_{1-x}As$ band gap was $(-3.95 - 1.15x)$ in units of 10^{-4} eV/deg [Adachi 1985]. The formula for the temperature variation of the GaAs band $E_{gap}(T)$ was that in J.S. Blakemore $E_{gap}(T) = 1519 - 540.5T^2/(T + 204)$ in meV. The dielectric constants for GaAs and $Al_xGa_{1-x}As$ were calculated using the formula $\epsilon = \epsilon_0(13.1 - 3x)$ (see Yamanishi *et al* 1988). In the case of coupled wells a weighted average was used because some of the wavefunction penetrates into the barrier. In practice it makes no significant difference to the modulation results predicted in chapter 4 of this thesis if the average value of ϵ or its value for $x = 0$

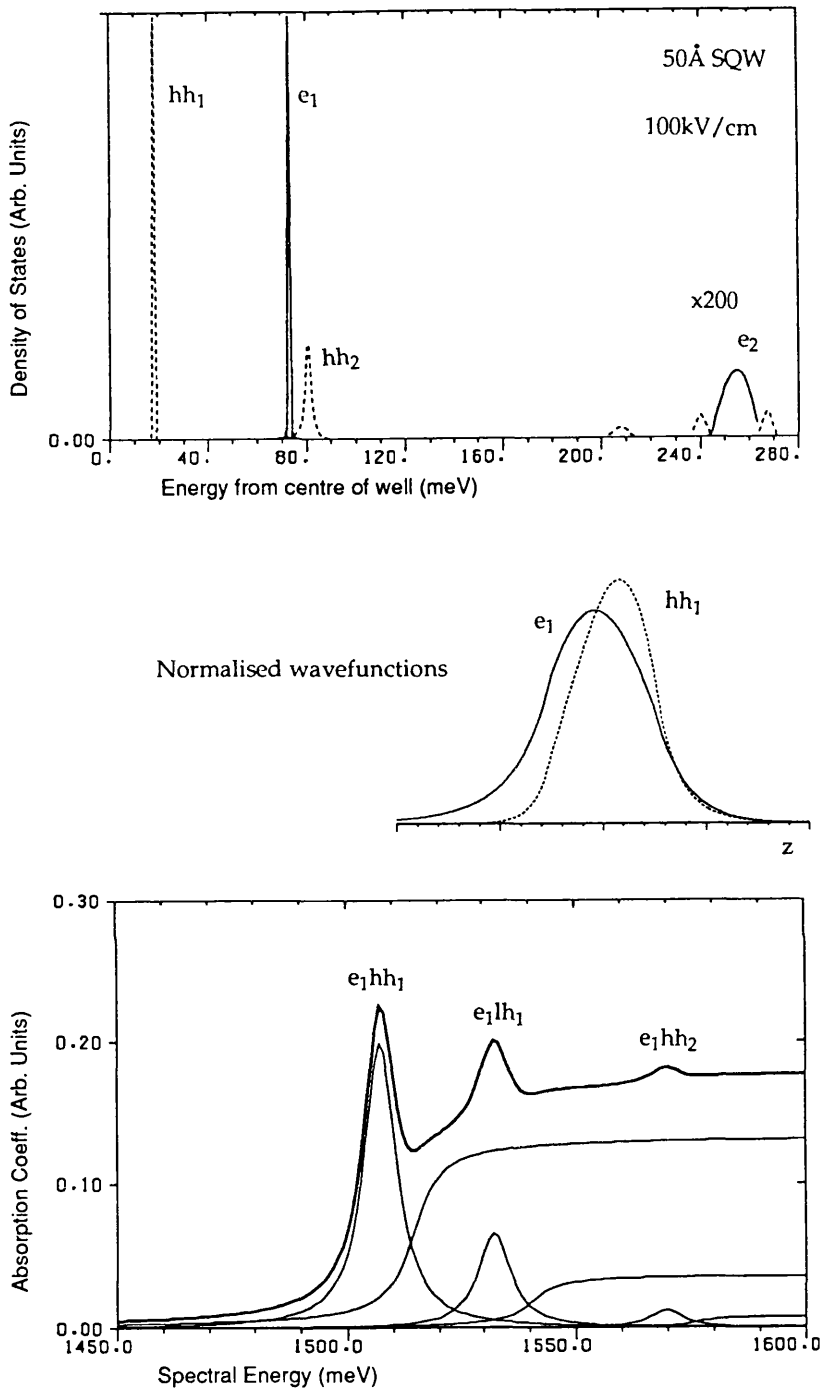

Figure 2.4 Summary of calculation. Top, density of states for a 50Å wide single quantum well at a field of 100kV/cm. Energy is measured from the centre of electron or heavy-hole well. The peaks in the densities of states occur at the carrier energy levels. These values are used to calculate wavefunctions - see middle figure. The overlap integral between the wavefunctions gives the Lorentzian peak height in the lower figure. This shows the Lorentzian and continuum contributions to the total absorption spectrum. The spectral energy of an absorption peak is determined by the energy level separation and the binding energy.

(GaAs) is used but it turns out to be more important in chapter 6 where wide barriers are included in the model. Room temperature and an aluminium concentration of 30% were used in all cases except the comparison with experimental data where the stated values were used.

The fitted parameters are the ratio, r_{e-h}, the FWHM Γ of the Lorentzian and the absolute value of the absorption coefficient all derived from experimental MQW data.

The exciton binding energy B_{e-h} in a CDQW has been calculated by Andrews *et al* (1988) and by Galbraith and Duggan (1989). The latter studied a CDQW structure consisting of two 50Å GaAs wells separated by an $Al_{0.67}Ga_{0.33}As$ barrier of variable thickness. They calculate that this can decrease the heavy hole binding energy by approximately 2.5 meV for their structure. The change in binding energy with field was studied by Andrews *et al* and by Galbraith *et al.* Andrews *et al* consider a 15Å barrier CDQW with 50Å wells and with 30% aluminium concentration in the barriers - a situation closer to my modelled structures than Galbraith and Duggan's. Andrews *et al* find a decrease of binding energy of up to approximately 1.5meV, with fields up to 40kV/cm, for both heavy and light hole excitons.

For all transitions and at all electric fields fixed light and heavy hole binding energies of 8.3 and 7.3 meV respectively are used. These were taken from the 100Å wide MQWs comparison in Stevens *et al* (1988). Thus I have taken a simplistic stand ignoring the variation of binding energy with barrier thickness and with field. The works mentioned above suggest that in chapter 4 I could be over-estimating the binding energy by up to approximately 4meV (the largest field considered there is 40 kV/cm)

.

The ratio, r_{e-h}, is linked to binding energy because both depend upon the dimensionality of the exciton, varying between 2D and 3D limits [Klipstein *et al* (1986)]. I used the binding energy corresponding to the dimensionality in a single 100Å well and hence I used the value 6 for the ratio, obtained from a single 100Å well spectrum fit [Stevens *et al* (1988)] allowing for a factor 2 as these authors use a Sommerfeld factor. The value of 6 is in reasonable agreement with Klipstein *et al*'s value of 5. The wavefunction calculation neglects the Coulomb interaction between electrons and holes which can cause the mixing of energy levels that are separated by approximately one exciton binding energy [Galbraith *et al* (1989)]. I suspect that for spectral peaks with a separation of approximately one binding energy (which is approximately one FWHM) then there may be a reduction in the height of the combined peak due to mixing of wavefunctions by the Coulomb interaction. This applies only to peaks about one binding energy apart.

In this chapter I have described the computational model used to calculate electroabsorption spectra. The matrix multiplication was developed independently by myself, the phase shift technique follows work by Austin *et al* (1985) who had previously calculated energy levels and wavefunctions from a coupled well structure but did not go on to calculate absorption spectra. My handling of wavefunction normali-

sation and overlap limits had not been published before [Atkinson *et al* (1990)] . The calculation of absorption spectra from energy levels and wavefunctions was adopted from Stevens *et al* (1988). These authors had previously modelled MQWs and I have extended this to coupled quantum wells. It is the application of the modelling in the subsequent chapters rather than the model itself that forms the majority of the novel work in this thesis.

Chapter 3 Model testing, problems and early applications.

§3.1 Testing the model.

The model developed in chapter 2 is tested in this section against existing published data. The purpose of this is to detect any errors in the computation and also to give an indication of how accurate the model is. The wavefunction calculation is tested first against published data, then the model is tested against uncoupled wells and finally for coupled structures the model is tested against itself and published experimental data.

Firstly the wavefunction calculation was compared with published data. The most suitable data for comparison was that for four coupled wells with and without electric field applied. There are (at least) two papers fulfilling these criteria - McIlroy (1986) and Austin *et al* (1987). McIlroy's calculation method differs more from mine than Austin *et al*'s so I have reproduced here the comparison with McIlroy, see figure 3.1. The good agreement provides considerable evidence that this aspect of the calculation works correctly.

Secondly the absorption spectrum calculation was tested. Multiple quantum wells in which there is no significant interwell coupling were compared first. Figure 3.2 shows the comparison with Stevens *et al* (1988) who give absorption derived from photocurrent measurements, and figure 3.3 shows comparison with Lengyel *et al*'s absorption measurements on wells with similar widths (≈100Å). The difference in material parameters between the two is that Stevens *et al* use 98Å wells with a 40% aluminium concentration in the barriers and Lengyel *et al* use 105Å wells with 32% aluminium barriers. Jelley *et al*'s (1989) absorption measurements on 35Å wells are also included for comparison in figure 3.4. The Lengyel *et al* and Jelley *et al* data is particularly useful as they measure absorption directly, minimise Fabry Perot effects by using an antireflection coating and estimate electric fields within their device. The axes of the calculated spectra are scaled to give my data, and that published, the same aspect ratio to aid visual comparison.

The modelling in this thesis goes beyond that of Stevens *et al* (1988) in that 'forbidden transitions' are included and not just the e_1hh_1 and e_1lh_1 transitions. (Forbidden transitions are those for which the overlap integral (2.47) is zero at zero electric field, but not at higher fields.) Consequently the peaks observed experimentally at around 840nm in figure 3.2a appear in the model. For modelling optical modulation in MQW material this is not very significant, however, it is crucial in coupled well modelling. In my modelling I have not found it necessary to introduce a drop in voltage of 1.4V somewhere in the device as Stevens *et al* did, nor have the curves been shifted in wavelength. The data in figure 3.2b assumes a Lorentzian broadening of constant width (FWHM=8.5meV). This gives good agreement for the zero bias spectrum but as field is applied it is evident that the experimental absorption peaks broaden. This field dependent broadening is largely due to unintentional background doping in the intrinsic

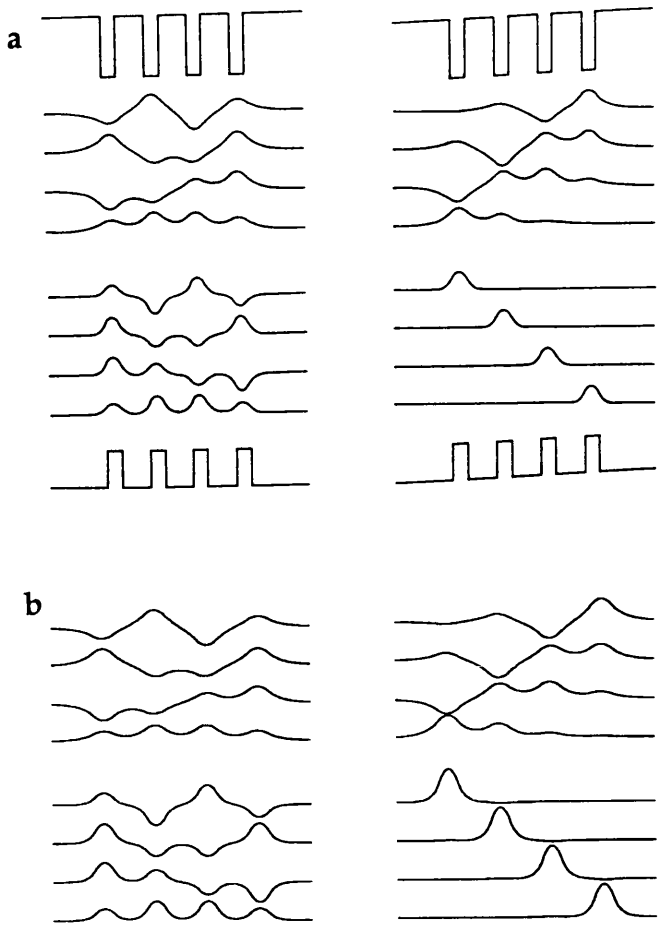

Figure 3.1a Wavefunctions reproduced from McIlroy (1986) figure 1. Structure is four 25Å GaAs wells separated by three 50Å $Al_{0.3}Ga_{0.7}As$ barriers. Electric fields are 10kV/cm (right) and 0kV/cm (left). Upper wavefunctions are electrons, lower are heavy holes.

Figure 3.1b Wavefunctions modelled here for comparison with McIlroy's. The same parameters as figure 3.1a were used.

region of the p-i-n diode (discussed in more detail later) . It is, therefore, dependent upon material quality. The results published by Lengyel *et al* show little sign of field induced broadening (although one should note that the maximum field in their figure is 68.5kV/cm as opposed to Stevens *et al*'s maximum of ≈100 kV/cm). Figure 3.3b shows the spectra calculated to correspond to Lengyel *et al*'s measured data (reproduced in figure 3.3a). This time the modelled growth of the peak at ≈843nm does not appear to be observed experimentally, the calculated and experimental peaks disagree in wavelength by about 8nm, the model being the higher and the calculated Stark shift is greater than that observed. (The latter two points are consistent with an inaccuracy in well width, the fit should be improved if a narrower well was modelled.)

The comparison with Jelley *et al*'s 35Å data in figure 3.4 is good in terms of relative peak heights and relative peak shifts. However the peaks in the model occur at wavelengths about 12nm above those measured. In order to obtain the spectra in figure 3.4b I have used a Lorentzian FWHM of 17.0 and a ratio r_{e-h} of 10 compared

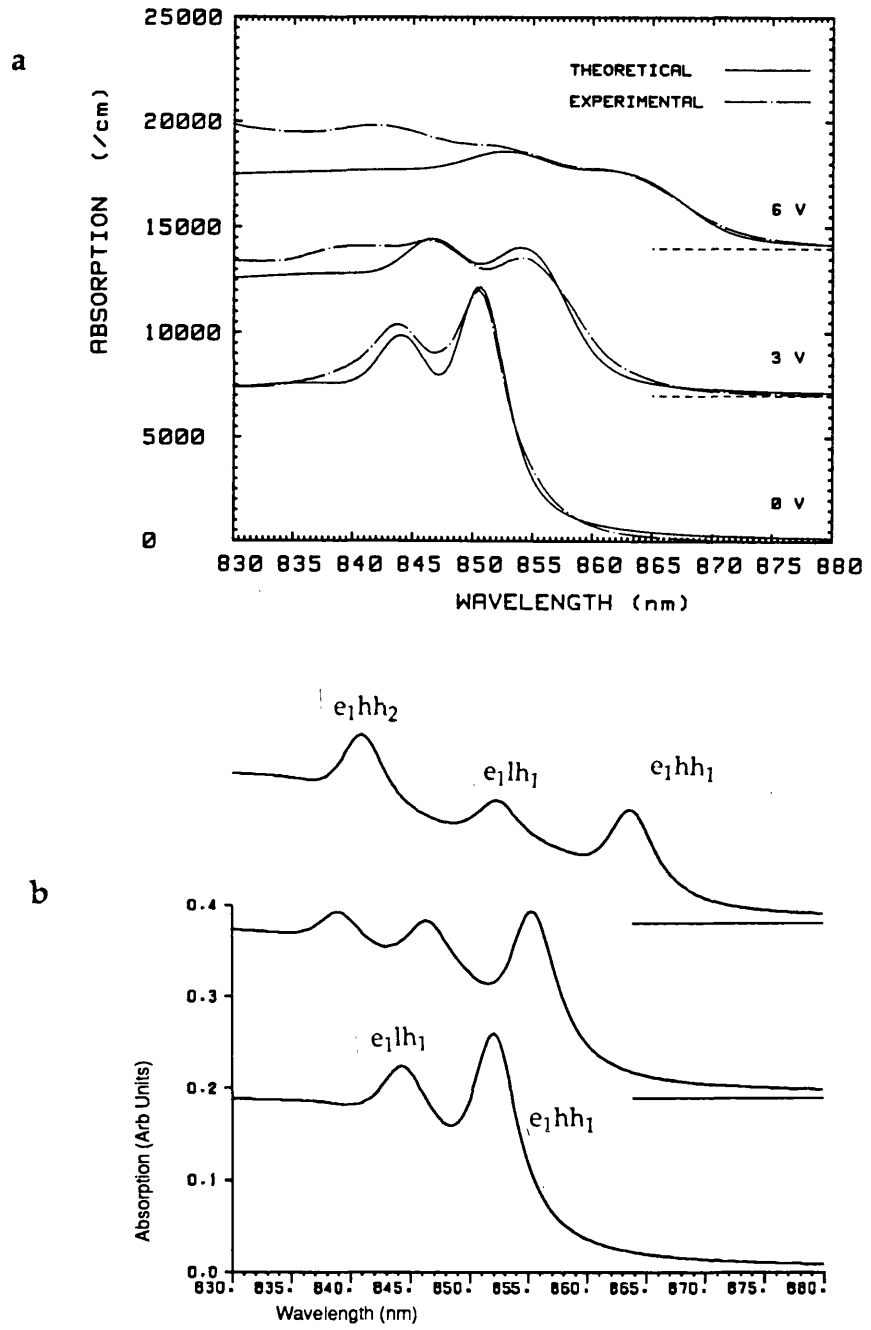

Figure 3.2a Absortion spectra reproduced from Steven's *et al* (1988) figure 10. 100Å wide GaAs wells between barriers of $Al_{0.4}Ga_{0.6}As$. Dashed curves are experimental, continuous are calculated by Stevens *et al*, they assume a 1.4V drop in the device when the theory calculates the field at the wells. Upper curves 6V, middle 3V and lower 0V.

Figure 3.2b My modelling of the structure in figure 3.2a. Data as for figure 3.2a. Electric fields used are 96kV/cm (upper curve), 48kV/cm (middle curve) and 0kV/cm (lower curve). Fields calculated from applied bias in figure 3.2a divided by the length of the intrinsic region.

a

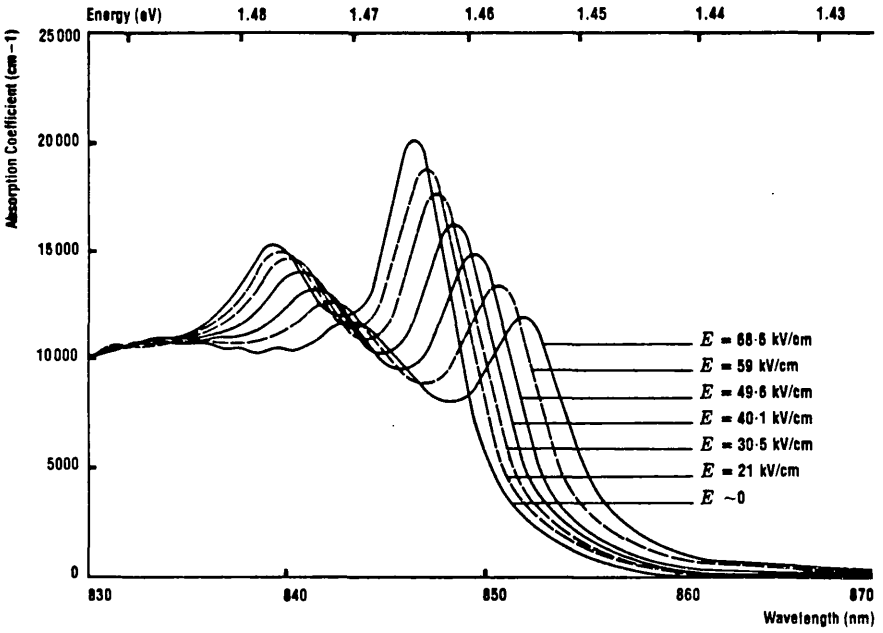

b

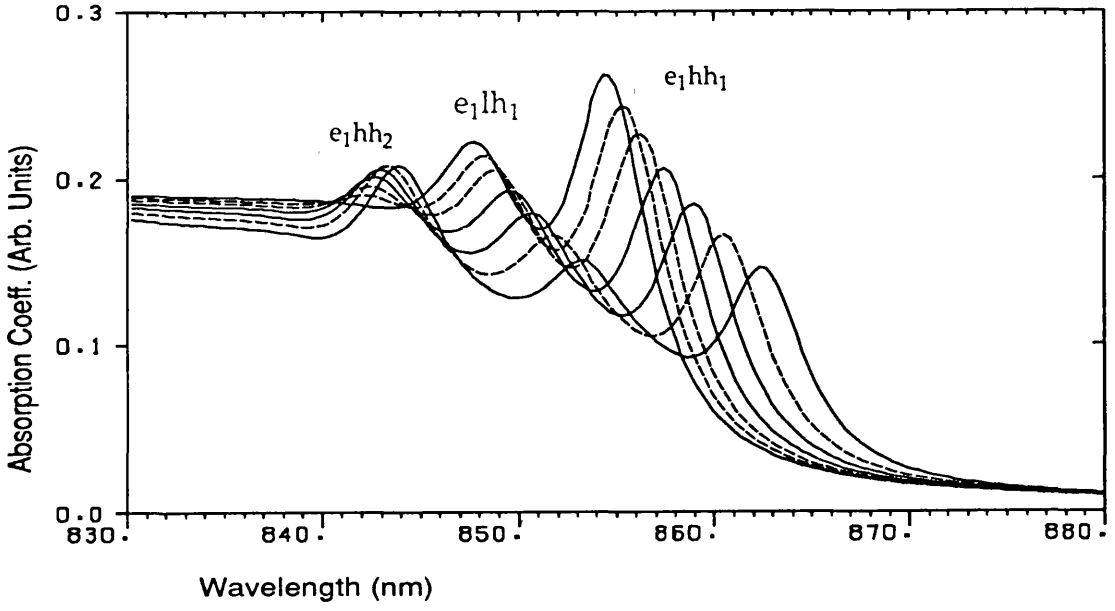

Figure 3.3a Absorption spectra reproduced from Lengyel *et al* (1990) figure 5. 105Å wide GaAs wells between barriers of $Al_{0.32}Ga_{0.68}As$.

Figure 3.3b My modelling of figure 3.3a.

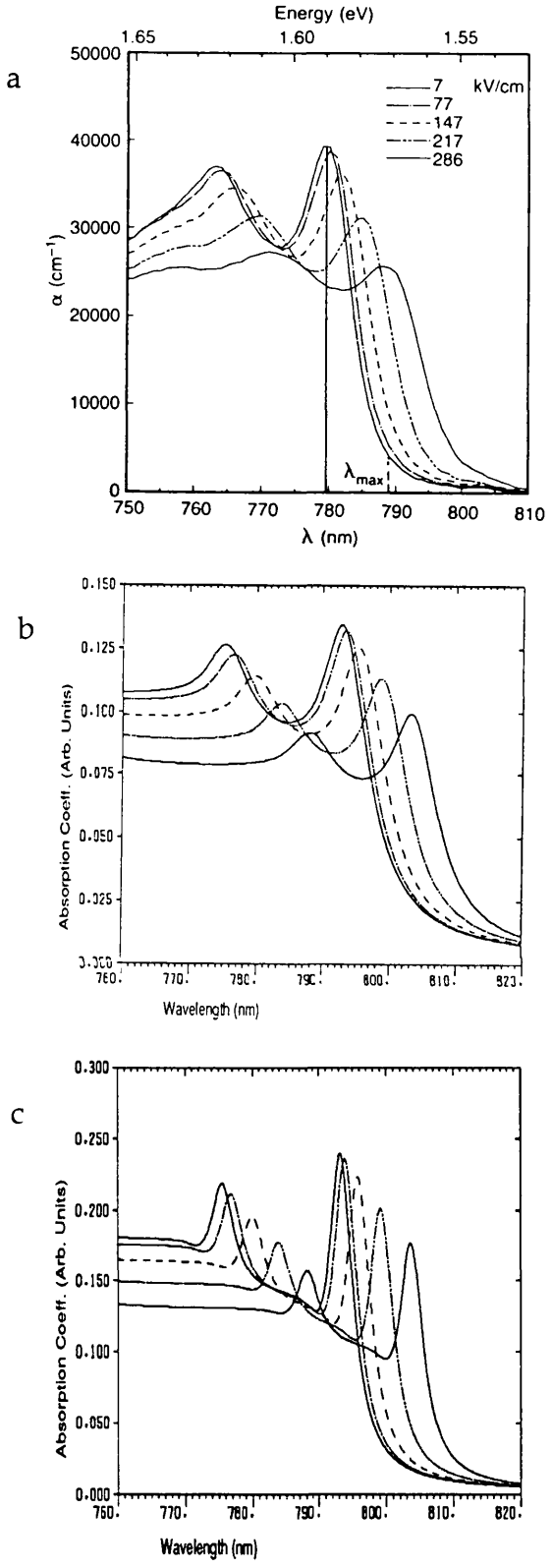

Figure 3.4a Absorption spectra reproduced from Jelley *et al* (1989) figure 1 for 35Å GaAs wells and $Al_{0.33}Ga_{0.67}As$ barriers.

Figure 3.4b My modelling of figure 3.4a assuming a ratio, r_{e-h}, of 10 and a Lorentzian FWHM of 17.0meV

Figure 3.4c As figure 3.4b but with $r_{e-h} = 6$ and a FWHM of 8.5meV, the values used for the modelling of wider wells.

with the previously used values of 8.5meV and 6 respectively. Jelley *et al* show that the Lorenztian FWHM increases rapidly for well widths below about 60Å, and the calculations for figure 3.4b use their value of 17.0 meV. The increase in ratio r_{e-h} can be justified on the grounds that the 35Å wide well is narrower than the 100Å and hence the exciton will be more two dimensional. The theoretical limits for the values of r_{e-h} are 2 in the 3D case and 16 in the 2D case, the binding energy should also increase as $r_{e-h}^{2/3}$ (Klipstein *et al* 1986), this corresponds to an increase in binding energy of about 3meV or a shift in the absorption peaks of about 5.5nm to shorter wavelengths, this is not included in the model. Figure 3.4c shows the result of keeping the ratio at 6 and the FWHM at 8.5meV for the 35Å wide well.

Turning now to coupled wells, in order to test the self-consistency of the model I compared the calculated spectra of a wide barrier CDQW with a single quantum well (SQW) of width the same as each well in the CDQW. The barrier width chosen was 70Å and the well widths 50Å . The CDQW and SQW spectra were very similar and almost identical at wavelengths around the e_1hh_1 peak and higher, both with and without field applied (doubling the single well spectra to allow for there being twice the amount of absorbing material in the double well case). The result is not quite as trivial as it may appear at first sight because there are twice as many energy levels and four times as many overlap integrals and peaks in the CDQW spectra than the SQW spectra. Also, I compared a narrow barrier (1Å) CDQW with the spectra calculated for a single well of width 100Å - twice that of one of the wells in the CDQW, again there was good agreement between double and single well calculated spectra, both with and without field applied.

These results provide confidence that the calculations of energy levels, wavefunctions, and overlap integrals are not suffering accuracy or other computer related problems.

Further credence and an insight into the model's validity is given by comparison of calculated spectra with those measured experimentally by Dingle *et al* (1975) and Debbar *et al* (1989). In both cases I used the well structure, composition and temperature quoted in their papers.

Figure 3.5 shows the spectrum calculated to correspond to Fig 1B in Dingle *et al* and this experimental data itself. (Optical density is the logarithm, base 10, of the ratio of incident light to the transmitted light. For a given thickness it is, therefore, proportional to the absorption coefficient.) The structure comprises two 50Å wells separated by a 15Å barrier, (denoted 50Å/15Å/50Å), at a temperature of 2K. The model gives a spectrum with peaks at similar energies to Dingle *et al*'s and the agreement would be improved by assuming larger well widths. The peak heights are in approximate agreement although the modelled peaks tend to be more pronounced. This discrepancy might be explained by material quality as their SQW spectra peaks (not shown here) are not as pronounced as those observed today.

More recently Debbar *et al* (1989) have measured absorption spectra at different

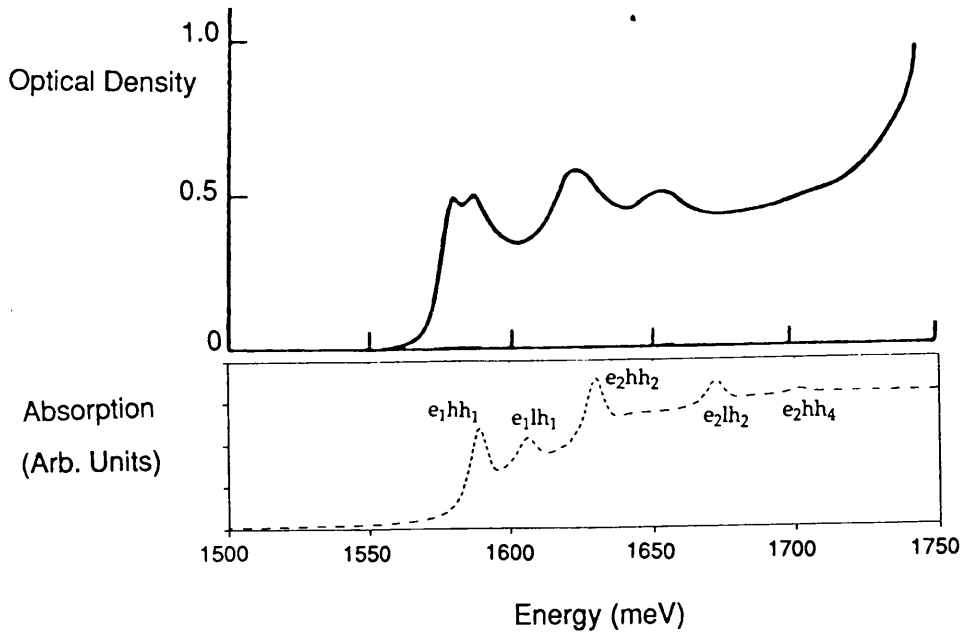

Figure 3.5 Zero-field absorption spectra for a 50Å/15Å/50Å CDQW with GaAs wells and $Al_{0.19}Ga_{0.81}As$ barriers at 2K. The upper curve is reproduced from Dingle *et al*'s figure 1b. The lower (dashed) curve is the calculated data.

applied voltages at a temperature of 10K. Figure 3.6 shows the results of calculations for the structure in their paper. The electric fields in figure 3.6 correspond approximately to the voltages at which the measurements were taken, a built in field of approximately 5 kV/cm and a Lorentzian FWHM of 3.5 meV were assumed. The model as a whole shows good agreement with experiment at wavelengths around the absorption edge - the usual region of interest for optical modulation. At higher spectral energies (approximately 1.62 eV) Debbar *et al* observe a light hole peak, my model places this at around 1.63 eV resulting in the observed discrepancy between experiment and theory. The discrepancy might result from the omission from the model of an energy dependent effective light hole mass. Watanabe *et al* and Andrews *et al* (1989) have found it necessary to use an energy dependent light hole mass in their modelling. Fortunately the light hole peak does not contribute much to the absorption spectrum at wavelengths close to the absorption edge where optical modulator devices operate.

The choice of a (fixed width) Lorentzian to model broadening, rather than say a gaussian, affects predominantly the high wavelength side of the spectrum. It is evident from figures 3.3 and 3.4 that the calculated absorption is not zero at wavelengths greater than $\approx$25nm from the e_1hh_1 exciton peak at zero field, yet the measured values are close to zero. Lorentzian lineshapes are used by many authors [eg Lee *et al* (1989) and Lengyel *et al* (1990)] because the dominant broadening mechanism is phonon broadening which applies to all carriers and is thus a homogeneous lifetime

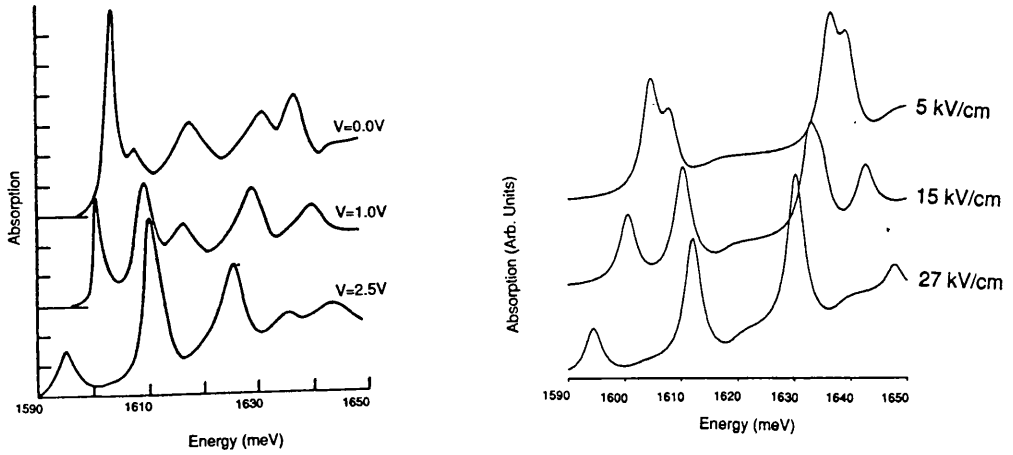

Figure 3.6 Left, measured absorption spectra, reproduced from Debbar *et al* (1989). The CDQW structure is a pair of 35Å GaAs wells coupled by a 30Å barrier of $Al_{0.2}Ga_{0.8}As$, measurements taken at 10K. Right, the calculated absorption spectrum using this structure.

effect that should be characterised by a Lorentzian lineshape. Lengyel *et al* claim this gives a good fit to their data, however, Chemla *et al* (1984) claim a guassian gives a good fit. To add to the confusion Shields *et al* reported that a gaussian lineshape gives a good fit to electroreflectance spectra at room temperature and a Lorentzian at lower temperature, the latter effect being contrary to what one would expect. Some authors convolve gaussian and Lorentzian functions to account for both homogeneous and inhomogeneous broadening effects, for example Stevens *et al* (1988) and Bailey *et al* (1989).

It should be noted that it is only in the tails of the absorption where the Lorentzian or gaussian lineshapes differ markedly and I do not use the model to make quantitative predictions in this region, nor do I consider waveguide devices where band tail absorption is important.

In conclusion, the model is good at predicting relative peak heights and shifts at wavelengths close to the absorption edge. The effects important for optical modulators, such as the absorption changes with electric field and consequent insertion loss and contrast ratio qualitatively appear to be modelled well. There is sometimes a discrepancy between the wavelengths at which absorption peaks are observed and modelled. There are sometimes discrepancies in the behaviour of absorption peaks at wavelengths sufficiently below the band edge to be of little concern for optical modulators. Field dependent broadening is sometimes observed experimentally, this could be easily added to the model by using a variable width Lorentzian, however the extent of this broadening is material dependent.

§3.2 Problems encountered in modelling.

This section briefly covers some of the practical problems and solutions encountered in the course of the computer modelling. The program in its present form is comprised of a main controlling program and a library of subroutines, all written in

FORTRAN. The more tedious, yet time consuming, problems I shall merely list here; network failures, mainframe downtime and congestion, enforced changes to the operating system and in the early days considerable inconvenience and delay obtaining hard copies of graphical output.

From a programming aspect the hardest part (and the section which now takes a significant portion of the running time) is the location of energy levels when the field is non zero. As mentioned in section 2.2 the energy levels can be as narrow as 10^{-100}meV whilst the well is hundreds of meV deep - a needle in a haystack. One can try to guess intelligently the position of the level based on its zero field energy (which is easy to compute) and the strength of the field applied . The guessing gets harder for energy levels above the groundstate where energy levels do not necessarily change in energy at the same rate as field is applied. The way around the problem is to look for the change in phase shift and apply a Breit-Wigner parameterisation as outlined in section 2.2 . This eases the problem but one has to be careful because as the FWHM (due to tunnelling) increases with field, or just due to higher energy levels being less confined. The Breit-Wigner parameterisation then becomes inaccurate and the peak in the density of states must be used. In the end I have used a 'belt and braces' approach, the entire well energy is scanned for peaks in the density of states and for Breit-Wigner resonances, the associated wavefunctions for all these energy levels are calculated and the nodal crossings within the confining structure counted. The ground state (n=1) has no nodal crossings, the next state (n=2) has one etc. Thus missing levels can be identified and a more detailed scan at greater resolution commenced to find them, and, levels found twice (due to the two methods) can be sorted out. Once located in this way another subroutine zooms in on the energy value of the level stopping when the resolution is such that the program can properly resolve the peak (not just one grid point higher than its neighbours) or the peak is so narrow that a Breit-Wigner parameterisation is valid. Although I only require absorption peak positions to an accuracy of the order of one meV it is important to find energy level positions to considerably greater accuracy because the wavefunction (and hence overlap and absorption peak height) can be very sensitive to the energy used.

A scatter plot of peak positions may be used to guess the energies of energy levels not picked up in the scan by interpolating between peaks that have been found - see figure 3.7 . The scan can then be repeated over a narrower range but with greater resolution.

Zero field calculations are much easier but in the case of a pair of identical wells separated by a wide barrier the energy levels occur in pairs, the separation between levels in a pair being small (as an example in a CDQW with 50Å GaAs wells and a 50Å $Al_{0.3}Ga_{0.7}As$ barrier the separation of the hh_1 and hh_2 energy levels is 0.07meV). If the energy assigned to a level is not sufficiently accurate the wavefunctions will not be symmetric, as they should be. In this case I count nodal crossings as before and also check that the wavefunctions are symmetric.

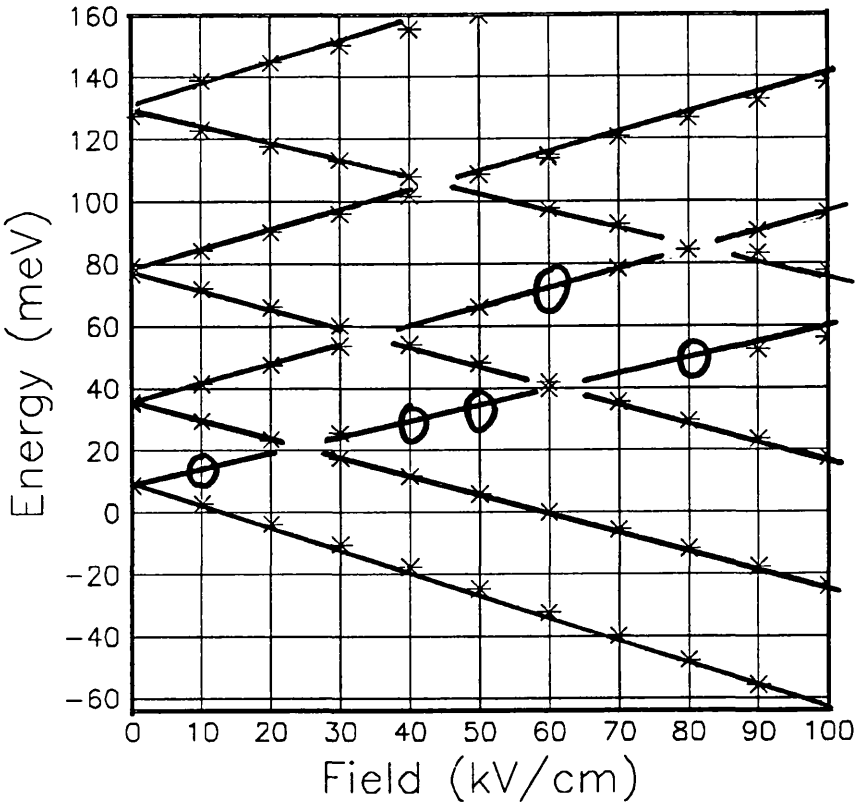

Figure 3.7 Scatter chart for heavy hole energy levels. The structure is two 90Å GaAs wells separated by a 30Å $Al_{0.3}Ga_{0.7}As$ barrier. The program has scanned the well for energy levels at each field, in 10kV/cm steps, stars mark energies at which energy levels are found. Lines linking stars are drawn by hand to show movement of energy levels, circles indicate energies where the scan has missed detecting an energy level.

Holes and electrons have opposite charge but substitution of a negative charge into the expression for y in equation (2.14) causes an error due to the attempt to find the cube root of a negative number. Inspection of Schrödinger's equation (2.1) shows that using a value of z that is the negative of its true value, yields the correct result (the qFz term remains unchanged in sign when both q and z have their signs changed) provided (a) the wavefunction is reflected afterwards, (b) a new potential $V'(z)$ is used in U such that $V'(z) = V(-z)$, and (c) the position dependent effective masses are likewise reflected.

Effective masses and potentials change as step functions at material interfaces and it is at these interfaces where the matrix matching takes place so care must be taken that machine inaccuracies do not place the z value under consideration just the wrong side of the interface.

§3.3 Applications of the model.

This section contains some of the ideas I had during the course of my work prior to the main coupled well modelling and a brief discussion about each of them.

§3.3.1 Switch from no coupling to coupling in a MQW as the barrier width is decreased. The thought behind this was the following; the wavefunctions for essentially uncoupled MQWs and for coupled wells look radically different. If one imagines decreasing the barrier widths in the initially uncoupled case, is there a rapid shift to the wells being effectively strongly coupled? The transition might be rapid because coupling is closely allied to tunnelling through the barrier which has an exponential type dependence upon barrier width. Although in a given device the barrier width is fixed, perhaps the tilting action of an electric field changes the effective barrier width, bringing on a rapid effect. It turns out that the device modelled in chapter 4 does the reverse in that wavefunctions are delocalised at zero field and become more localised as field is applied. This is discussed more fully in chapter 4 and is known as the Wannier Stark effect.

§3.3.2 Variable well widths to compensate for the built in field. This work is not directly related to coupling between wells although had the conclusions been more positive it would have had applications to coupled well systems as well as uncoupled ones.

The unintentional background doping from impurities in the i region of a p-i-n diode results in the electric field varying across the intrinsic region. The variation of field across each individual well is small but from one end of the intrinsic region to the other there can be a significant change in field. (This later turns out to be a problem in experimental measurements.) The variation of field can be found by solving Poisson's equation (Bleaney and Bleaney) :

$$\frac{d^2V_q}{dz^2} = -\frac{\rho_q}{\epsilon_r\epsilon_0} \tag{3.1}$$

where V_q is the potential due to the charges from the impurity charge density ρ_q . This leads to the following expression for the rate of change of electric field across the intrinsic region due to there being a density N_i of impurities, each with charge q:

$$\frac{dF}{dz} = \frac{qN_i}{\epsilon_r\epsilon_0} \tag{3.2}$$

For example, an intrinsic region 1μm long with a background doping of 10^{15}cm^{-3} has a variation in field of 1.4×10^{-6} V/m = 14 kV/cm (assuming a dielectric constant ϵ_r of 13).

In order to relate this change of field to the electric field within a p-i-n diode two rules apply. a) If the field is non zero, its slope with distance in either the p, i or n region is given by (3.2). b) The area under the plot of field versus distance must equal the voltage across the p-i-n regions (from equations 3.1 and 3.2). These rules will be used later, for now it is the slope of field with distance that concerns us.

For bias absorbing operation (see figure 3.8 for definition) which is the most common mode of operation for MQW devices with well widths of the order 100Å or less,

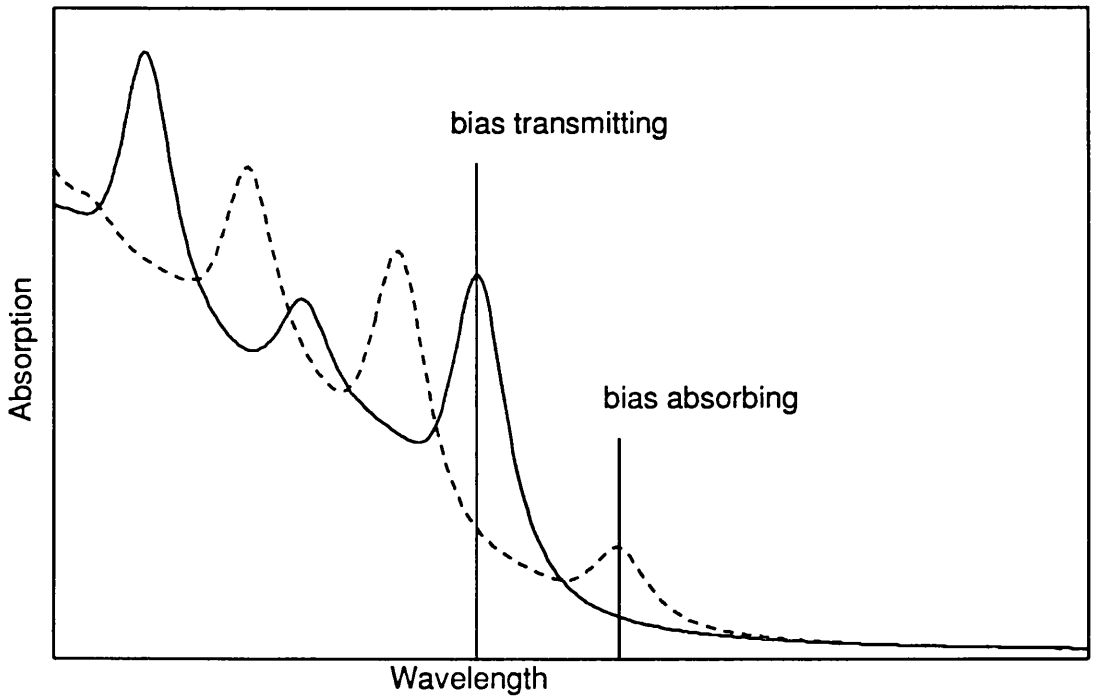

Figure 3.8 Diagram showing 'bias absorbing' and 'bias transmitting' operation. The dashed curve represents absorption with electric field (bias) applied, solid curve is for no bias.

a voltage is applied to the device and the e_1hh_1 absorption peak shifts to a longer wavelength or lower spectral energy.

The variation of electric field due to doping in the nominally intrinsic region results in a range of electric fields across the intrinsic region, and, a range of wavelengths at which the e_1hh_1 peak maximum is seen. However, as figure 3.9 shows, the position of an e_1hh_1 absorption peak depends upon well width in addition to electric field.

Hence it is theoretically possible to keep the wavelength of the e_1hh_1 absorption peak constant at different electric fields by changing the well width. The practical situations considered were MQWs with wells of $\approx$35Å and $\approx$105Å and for background doping levels of $5 \times 10^{14}cm^{-3}$ and $5 \times 10^{15}cm^{-3}$. The variations of electric field due to these doping levels in one micron of material are 7kV/cm and 70kV/cm respectively (from equation 3.2).

For the 35Å wells the operating field with bias applied is 286kV/cm in figure 3.4a. A $5 \times 10^{15}cm^{-3}$ background doping over one micron gives a field variation of 251kV/cm to 321kV/cm. Figure 3.10 shows the spectral energies of the e_1hh_1 peak for different well widths at fields of 251, 286 and 321 kV/cm. The horizontal dashed lines show the range of peak energies that would be present in a device if all wells were 35Å wide across one micron of 'intrinsic' material.

This range is $\approx$9meV, about half the FWHM (17.0meV) of the e_1hh_1 peak and so would yield some broadening. The continuous horizontal line at 1534meV is the 'ideal' operating energy, to operate at this spectral energy when the field is 251 kV/cm

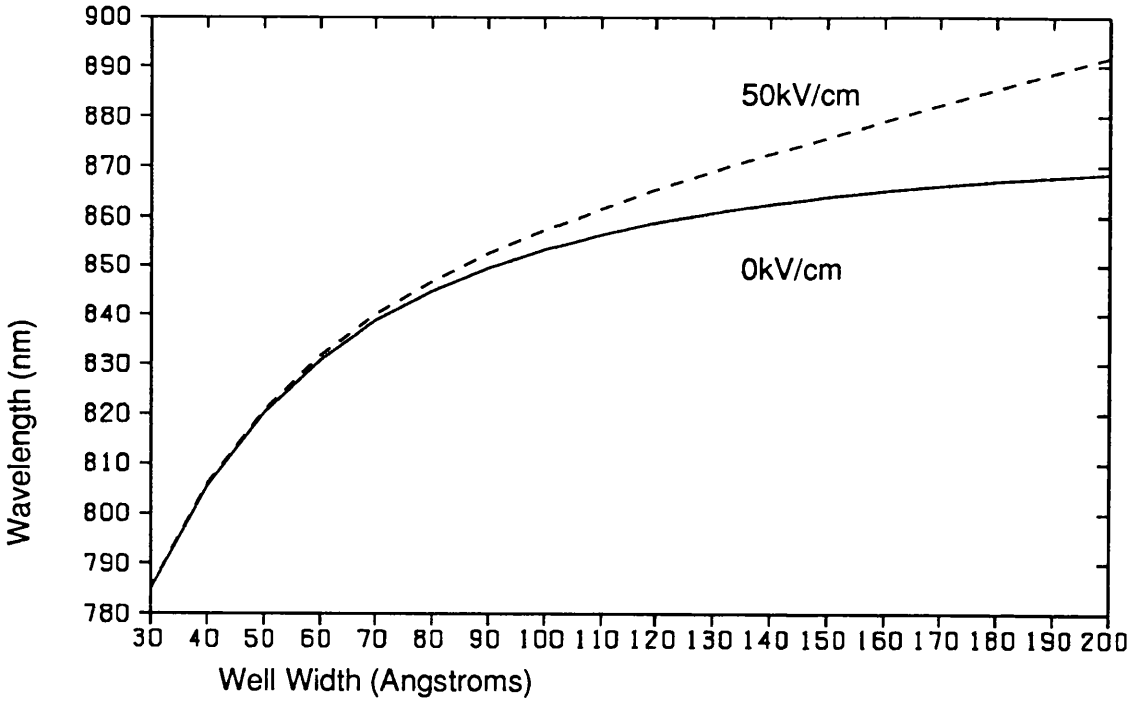

Figure 3.9 Wavelength of the e_1hh_1 absorption peak as a function of well width at 0 and 50 kV/cm. Single GaAs quantum well with $Al_{0.3}Ga_{0.7}As$ barriers.

requires a well width of ≈34Å , and of ≈36Å when the field is 321kV/cm. So, to achieve a constant peak wavelength would require a gradual variation in well width of ≈2Å from one side of the intrinsic region to the other. This is not a practical proposition as the thickness of one monolayer is 2.83Å.

In the 105Å well case figure 3.11 shows that there is a change in peak position of ≈3meV around the operating energy of 1440meV when a doping of $5 \times 10^{14}cm^{-3}$ is assumed. This could result in a small broadening of the spectral line (FWHM= 8.5meV) and in order to compensate would require a total well width change of the order a monolayer. However, for 105Å wells and a background doping of $5 \times 10^{15}cm^{-3}$ figure 3.12 shows that, uncorrected, there is a large (21meV) difference in peak position, to compensate a range of well widths in excess of 20Å is needed - a feasible range.

In conclusion, for 105Å wells a background doping of $5 \times 10^{15}cm^{-3}$ can be a real problem, but $5 \times 10^{14}cm^{-3}$ is much less so. It would be possible to offset electric field variations in the wider well situation by varying the well width across a structure. Unfortunately, this requires prior knowledge of the background doping which is not always the case as it originates from impurities. Narrower 35Å wide wells are less susceptible to field variations and this idea would not be applicable there.

§3.3.3 Superlattice and multiple quantum well at once. The differences in electron and hole effective masses result in the heavy-hole ground state being more confined than that for electrons (for example see figure 3.1). Hence it may be possible to design a structure in which the electrons are effectively strongly coupled and the heavy-holes uncoupled. I thought this might have novel properties or exhibit a cross between

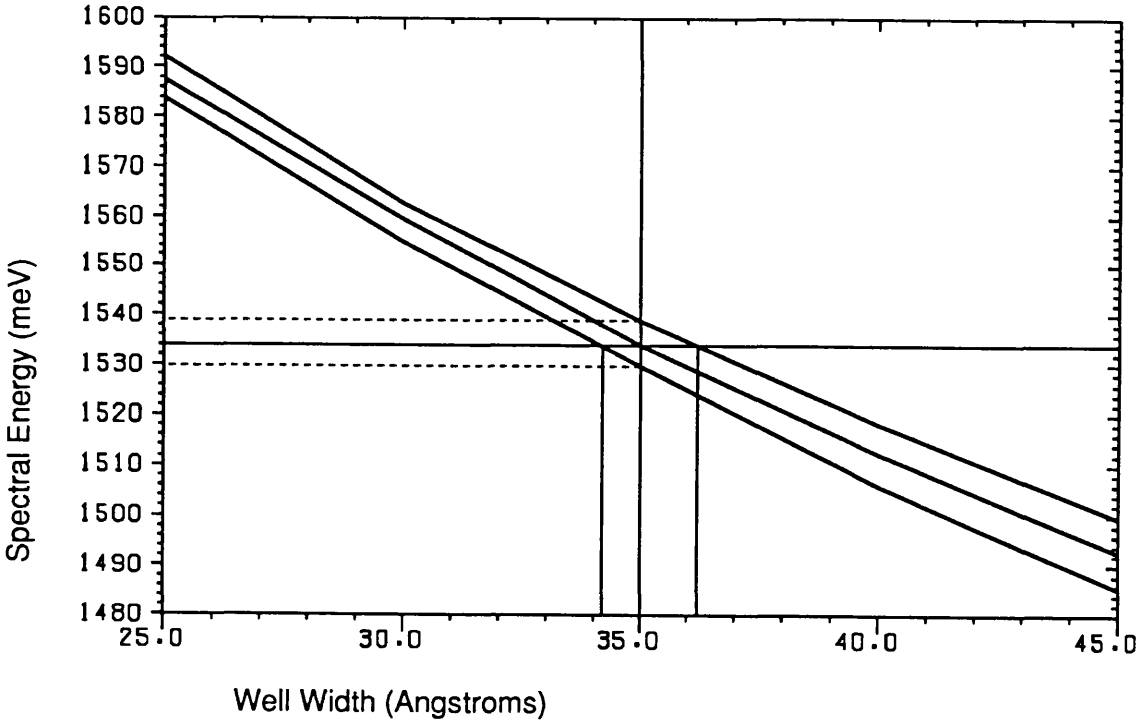

Figure 3.10 Spectral energies of the e_1hh_1 absorption peak as a function of well width for a narrow well and an intrinsic region doping of $5 \times 10^{15}cm^{-3}$. Of the three curves (not vertical or horizontal lines) upper is for a field of 251kV/cm, middle is for 286kV/cm and lower is for 321kV/cm. The long vertical and horizontal solid lines denote 'ideal' well width and spectral energy respectively. Dashed horizontal lines show range of energies over which peaks would occur if well width was fixed at 35Å due to the field variation. Short solid vertical lines show range of well widths needed to keep the e_1hh_1 peak fixed at a spectral energy of 1534meV.

superlattice and multiple quantum well behaviour. The carrier transport properties could also be interesting because the less localised electrons are probably swept out of the wells faster than the holes by an electric field. Similar arguments can be applied to wells separated by barriers that effectively isolate groundstate (n=1) energy levels but strongly couple the n=2 and higher states. In this case it would be intersubband transitions that would be of interest.

With hindsight I have never properly pursued this although my work went on to study the effects of different barrier widths on optical properties which is the first stage of following this up. I can now think of some problems for the electron superlattice, hole MQW structure; from a modulator point-of-view the confined heavy-holes would probably cause the exciton to be restricted to a region of the order of a well width, this situation is very similar to an ordinary MQW. The possible faster transport of electrons than heavy-holes might leave the heavy-holes in the wells, charge could accumulate and the potential due to the wells would be distorted. This may lead to a worsening of modulator performance, or, interesting non-linear effects.

Since I originally had these thoughts I have become aware of a few papers related

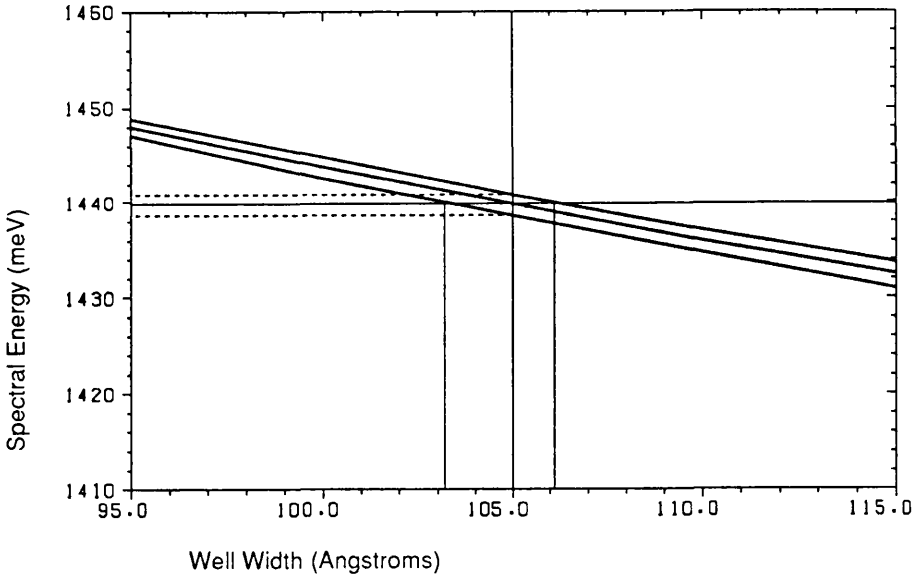

Figure 3.11 Spectral energies of e_1hh_1 peak as a function of well width for a wide well and a doping of $5 \times 10^{14}cm^{-3}$. Electric fields are 56.5kV/cm (top curve), 60kV/cm (middle curve) and 63.5kV/cm (bottom curve). Dashed horizontal lines show range of spectral energies over which peaks would be seen if the well width was fixed at 105Å. Range of well widths needed to compensate for field variation is shown by shorter vertical lines.

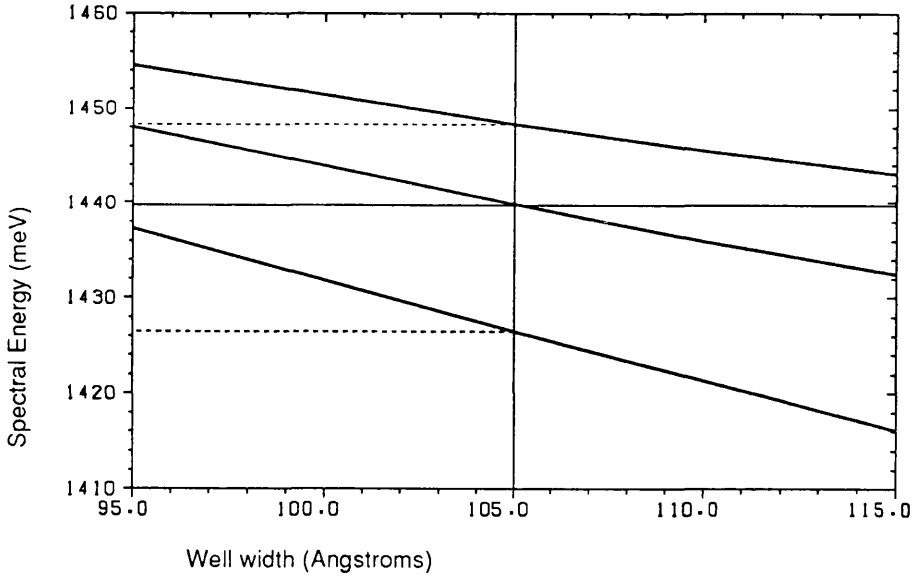

Figure 3.12 Spectral energies of e_1hh_1 peak as a function of well width for a wide well and a doping of $5 \times 10^{15}cm^{-3}$. Electric fields are 25kV/cm (top curve), 60kV/cm (middle curve) and 95kV/cm (bottom curve). Dashed horizontal lines show range of spectral energies over which peaks would be seen if the well width was fixed at 105Å. Range of well widths needed to compensate for field variation is greater than that shown here.

to these effects. Lang *et al* observed the 'trapped' heavy holes by using a capacitance-voltage measurement in an InGaAs/InP superlattice at temperatures below 100K. Capasso *et al* report large photocurrent amplification in an $Al_{0.48}In_{0.52}As/Ga_{0.47}In_{0.53}As$ superlattice, an effect they attribute to 'effective mass filtering' due to the different tunnelling rates of electrons and holes. Sauer *et al* demonstrate from photoluminescence measurements the different electron and hole tunnelling times in asymmetric coupled quantum wells of $In_{0.53}Ga_{0.47}As/InP$. The photoinduced space-charge build up is excitation dependent and they discuss the possibility of achieving optical bistability. However, I am unaware of any study of these effects upon electro-optic modulators.

§3.3.4 Energy level repulsion. In my early evaluations of the positions of energy levels in double coupled well structures I noticed that the energy levels of a given carrier repel each other if they come close in energy (see figure 3.13) and that the repulsion is greater when the coupling between wells is greater. This is closely analogous to the mixing of states seen in atomic spectroscopy (for example figure 8.6 in Woodgate). When translated into a plot of spectral peak positions against field, the repulsion manifests itself as what I now know are called "anti-crossings". At the time I hoped to exploit the enhanced shift of the e_1hh_2 exciton at the turn around point for the following reasons.

From figure 3.13 one can see that the energy separation between the e_1 and hh_1 energy levels rapidly decreases, at the same time their wavefunction overlap integral falls; consequently the e_1hh_1 absorption peak moves rapidly to high wavelengths and falls rapidly in height with applied field.

For fields below 15kV/cm in this structure the energy separation of e_1 and hh_2 changes little, both these levels are decreasing in energy with applied field. At the turn around of the hh_2 energy level the e_1hh_2 spectral energy rapidly decreases (for fields greater than $\approx$40kV/cm). It was this feature that created my interest in the avoided crossings - with the e_1hh_1 peak disappearing quickly it is possibly of no use for bias absorbing modulation, perhaps the turn around of hh_2 could be used to move the e_1hh_2 peak's wavelength and thus give bias absorbing modulation.

Energy level repulsions and anti-crossings are often observed in experimental data in the literature for example Golub *et al* (1988), Salvador *et al* (1990), and also in modelling work, for example, Yuh P-F *et al* (October 1988) and Fox *et al* (1990) but have received little attention with optical modulators specifically in mind. In chapter 6 I will model a structure that exhibits an anti-crossing behaviour.

§3.4 Future directions

In this chapter I have demonstrated the use of the model for a range of structures. The model was used to evaluate the possibility of using graded well widths to overcome the problem associated with impurity dopants. The conclusions were that this was unlikely to be of practical use. This latter idea had not previously been reported. Other ideas all require a more detailed study of the coupling between wells and the

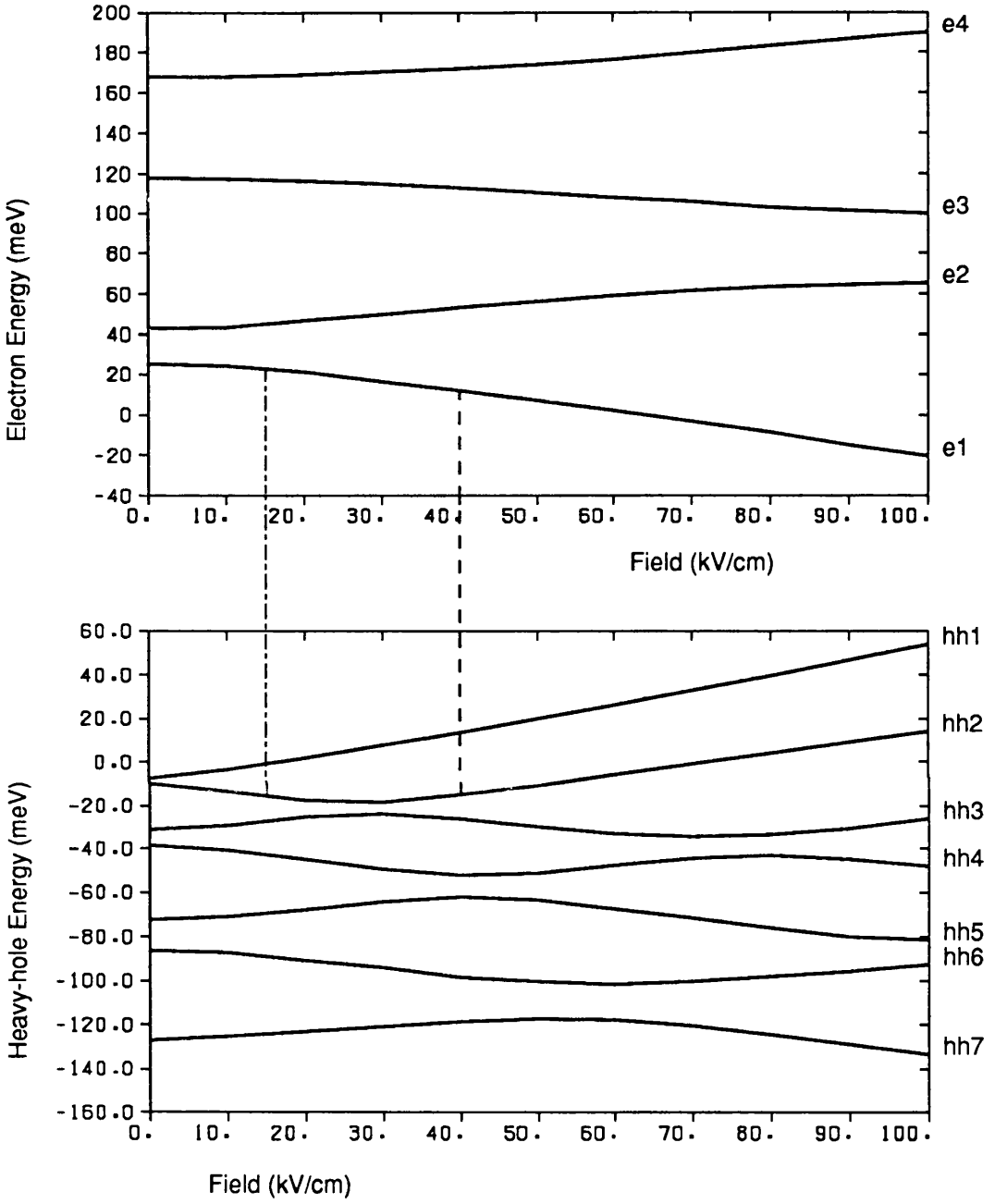

Figure 3.13 Energy level repulsions. Graphs show calculated changes of energy levels with field for two 90Å GaAs wells coupled by a 10Å $Al_{0.3}Ga_{0.7}As$ barrier. Dot dash vertical line denotes e_1hh_2 spectral energy at 15kV/cm, a field less than the turn around of the hh_2 level. Dash-dash vertical line denotes e_1hh_2 spectral energy at fields where this energy changes rapidly with field. Zeroes of energy refer to potential energy at the bottom of quantum wells at zero field, energies increase in the same sense as increasing electron potential energy. (Slight jagged appearance is a consequence of limited number of data points.)

most basic coupled structure upon which to start this investigation is a pair of identical wells - this forms the basis of chapter 4.

Chapter 4 Coupled Well Devices

§4.1 Introduction

In §3.1 I stated that there was a small difference between absorption spectra calculated for two 50Å wells with a 1Å barrier between them and a 100Å wide single quantum well (this was used as a consistency check of the model). The coupling barrier width of 1Å was not the first one chosen, initially I used a barrier of width 5Å but found that even this narrow a barrier caused significant coupling effects to be observed see figure 4.1 .

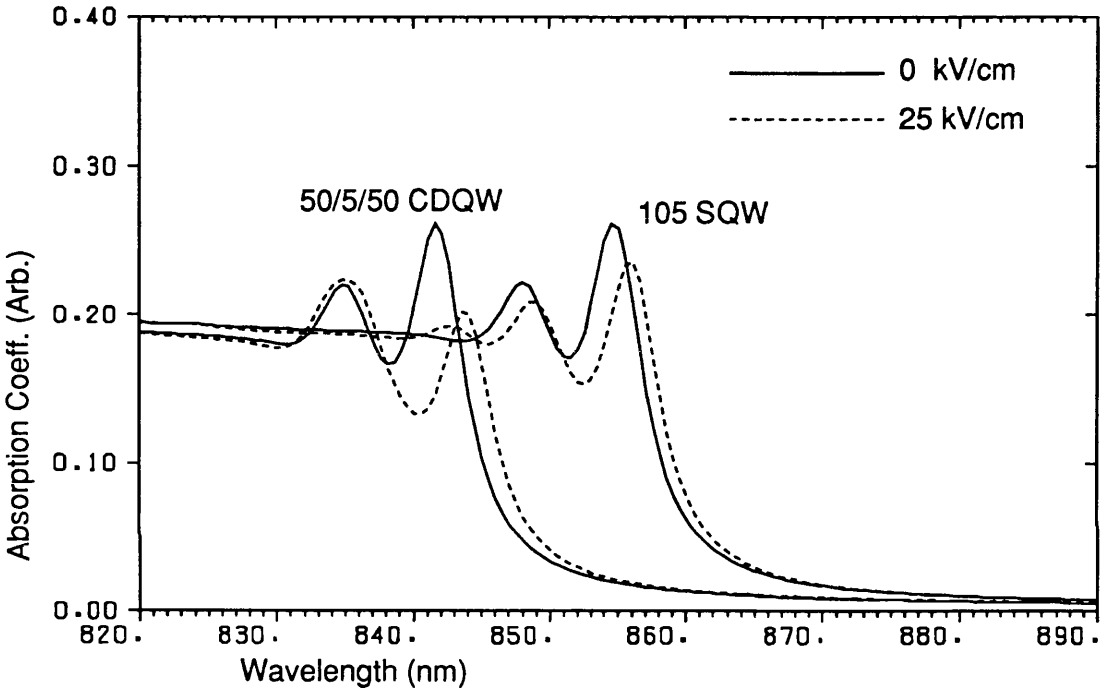

Figure 4.1 Absorption spectra calculated for a single 105Å wide well and for a coupled well pair, each well being 50Å wide and separated by a barrier of only 5Å . (Well material is GaAs, barrier $Al_{0.3}Ga_{0.7}As$.)

Because one monolayer has a width of 2.83Å and the definition of a single monolayer is unclear when one is dealing with an alloy material (AlGaAs), the assumption that a ≈5Å barrier would be practically very hard to grow inspired further work into barriers wider than this. (However, it is interesting to note that since I started my work Onose *et al* have reported results in 1989 on coupled double quantum wells with AlAs barriers of 5.7Å). The work in chapter 3, mentioned above, shows that narrow barriers can have significant effects upon electro-absorption for small electric field changes. At this time (Summer 1988) there were results in the literature demonstrating related aspects of the physics of coupled well pairs and these are summarised below.

Dingle *et al* (1974) measured the optical density from pairs of coupled wells and showed for the first time that coupling does take place in semiconductor quantum wells - see figure 3.5. Their work was for zero field only.

Kawai *et al* (1985) observed the change of wavelength of the e_1hh_1 exciton peak with changing barrier $Al_{0.5}Ga_{0.5}As$ widths in the range 12 to 40Å between 30Å GaAs wells. The measurements were performed using photoluminescence at zero electric field and room temperature.

Chen *et al* (1987) measured low temperature exciton energies using a variety of techniques - photoluminescence (PL), photoluminescence excitation (PLE) and photocurrent spectroscopies. (The application of the first two of these experimental methods to the measurement of quantum well parameters is reviewed in Orton *et al* (1987); photocurrent is a measure of the number of photogenerated carrier pairs at a given applied electric field and is closely related to absorption, see §4.6.3 for more details.) Chen *et al*'s measurements demonstrated the effects of electric fields on the carrier energy levels and they state that coupling can enhance the quantum confined Stark effect over that of a single quantum well. They also infer carrier localisations from lifetime measurements, this is explored by them and other authors in Charbonneau *et al* (1988). These measurements all provided considerable evidence that the energy levels and wavefunctions behaved as expected. Both these authors report agreement with the theoretical work of Austin *et al* (1986) on carrier lifetimes and localisations in coupled wells.

Le *et al* (1987) presented photoluminescence excitation data from a sample at 2K containing an asymmetric pair of wells, one having a width of 105Å and the other 85Å , separated by a 20Å barrier. The movement of peaks with bias shows quite good agreement with their numerical calculation of peak energies with field.

Independently of Chen *et al* and Le *et al*, Islam *et al* published room temperature electroabsorption results in 1987 on a structure consisting of two pairs of 46Å GaAs wells coupled by 11.5Å $Al_{0.3}Ga_{0.7}As$ barriers. They reported a 14:1 modulator operating with a change in bias of 3.5V, this was a waveguide device working in the polarization for which the electric field vector is perpendicular to the quantum well layers (ie the polarization unobtainable in transmission - see figure 1.2). They also showed electroabsorption data for the parallel polarisation. The shifts of lower energy absorption peaks and their changes in heights behave as they predict from a tunnelling resonance calculation but there is evidence that light and heavy hole mixing is occurring at higher energies.

Andrews *et al* published in 1988 the photoluminescence excitation spectra from two 48Å GaAs wells separated by a 16Å $Al_{0.3}Ga_{0.7}As$ barrier at 5K. Again rapid changes in the positions of peaks are seen for small electric fields ($\approx$50kV/cm).

Most of the authors cited above provide calculations of energy levels and often wavefunction overlaps as well. All these results provide useful confirmation of the physics of CDQWs, however their application to optical modulators receives less attention. There had been no modelling of the coupled-well-pair absorption spectrum that included excitonic effects and forbidden transitions. There was little explanation of why the authors chose the particular structure except Islam *et al* who chose the coupled

quantum well (CQW) structure giving a large absorption change (in the perpendicular polarization), this is an important aspect of modulator performance. The work in this chapter considers how best to exploit the low electric field performance of coupled wells to produce an electrooptic modulator showing reasonable modulation for small electric field changes at room temperature. Particular attention is paid to the barrier coupling the wells and growth fluctuations receive attention. Photocurrent spectra are presented showing clearly that at room temperature reasonable optical modulation should be achievable at low electric fields in the transmission mode of operation.

§4.2 Coupled double quantum wells vs superlattices

Prior to discussing the thicknesses of the coupling barrier, the reason for choosing coupled double quantum wells rather than a greater number of coupled wells is explained. Quantum well electro-optic modulators benefit from large changes in absorption and this is normally achieved by exploiting the excitonic nature of quantum well absorption. As indicated in chapter 1, to benefit from exciton absorption the carriers should be confined to distances of the order of 100Å, this is less than the bulk Bohr diameter of ≈300Å. For a suitably designed superlattice at zero field the carrier wavefunctions may theoretically be spread over many wells and many hundreds of angstroms ie 'delocalised' and the carriers would not be constrained to distances less than the bulk Bohr diameter, consequently there may be little excitonic absorption. By modelling coupled well pairs and not many wells all coupled together I was able to restrict carrier confinement to lengths of around 100Å in order that the excitonic features should be usable for optical modulation.

It occurred to me that there might also be the possibility of achieving good modulation by using a superlattice between zero field and an applied field. When an electric field is applied, Wannier-Stark localisation of the wavefunction takes place (observed by Mendez *et al* 1988) in which the carriers effectively localise on individual wells. This is the so-called 'Stark ladder' and can be seen in the heavy-hole wavefunctions of figure 3.1. At zero field the four heavy-hole wavefunctions are spread over the four wells, with 10kV/cm applied each wavefunction localises on a different well in a 'ladder' formation. Hence with field applied the carriers may be constrained to lengths the order of a well width and the excitonic absorption should be recovered. I thought this had potential as a bias absorbing optical modulator because absorption goes from a low to high value as the wavefunctions change from bulk like to multiple quantum well like with electric field. I did not pursue this because unfortunately the carrier wavefunctions at zero field are only delocalised (ie bulk like) if all the wells are of very similar width and depth. Fluctuations in well width or barrier alloy composition can cause carriers to localise on a particular well or group of wells, this will enhance excitonic absorption at zero field and the advantages mentioned above may be lost.

There has been some modelling of this localisation in the literature, Littleton *et al* (1986) considered a 10 period superlattice in the InGaAsP/InP system and showed that variations of well width of ≈5% cause little significant shift of energy levels but

cause carriers to localise strongly around the wider well. The effects of this have been observed experimentally by Moore *et al* (1990) in the InGaAs/GaAs system and by Pavesi *et al* (1989) in a deliberately disordered GaAs/AlGaAs superlattice. The 'problem' can be lessened by increasing carrier coupling by using narrower and/or lower barriers and/or narrower wells (R. Lang *et al*). Nevertheless I decided to focus on coupled double quantum wells of total width less than the bulk Bohr diameter so that I could be sure of keeping excitonic features and not be too reliant on good quality growth and be restricted to strong coupling.

It is pertinent to note that Law *et al* (1990) have recently demonstrated a high contrast (greater than 60:1) asymmetric Fabry-Perot reflection modulator using Wannier-Stark localization in a 100 period 30Å GaAs/30Å $Al_{0.3}Ga_{0.7}As$ superlattice. Their device relies upon the blue shift associated with Wannier- Stark localisation to decrease absorption with field rather than the idea discussed above. (The zero field energy levels of a superlattice form a miniband of energies, approximately centred on the energy level of one of the wells if it were isolated, thus the superlattice band gap is smaller than that of the isolated quantum well. When field is applied the coupling is 'turned off', Wannier-Stark localisation takes place, the miniband is lost resulting in an increase in the band gap ie a blue shift. This was investigated and demonstrated by Bleuse *et al* (Jan 1988 and Dec 1988) and Mendez *et al* (1988).)

§4.3 Choosing the barrier width for bias transmitting operation

§4.3.1 Discussion

Having decided initially upon coupled double quantum wells to retain the benefits of excitonic absorption how wide should the coupling barrier between the wells be for a structure to give good optical modulation for low drive voltages?

Firstly consider bias transmitting operation as defined in figure 3.8. With no field across the wells the device is strongly absorbing at the wavelength of the e_1hh_1 exciton peak (the operating wavelength). To achieve good modulation at this wavelength this peak must shift away rapidly in wavelength and/or decrease rapidly in height as field is applied. It is also necessary that no other absorption peaks move to this wavelength or increase rapidly in height in close proximity to this wavelength.

The effective mass of the electrons is lower than that of the heavy-holes by a factor of about 5, consequently the electrons are less confined and the separation in energy of e_1 and e_2 is greater than that of hh_1 and hh_2. Hence the features in the absorption spectrum close to the absorption edge are transitions from the lower hole states to e_1 states (Other transitions e.g. e_2hh_1 and e_2hh_2 occur at higher photon energies.) The absorption spectrum calculations in this thesis include all transitions for accuracy but in this discussion I focus on e_1hh_1 and e_1hh_2.

Figure 4.2 shows schematically the variation of e_1, hh_1 and hh_2 zero field energy levels with barrier width (and also how the energy levels tend to those of single quantum wells in the limit of very wide and very narrow barriers). The main point here is that

the narrower the barrier the greater the separation of hh_1 and hh_2 in energy and that as I will show, this is desirable.

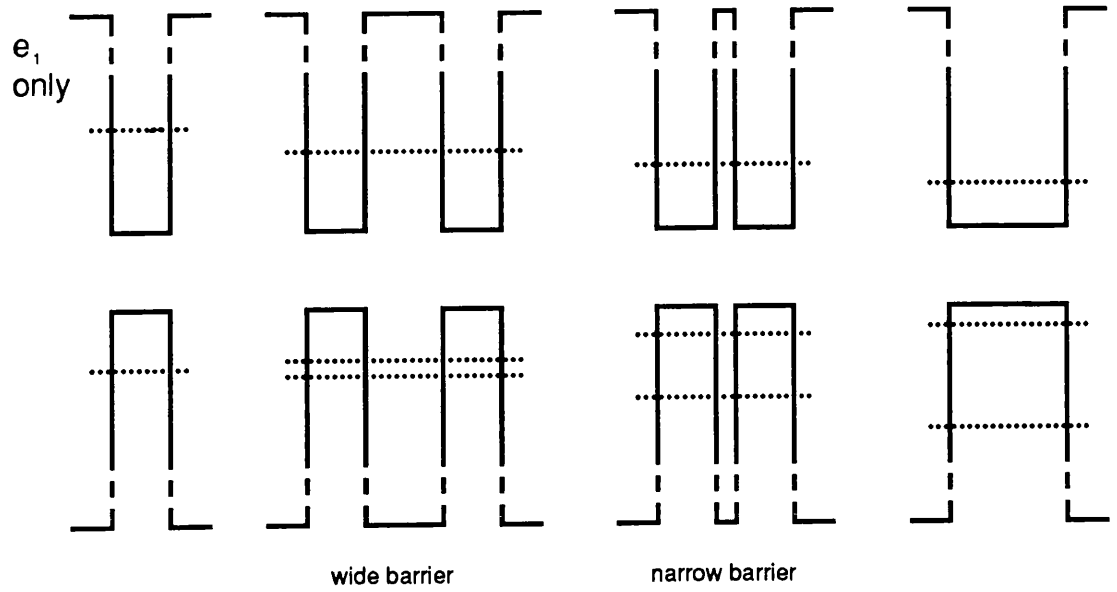

Figure 4.2 Schematic representation of the energies of the e_1, hh_1 and hh_2 levels at zero field in four structures. All wells have the same width except the rightmost one which is double the width of the others. Note how as the barrier is widened the hh_1 to hh_2 separation decreases and the energy levels tend to that of the isolated well.

Figure 4.3 depicts the behaviour of e_1, hh_1 and hh_2 wavefunctions when an electric field is applied. Note that with field applied to the coupled wells (figure 4.3 d) there is considerable localisation of all these wavefunctions.

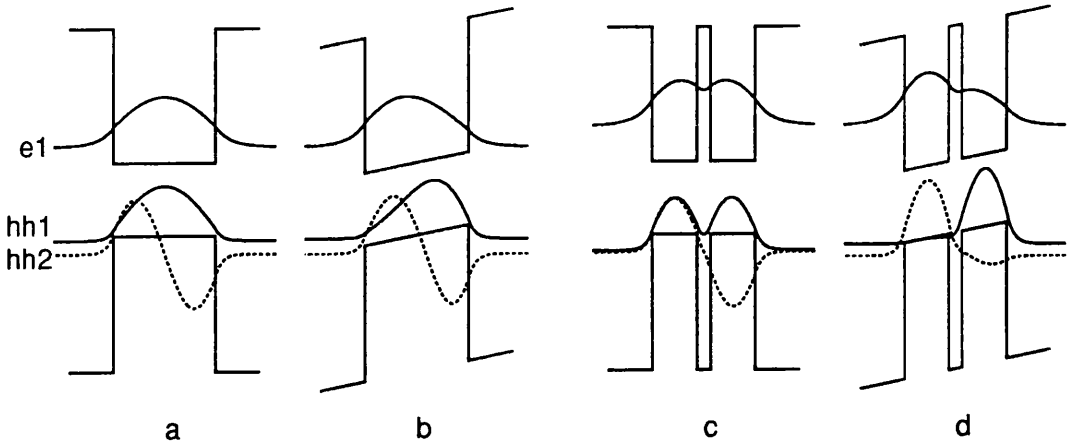

Figure 4.3 Wavefuctions overlaid upon the potential profile for: (a) a 115Å SQW at zero field, (b) at 25kV/cm, (c) a pair of 50Å wells separated by a 15Å barrier at zero field, and (d) at 25kV/cm. The zero of wavefunction is placed at the position of the corresponding energy level. Note the more rapid localisation of wavefunctions and larger changes in the hh_1 and hh_2 energy levels for coupled wells with the same field.

The wavefunctions become 'pinned' to one well (see figure 4.4) and to a first

approximation their energies change with field as the potential energy of the bottom of that well changes with field. The wider the barrier the greater the decrease in energy separation between e_1 and hh_1 as the applied field changes from zero to a given value; this is because these levels are pinned to opposite corners of the structure. So a wide barrier gives a large shift in wavelength of the e_1hh_1 peak, furthermore, the wider the barrier the greater the spatial separation of e_1 and hh_1 wavefunctions when field is applied and the quicker the overlap decreases and absorption peak height falls. Both this large wavelength shift and loss in peak height are desirable. However, the e_1 and hh_2 wavefunctions become localised in the same well as field is applied initially and hence the wavelength of the e_1hh_2 peak changes little at these low fields but their overlap integral increases so the corresponding absorption peak increases in height at a roughly constant wavelength. The wider the barrier, the closer this wavelength is to the operating wavelength.

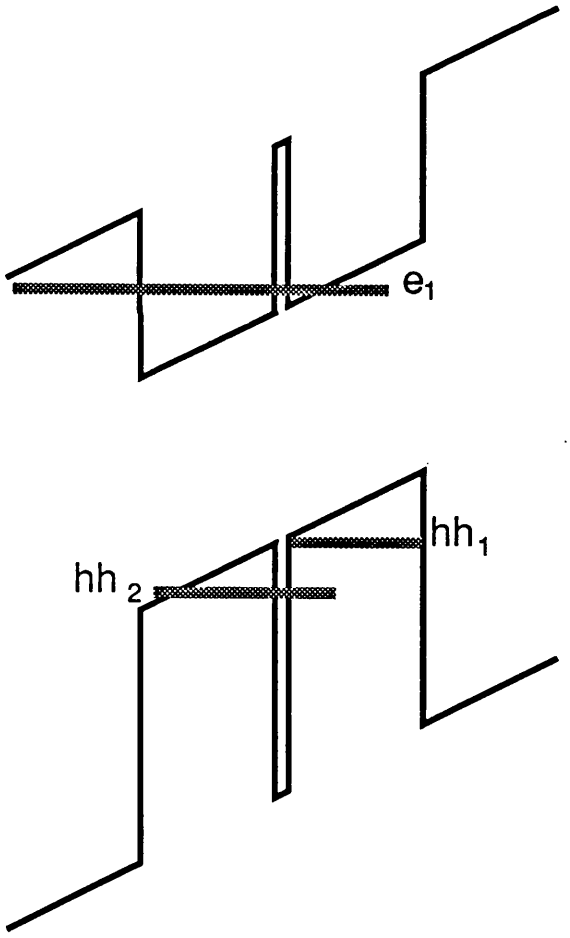

Figure 4.4 Schematic representation of energy levels and their localisations in a coupled quantum well with field applied

To summarise, the narrower the barrier the greater is the e_1hh_1 and e_1hh_2 peak separation, but, the wider the barrier the better the electric field performance. Hence

there must exist an optimum barrier width, the optimum being dependent upon operating wavelength, well widths, widths of absorption peaks and the electric field performance acceptable.

§4.3.2 Determination of barrier width

To determine a good barrier width I chose to study two 50Å GaAs wells separated by an $Al_{0.3}Ga_{0.7}As$ barrier. The aluminium concentration of 30% was used because this concentration had been established to be reliable in devices grown previously by the III-V group at the SERC central facility in Sheffield University. The well width of 50Å ensured that the total confining length was approximately 100Å, as discussed in section 4.2 .

The FWHM of the Lorentzians used in calculating absorption peaks at room temperature in the model is 8.5meV, because each Lorentzian is multiplied by its corresponding electron-hole overlap integral, which lies between 0 and 1, the apparent FWHM may be less than 8.5meV. (When considering absorption spectra it is useful to remember that at ≈830nm an energy difference of 8.5meV is equivalent to a wavelength difference of ≈15.5nm). Consequently I would like the e_1hh_2 peak to rise with field at a spectral energy different from the e_1hh_1 zero field spectral energy by about 4meV (≈7nm) to achieve a change in absorption coefficient of about 50% .

At the same time I require the e_1hh_1 peak to have shifted to a higher wavelength, in practice this results in a trough between the e_1hh_2 and e_1hh_1 peaks at an applied field and the trick is to choose the barrier width to place this trough at the same wavelength as the e_1hh_1 exciton at zero field.

Plots of absorption peak position against field for various barrier widths are shown in figure 4.5. The vertical lines denote operating wavelength, the horizontal lines denote a field of 25kV/cm. For the 5Å barrier structure the e_1hh_1 peak is too close to the operating wavelength, for the 25Å barrier structure the e_1hh_2 peak is too close to the operating wavelength. In trying to pick the structure for which the trough between the e_1hh_1 and e_1hh_2 peaks is at the operating wavelength I chose the 15Å barrier because the operating wavelength is best centred between the e_1hh_1 and e_1hh_2 peaks. This is only an estimate of the best structure because the exact location of the trough will depend upon relative peak heights as well as each peak's separation in wavelength from the operating wavelength. It would appear from the figures that for barrier widths in the range 10 to 20 Å the operating wavelength is fairly well centred between e_1hh_1 and e_1hh_2. This is encouraging because if growth calibrations are inaccurate and the barriers grown are consistently slightly less or greater than the 15Å the device should still work, although at a different wavelength. Furthermore, over this range of barrier widths the e_1hh_2 peak moves away from the operating wavelength for electric fields from 25kV/cm to at least 50kV/cm, implying that the good modulation is achievable for a range of electric fields.

§4.4 Absorption spectra

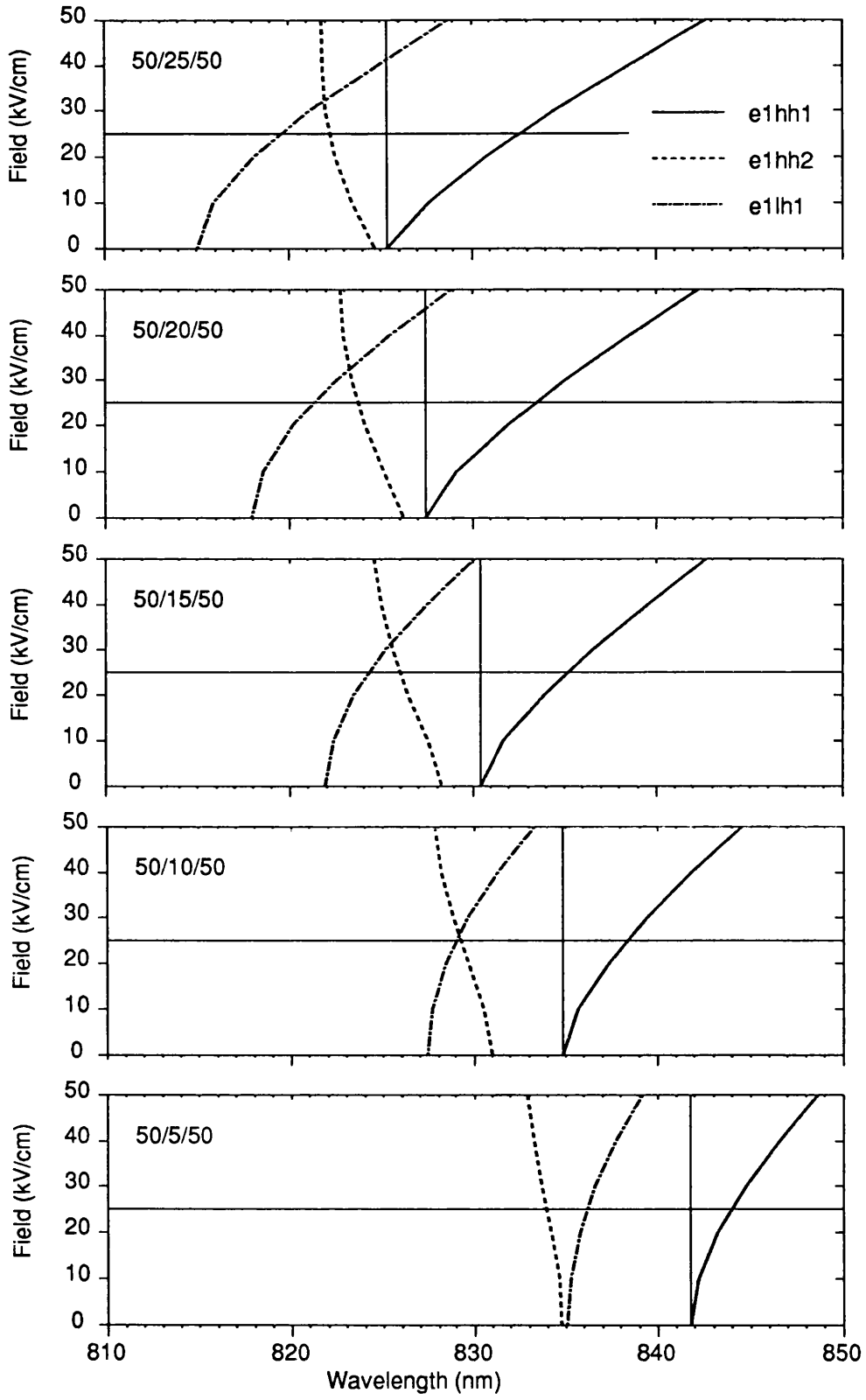

Figure 4.5 Variation of absorption peak wavelengths with field for 5 different barrier widths. Solid horizontal lines denote 25kV/cm, vertical lines denote operating wavelengths.

The modelled spectra for the 15Å barrier structure are shown in figure 4.6. Bias transmitting modulation occurs at ≈831nm , the magnitude of which is similar for both 25kV/cm and 40kV/cm electric fields. The trough in absorption at 25kV/cm occurs as predicted close to the e_1hh_1 zero field exciton wavelength of ≈831nm. For comparison, the modelled spectra of a 115Å SQW and a 50Å SQW are included in figures 4.7 and 4.8 . In all cases room temperature is assumed, the wells are GaAs and the barriers are $Al_{0.3}Ga_{0.7}As$. The 115Å SQW spectra were evaluated because a 115Å SQW contains approximately the same amount of absorbing material as the CDQW.

A similar on/off ratio is obtained in the CDQW at 25kV/cm as opposed to the 115Å SQW operating at 40kV/cm. The absorption data presented here are in arbitrary units linearly proportional to absorption coefficient measured in cm^{-1} which is also proportional to intensity absorption in dB. Because there is a similar amount of absorbing material in the CDQW and the 115Å SQW it was expected that the absorption scales would be similar in these two cases. Hence devices based on these CDQWs should be capable of operating at a lower drive voltage than those based on SQWs at room temperature. For comparison a zero and 40kV/cm spectrum are shown in figure 4.8 for a 50Å SQW. In this case the field is too small to cause much useful shift of the absorption spectrum.

§4.4.1 Broadening of absorption spectra due to growth fluctuations.

Growth of quantum well layers is not perfect in the sense that the layers are not always atomically flat. The narrow coupling barrier of 15Å is both the smallest feature in the structure and very important in determining the electro-absorption features because it controls the coupling between wells. For these reasons, the effect of fluctuations in growth upon the width of the barrier is expected to be the most significant.

If the barrier width fluctuates rapidly in the plane of the layer (the x-y plane) on a scale smaller than the exciton diameter then the exciton will see an average barrier width. Fluctuations extending over the size of an exciton or greater can be viewed as regions in the x-y plane where the barrier width is different, the effective barrier width experienced by the excitons depends upon their size, the size of the fluctuation and the temperature. Temperature and related thermalisation effects change the effective well width seen by excitons in quantum wells [eg Orton *et al* (1987)] and one expects similar arguments to apply to barrier widths.

To obtain a qualitative feel for the effect of barrier width variation I averaged the spectra from three CDQWs with barriers of 13.58Å, 15Å and 16.42Å, see figure 4.9. This range gives a total fluctuation of one monolayer (2.83Å) in the coupling barrier width and is intended to represent the situation where excitons in different coupled well pairs experience different average barrier thicknesses, the total range being one monolayer. Similarly I averaged spectra for CDQWs with barriers of 12Å, 15Å and 18Å, see figure 4.10 (the slight lumpiness of the zero field spectrum in figure 4.10 is due to averaging only three peaks).

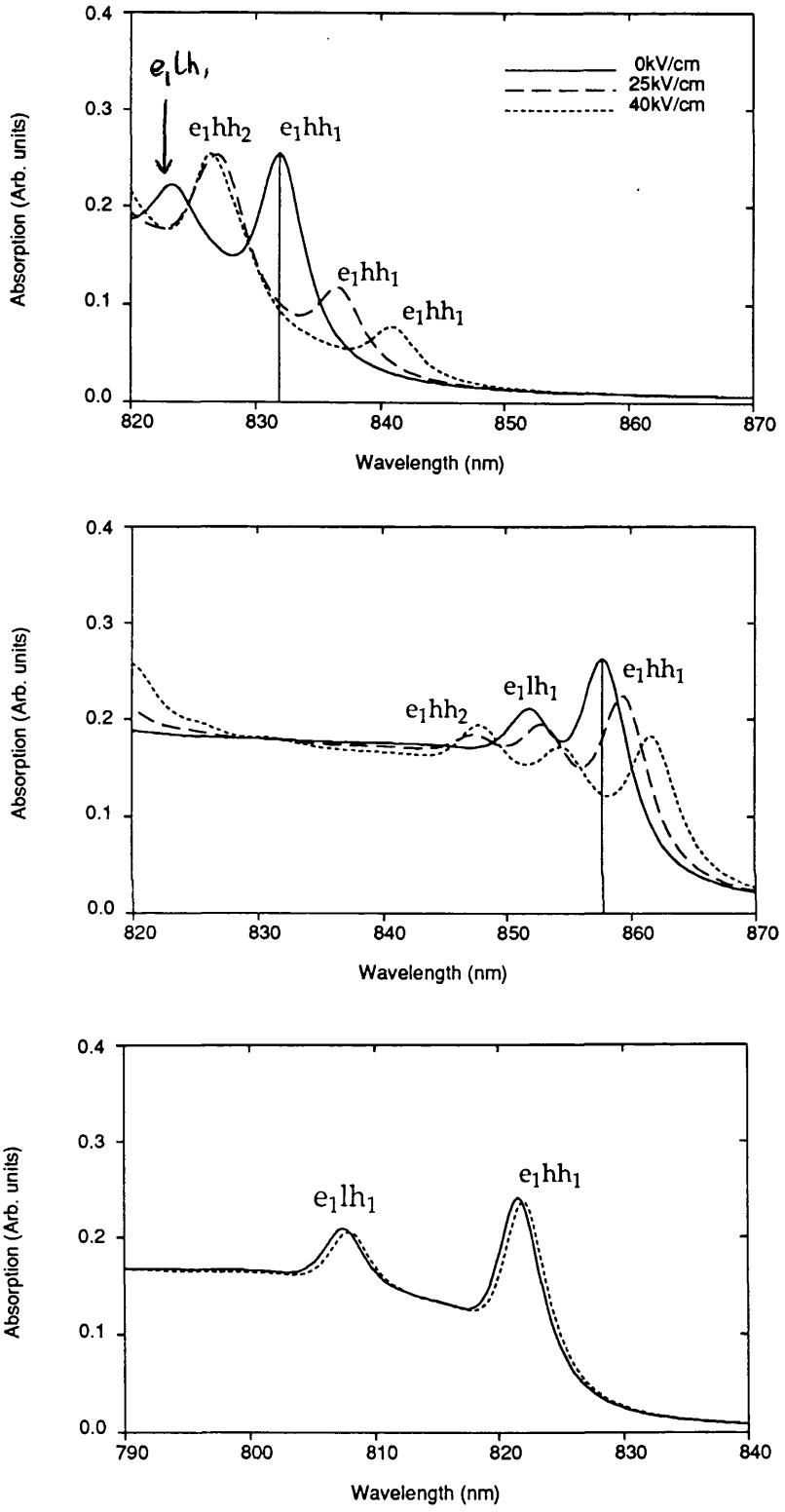

Figure 4.6 (top) showing calculated electroabsorption for two 50Å GaAs wells coupled by a 15Å $Al_{0.3}Ga_{0.7}As$ barrier at room temperature. The vertical line denotes the wavelength for 'bias transmitting' operation. **Figure 4.7** (middle) as figure 4.6 but a 115Å SQW. **Figure 4.8** (lower) as figure 4.6 but a 50Å SQW.

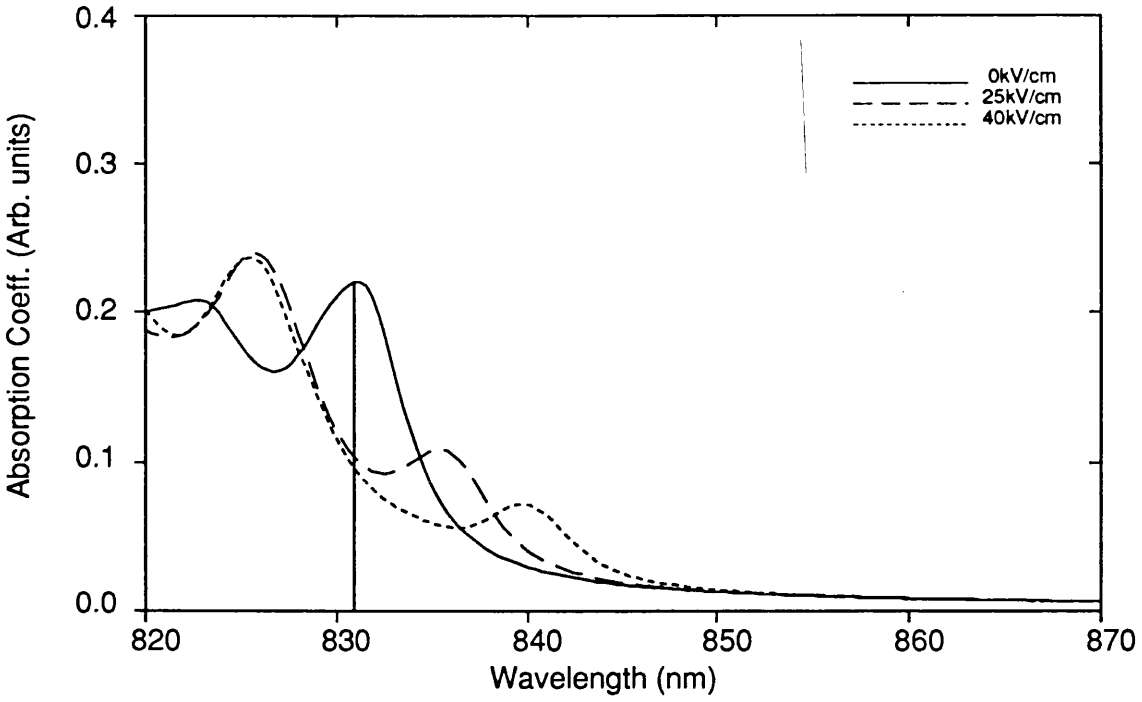

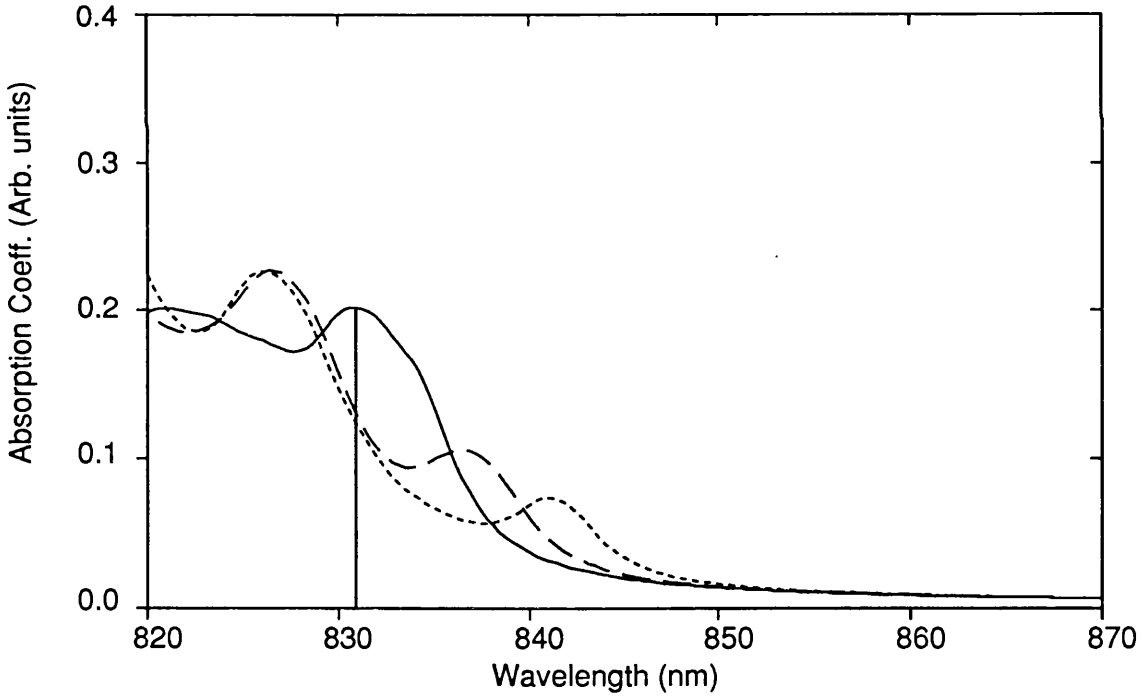

Figures 4.9 (upper) and 4.10 (lower). The average spectra for three CDQWs, all with 50Å wells and the same electric fields as figure 4.6. In figure 4.9 the barriers are 13.58Å, 15Å and 16.42Å representing a fluctuation of one monolayer, in figure 4.10 the barrier widths are 12Å, 15Å and 18Å. The vertical lines denote the wavelengths for reflection modulator calculations.

Figure 4.9 was encouraging as the spectra retained their general features although a worsening of the modulation can be seen. In figure 4.6 the ratio of absorption when the device is unbiased and biased is 2.5, in figure 4.9 it is 2.15. As the barrier width variation increases in figure 4.10 the modulation worsens again, the ratio above now being 1.54. This work showed that although growth fluctuations might decrease the amount of modulation observed, they need not render the device useless.

§4.5 Bias absorbing operation

Coupled double quantum wells offer more rapid movement of the e_1hh_1 peak with field than a SQW, as can be seen from figures 4.6 and 4.7, and as has been demonstrated in the literature (see §4.1). In the bias absorbing mode of operation, modulation normally takes place at a wavelength in the zero field absorption tail, with bias the e_1hh_1 peak shifts to this wavelength and absorption increases giving modulation. The wider the coupling barrier the more rapid is the shift in wavelength of this peak but the greater is its loss in height. In order to design a structure for an optical modulator device the minimum acceptable modulation and field performance must be known, and then the relevant barrier width can be chosen from a consideration of the variation of overlap integral or peak wavelength with barrier width.

Quantitative predictions of modulation are difficult to make from the model because of the inaccurate Lorentzian tail (§3.1). Furthermore, one of the applications of these electroabsorption effects is in an asymmetric Fabry Perot reflection modulator (AFPM) [Whitehead *et al* (July 1989), Yan *et al* (1989)], this forms the basis of chapter 5, in these devices the product αd of absorption coefficient and length of absorber, is important. The product αd can reach a given value either by choosing a large α (bias transmitting) and less absorbing material, or, a smaller α (bias absorbing) and a greater d. The disadvantage of the latter is that a larger d requires more absorbing material ie more wells, which increases the length of the intrinsic region and hence the voltage which must be applied to achieve a given change in electric field. The larger d increases the likelihood of greater broadening due to variations of electric field across the wells and growth non-uniformities within the well/barrier region. An AFPM operating in bias transmitting mode has recently been reported by Whitehead *et al* (1990), using a MQW with 150Å wide wells this exploits the larger value of α to give an AFPM with a lower operating voltage (3.5V swing vs the more normal 9V). Bias transmitting mode has two further advantages, a) it is compatible with SEED devices and b) the operating wavelength is similar to that of readily available, commercial semiconductor lasers.

For these reasons and the reasonable modulation in figure 4.6 I concentrated on bias transmitting operation.

§4.6 Experimental Results

§4.6.1 Growth and processing

To test the modelling above two structures were grown [by Dr John Roberts and

Chris Button] at Sheffield University, in an MOVPE reactor and the wafers processed [by A. Rivers and A. Stride , University College London] into p-i-n diode mesa structures to allow photocurrent measurements to be taken (see figure 1.3).

The MOVPE growth technique is summarised here, more details of the work at Sheffield can be found in Roberts *et al* (1984) and Roberts *et al* (1988), a review of MOVPE growth is given in Stringfellow (1985) with more recent reviews appearing in Stradling and Klipstien. The essential feature is that gases which are compounds of Al, Ga and As enter a chamber and react chemically after being heated in the region around the substrate. The reactions result in the formation of GaAs or AlGaAs and this is deposited epitaxially on the substrate. Control of the gas flows gives control of the chemical compostion of the layer deposited and its thickness (through varying the time for epitaxial growth). In this case the arsenic originates from arsine (AsH_3), the gallium from trimethylgallium (TMG) and aluminium from trimethylaluminium (TMA). Intentional doping is achieved by introducing silane to give an n-type region or dimethylzinc to give a p-type region. The background doping in the intrinsic region is p-type.

A typical layer design is shown in figure 4.11.

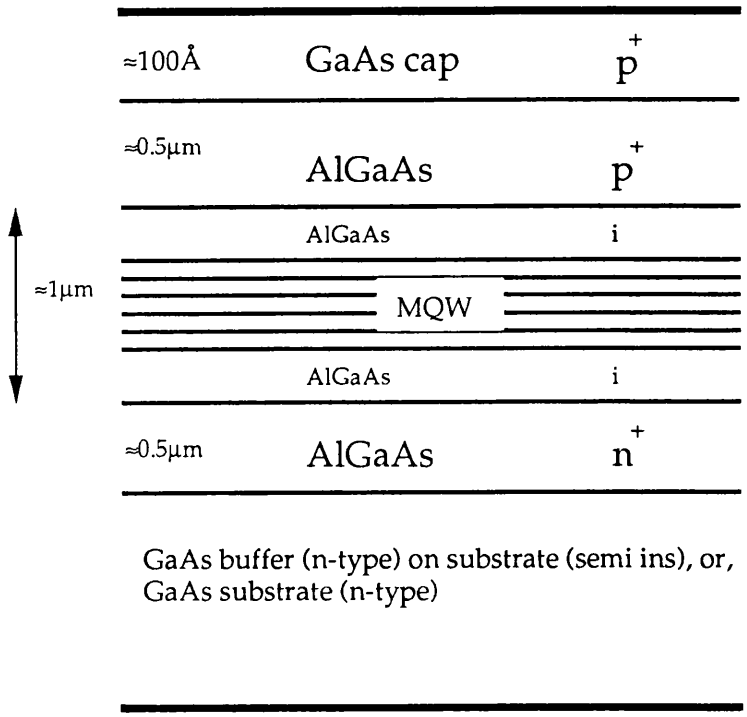

Figure 4.11 Sketch of a typical layer structure (not to scale).

The GaAs substrate provides mechanical support for the quantum wells. Substrates are available that can be either n-type or semi-insulating. On top of the substrate a doped gallium arsenide buffer layer is grown, this is used for contacting and smooths roughness originating from the substrate surface. Then a doped layer of AlGaAs is deposited, on top of this an undoped AlGaAs layer may be grown to prevent

carrier diffusion from the highly doped region into the quantum wells above. Similarly above the quantum wells there may be another undoped AlGaAs region between the doped layer and the quantum wells. The upper AlGaAs layer is doped and capped with a layer of GaAs which is similarly doped. The purpose of the GaAs cap is to provide a material for contacting. Oxidation of AlGaAs makes successful contacting to it difficult so GaAs is used. It is important to note that 'bulk' GaAs is absorbing at wavelengths less than ≈870nm (ie absorbing at the quantum well operating wavelengths) and so the GaAs capping layer must either be thin or etched away in processing to allow light to reach the quantum wells. Bulk AlGaAs is absorbing at wavelengths below the operating wavelength (for $Al_{0.3}Ga_{0.7}As$ absorption occurs below ≈690nm).

The layer structure in figure 4.11 is then processed to produce a mesa structure, sketched in figure 4.12, the purpose of the mesa being to provide electrical isolation.

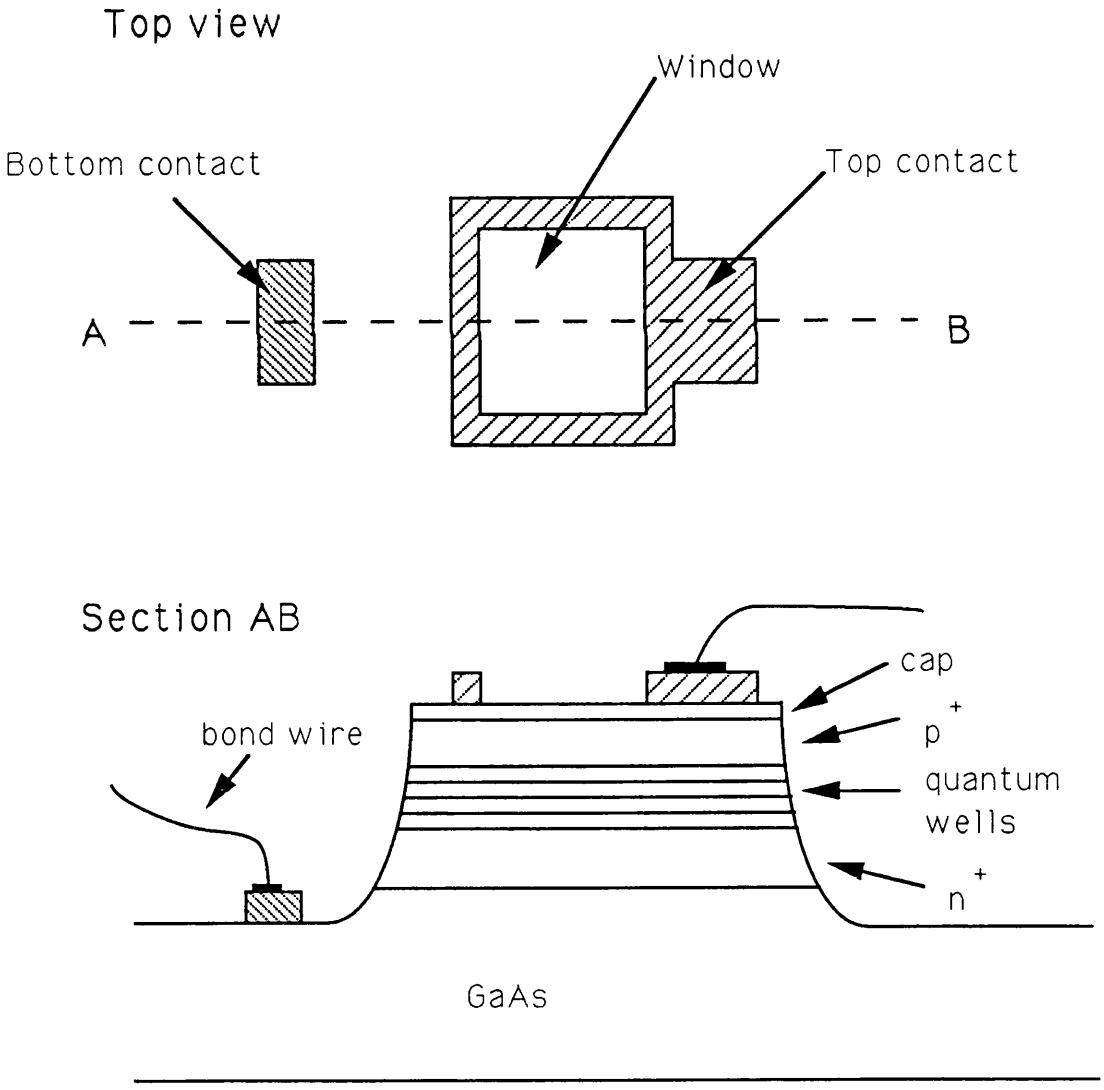

Figure 4.12 Schematic view of the mesa structure used for photocurrent measurements.

In summary, the device processing involves laying down the Cr:Au top p^+ contact, etching away a window in the p^+ GaAs cap if necessary, then etching the mesa and finally laying down the Sn:Au contact. The Cr:Au contacts are composed of a thin layer of chrome followed by a thicker layer of gold. After alloying the chrome adheres to the p-type material and the gold gives a good electrical contact. Similarly for the Sn:Au n-type contact. The contact patterning and protection of parts of the device during etching of other parts is achieved using photoresists. Mesas are tested for electrical breakdown and dark current, and the good devices are mounted on a TO5 header and bond wires attached.

§4.6.2 Experimental apparatus

§4.6.2.1 Photocurrent

Photocurrent measurements were taken using a grating monochromator. The light source was a current stabilised 100W quartz halogen lamp, the output from which passes directly through a rotating wheel chopper and then into the monochromator. At the exit to the monochromator a filter removes second order light before the beam is focussed onto the mesa of the device. The linewidth of the light falling on the device is $\approx$0.6nm [Mark Whitehead thesis].

The device is biased and the photocurrent determined by measuring the voltage across a 100kΩ resistor placed in series with the device. A lock-in amplifier is used, the chopper providing the reference signal. Computer control of the monochromator's wavelength and the bias voltage and acquisition of the lock-in output allows photocurrent spectra at various biases to be taken fairly easily.

§4.6.2.2 Doping profile

A computer controlled 'LCZ' meter was used to acquire capacitance-voltage measurements [measurements taken by A. Rivers, software written by C. Tombling]. A DC reverse bias is applied to the device and the LCZ meter superimposes a 1MHz AC signal, from the out of phase current the capacitance is calculated. The change in capacitance with reverse bias can then be used to determine the doping profile [see Blood *et al* (1978) and Blood (1986) for reviews of this technique].

§4.6.3 Photocurrent and absorption

Photocurrent measurements are used here as a means of measuring absorption coefficient. The equation relating the photocurrent and absorption is given below; from Whitehead *et al* (Feb 1988)

$$I(V,\lambda) = P(\lambda)(1-R_f)(\lambda e/hc)\eta(V).\{1-\exp[-\alpha(V,\lambda)d]\} \qquad (4.1)$$

where I is the photocurrent, V is the bias voltage, λ is the wavelength, $P(\lambda)$ is the optical power falling on the device, R_f is the front surface reflectivity, e is the electronic charge, h is Planck's constant, c is the velocity of light, $\eta(V)$ is the diode quantum efficiency, α is the absorption coefficient of the absorbing material and d is the thickness of absorbing material. In all the photocurrent measurements in this

thesis the quantum wells remain on the GaAs substrate, Fabry Perot effects can thus be neglected and the front reflectivity R_f assumed to be constant with wavelength. The diode quantum efficiency $\eta(V)$ is the fraction of photo generated carriers which reach the contacts and contribute to the measured photocurrent.

The equation above can thus be simplified :

$$I(V,\lambda) = \text{constant} \times \lambda\eta(V).\{1 - \exp[-\alpha(V,\lambda)d]\} \tag{4.2}$$

where the photocurrent I is now normalised to the power spectrum of the light source. Hence for $\alpha(V,\lambda)d < 1$ and over a short range of wavelengths, and with spectra scaled to allow for the variation of $\eta(V)$,

$$I(V,\lambda) = \text{constant} \times \alpha(V,\lambda)d \tag{4.3}$$

ie the photocurrent is proportional to the absorption coefficient α.

§4.6.4 Experimental Results

The first of the two structures ordered had a well/barrier structure of 50 pairs of coupled wells, each pair separated by an 85Å barrier of $Al_{0.3}Ga_{0.7}As$. The coupled wells were two 50Å GaAs wells separated by a coupling barrier of 15Å of $Al_{0.3}Ga_{0.7}As$. The 85Å barrier separating each pair was assumed to be wide enough to prevent coupling between coupled quantum well pairs. The second sample acted as a control, this was the same structure but with each coupled well pair replaced by a 115Å well of GaAs. Thus the intention was to be able to make the direct comparison between figures 4.6 and 4.7.

The first sample ordered (CB191) gave the photocurrent data in figure 4.13 , that of the control sample (CB194) gave the photocurrent data in figure 4.14. The data in these figures is NOT scaled to compensate for the different efficiencies of photogenerated carriers escaping from the quantum wells at different electric fields. This has the effect of giving spectra at low biases an 'artificially' low absorption coefficient if equation (4.3) is used.

In each case the e_1hh_1 exciton peak at 0V is observed close to the modelled wavelength, however the clarity of the features is poor, especially as bias is applied to the devices. Room temperature photocurrent measurements on multiple quantum wells with (uncoupled) wells of width ≈100Å are fairly common [for example Whitehead *et al* (Feb 1988)] and comparison with the data here is poor in that there is very little shift of the exciton peak, just a loss of peak height. Because the results for the control are poor it is not surprising that the CQW results are also poor. (Mark Whitehead also had a sample grown at the same time (CB190) and this also exhibited poor characteristics, other diodes from these wafers showed similar behaviour). The cause of this was attributed to a high background doping in the 'intrinsic' region. The arsine source had been contaminated with impurities [C.Button private communication]. From C-V measurements the doping in CB191 and CB194 was calculated to be $\approx 10^{16}\text{cm}^{-3}$. The

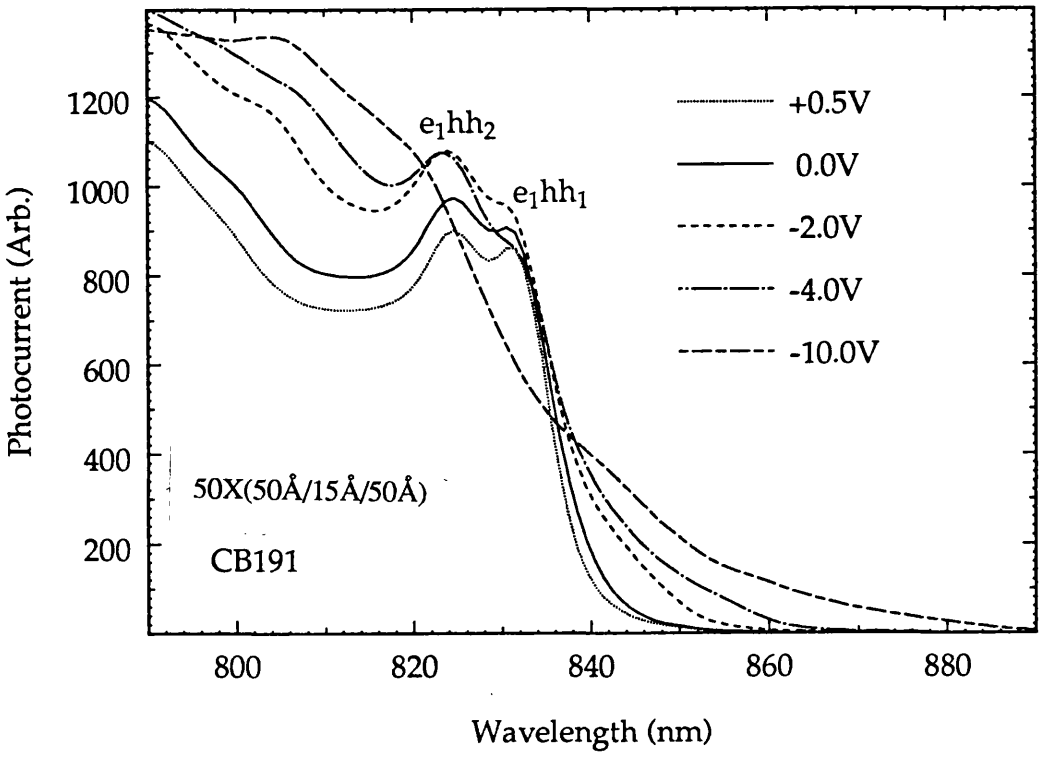

Figure 4.13 Photocurrent from CB191, a p-i-n diode containing CDQWs. Key shows the reverse bias (negative voltage) applied.

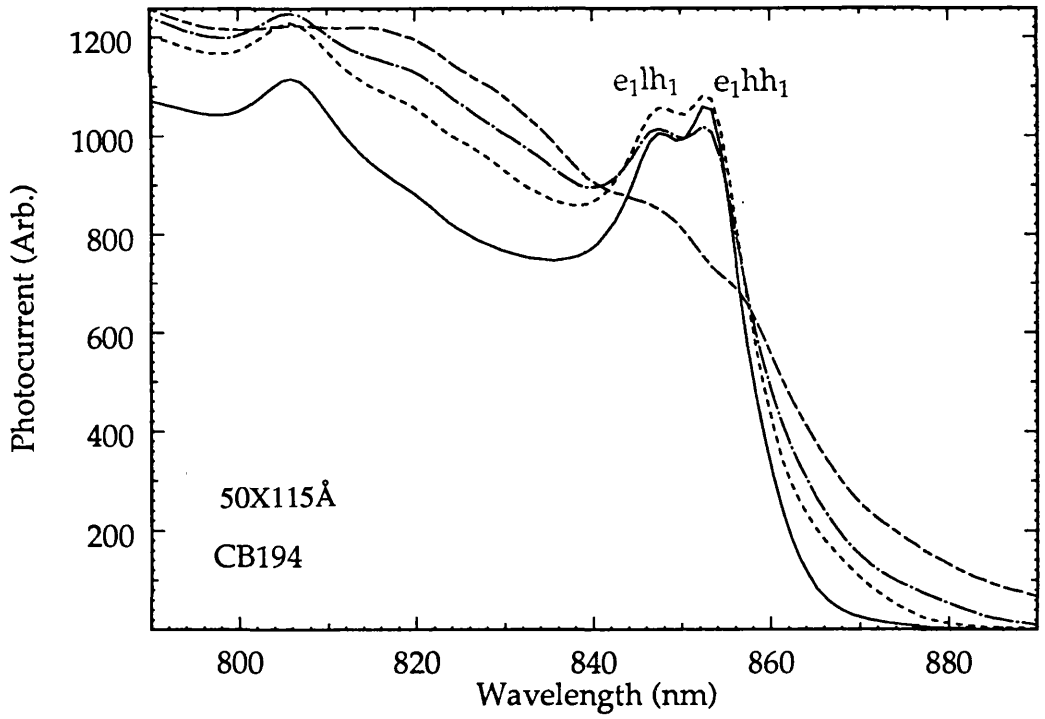

Figure 4.14 Photocurrent from CB194, a control sample with uncoupled wells. Reverse biases as in figure 4.13.

effect of this is to give a very large variation of field with distance across the whole intrinsic region when sufficient reverse bias is applied and to give a smaller variation

in field across about 40% of the wells with no bias applied, the remaining 60% of wells experiencing no electric field. This is depicted in figure 4.15.

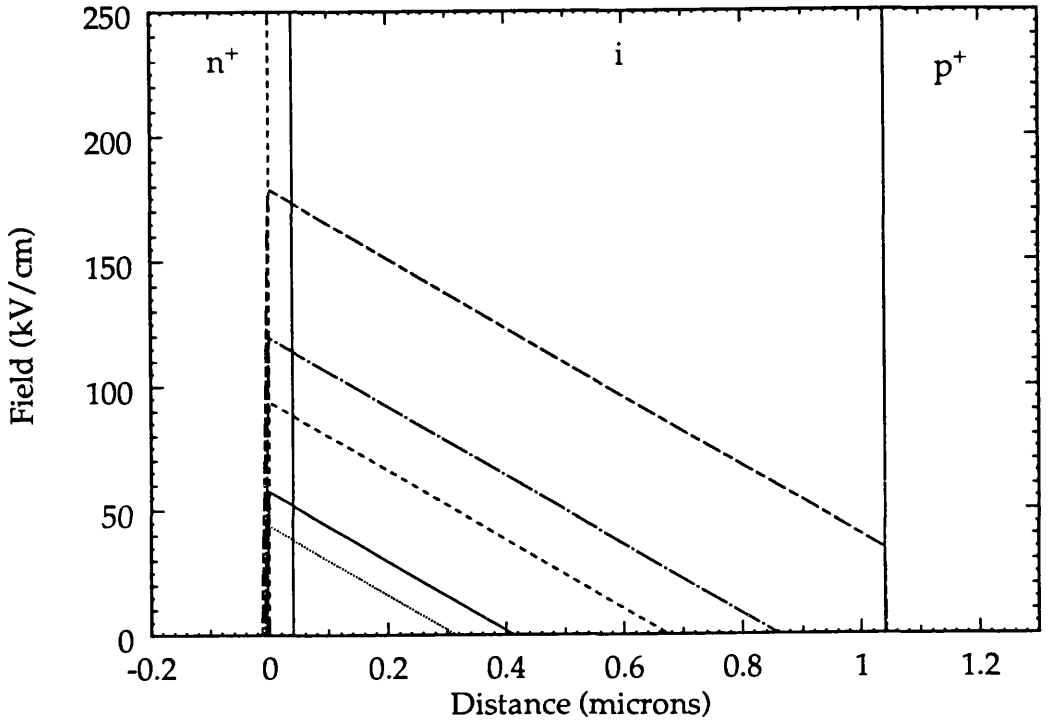

Figure 4.15 Calculated electric fields in CB191 and CB194. The quantum wells are located in the micron of material between the solid vertical lines. Reverse biases as in figure 4.13. Assumed background doping is 10^{16}cm^{-3} and built in voltage is 1.2V.

The assumed diode built in voltage is 1.2V. This is close to the value of 1.3V used by Lengyel *et al* (1990) (deduced from their figure 6), who relate their bias voltages to electric fields for a room temperature p-i-n diode with $Al_{0.32}Ga_{0.68}As$ barrier material doped to $5 \times 10^{17}\text{cm}^{-3}$ - a situation similar to those in this thesis. An exact value of the built in voltage is not determined here but it is not simply the $Al_xGa_{1-x}As$ band gap (1.8eV for $x = 0.3$ at 300K) as one might expect from an equalisation of Fermi levels in a highly doped pn junction. Further evidence for this comes from Golub *et al* who used a value of 1.2V for barriers with $x = 0.3$ although the measurements are at 10K where one could expect a larger band gap, and, Chen *et al* found the flat band condition (0 field) to be a forward bias of 1.6V at 5K for barriers with $x = 0.27$; in both cases these voltages are less than the $Al_xGa_{1-x}As$ band gap.

Now consider first the coupled well results in figure 4.13. At zero bias both e_1hh_1 and e_1hh_2 are observed because some wells experience no field and some see a range of fields. From figure 4.6 it can be seen that the e_1hh_2 peak remains roughly at the same wavelength for a range of electric fields, whereas e_1hh_1 does not. Consequently many of the coupled wells that experience different fields contribute to the e_1hh_2 peak at a similar wavelength but the e_1hh_1 contributions occur at different wavelengths. Hence the zero bias spectrum is composed of the zero field spectrum and e_1hh_2 contributions.

When bias is applied fewer wells experience no field (flat band) but more see a range of fields, hence the e_1hh_2 peak begins to dominate the spectrum around the absorption edge.

For the uncoupled wells there are no peaks in figure 4.7 that remain roughly fixed in wavelength like the e_1hh_2 peak in the coupled wells case. Hence, as bias is applied one observes a decreasing proportion of the zero field spectrum and an increasing proportion of the 'washed out' spectrum due to the absorption peaks all being at different wavelengths because the wells in the depletion region all see different fields.

(Dark currents of $\approx$10nA were observed at reverse biases of about 5V in these devices compared with about 20V reverse bias in similar devices showing better characteristics [A. Rivers private communication])

CB191 and CB194 were regrown as CB234 and CB235 respectively. Again the C-V measurements gave a doping of $\approx 10^{16}\text{cm}^{-3}$ and the spectra showed similar behaviour except that the CB234's e_1hh_1 zero field wavelength was 841nm - this receives more attention in §4.6.5 .

Background doping seemed to be a recurrent problem, but in order to test much of the theory I only needed photocurrent data from a few pairs of wells. A structure with only a few pairs of wells could not be made into a useful optical modulator because there is insufficient absorbing material but photocurrent spectra can still be taken. Consequently a structure with only 5 pairs of wells located approximately centrally in one micron of intrinsic material was requested (QT67). With only 5 pairs of wells the electric field variation over the wells is comparatively small (14kV/cm for 10^{16}cm^{-3} doping) when the field is non zero so the 'washing out' should not occur. Placing the wells in the centre of one micron of intrinsic material meant that with no applied bias the wells would hopefully be in a region where the electric field is zero, as bias is applied the depletion boundary moves through the wells and they experience an electric field. Hence the wells can be made to see both zero electric field and an approximately constant one when bias is applied - see figure 4.16.

The results for this sample (QT67) are shown in figure 4.17 together with a copy of figure 4.9 for comparison with the modelled data. The experimental data has been normalised to a reference spectrum and scaled to account for the poor quantum efficiency η at low biases. The scaling factors used were $\approx$10 for 0V, $\approx$1.2 for -2V and $\approx$1 for the rest. The data was scaled such that the photocurrent at 750nm is equal in all cases. The justification for this is that from calculations the absorption spectra should all have the same value around this wavelength. This effect is seen in many published absorption spectra (eg figures 3.3a) and is a consequence of the sum rules discussed by Miller D A B *et al* (Sep 1986) [Andrews *et al* (1988)]. Furthermore, the fact that the scaling factor is approximately 1 for the higher biases implies that this is the case and that we are genuinely dealing with a carrier escape problem. It is interesting to note that in figures 4.13 and 4.14 I have not applied scaling and the 0V spectrum does not suffer a factor 10 loss in quantum efficiency. This is probably because in these cases

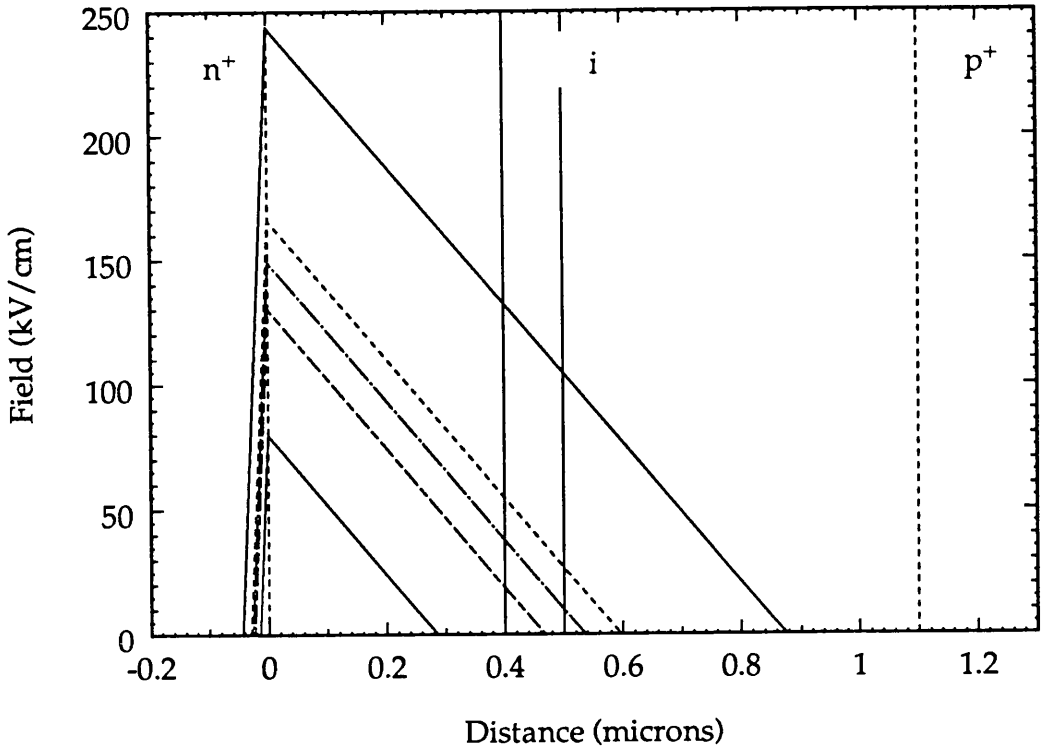

Figure 4.16 Calculated electric fields in QT67. Intrinsic region located between vertical dashed lines. Coupled wells located between solid vertical lines. Reverse biases are 0, 2, 3, 4 and 10V. Background doping is $2 \times 10^{16}\text{cm}^{-3}$. Note that the depletion boundary moves through the wells as bias is applied.

some wells always experience a field that can sweep out the carriers.

§4.6.5 Comments on experimental results

The thickness of absorber d in this case is approximately 5×115Å and if the absorption coefficient is of the order 15000 cm^{-1}, as it is in uncoupled quantum wells, then αd has a value of $\approx$0.09 which is considerably less than 1. Hence one can consider the photocurrent (normalised and scaled) to be proportional to absorption coefficient α (section 4.6.2.1). The most important conclusion to be drawn from the results in the previous section is that the shifts of peaks in terms of their wavelengths and heights agree well with theory, also the separation of absorption peaks is in good agreement. The 'modulation' observed at the wavelength of the zero bias e_1hh_1 exciton peak is the same as that predicted although this may be a little fortuitous given that the one monolayer barrier width fluctuation chosen was just an estimate. Nevertheless, the photocurrent measurements imply very strongly that the model is performing well in its aims of predicting useful structures and predicting shifts in peak wavelengths and heights. The assumptions of ignoring light and heavy hole mixing, band non parabolicity and the change of binding energy with field do not appear to be causing problems. The fitted parameters appear to be correct. Bias absorbing modulation is better than that modelled because the Lorentzian lineshape gives too large an absorption tail (§3.1).

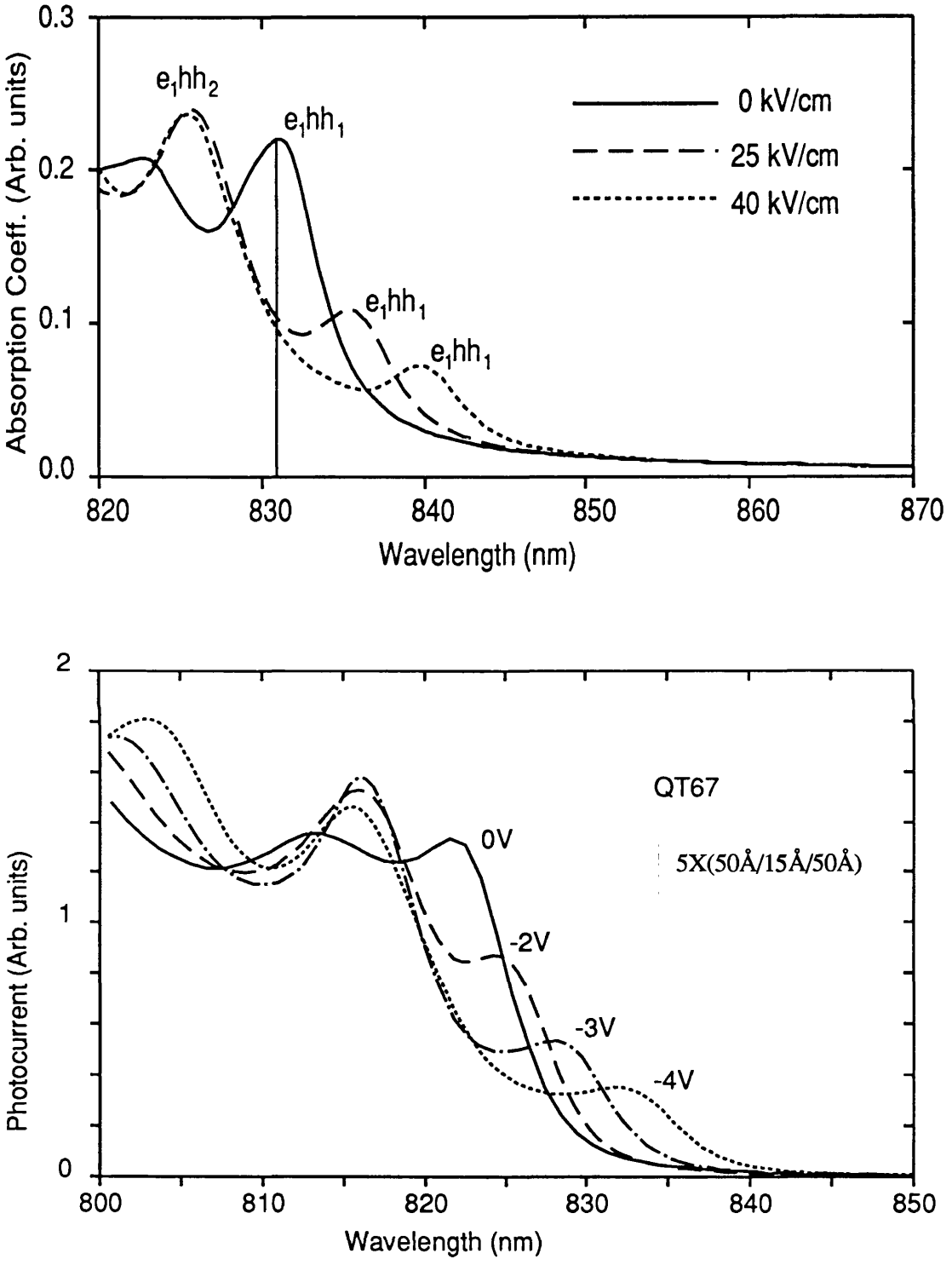

Figure 4.17 Calculated absorption coefficient (upper) from figure 4.9 and scaled photocurrent (lower) from QT67. To relate reverse biases to electric fields consult figure 4.16

Device	Wavelength (nm)	Structure
CB191	831	50 CDQW units
CB234	841	50 CDQW units
CB294	826	32 CDQW units in complex structure
QT67	821	5 CDQW units in 1μm
CB345	814	50 CDQW units, no p or n layers
QT133	829	14 CDQW units in 1μm

Table 4.1 showing device code, wavelength of the zero field e_1hh_1 exciton peak and the device structure. One CDQW unit is two 50Å GaAs wells separated by a 15Å $Al_{0.3}Ga_{0.7}As$ barrier.

There is, however, a discrepancy in the wavelengths at which the modelled and measured peaks occur. In this instance the modelled e_1hh_1 zero field peak is at ≈831nm and the measured one is at ≈821nm. There are three possible explanations; a) an error in the modelling, b) the devices grown are not as specified, c) a combination of the two.

In the model testing of section 3.1 some of the modelled data similarly was at too high a wavelength. However, the table 4.1 lists the e_1hh_1 zero field wavelength from all the devices containing this CDQW structure grown by Sheffield University for us and there is a large variation in observed wavelengths. Possible reasons for the wavelength shift are; incorrect calibration of AlGaAs growth rate (affecting coupling barrier width), incorrect calibration of GaAs growth rate (affecting well widths), inaccurate AlGaAs concentrations in the barriers and AlGaAs contamination in the wells (affecting the band gap). A full investigation of these is out of the scope of this thesis but it should be noted that so long as the variations or inaccuracies are fixed for any given sample it is likely that the essential features of the model will work. In each case distinct excitons were observed implying that growth is consistent within that sample.

§4.7 Concluding remarks and related works

Similar structures have been investigated and some are listed below with more details on the earlier works in §4.1. I have excluded work on superlattices and optical non-linearities as these are not directly related to the results in this chapter. Work published after Summer 1988 is independent of mine. The notation used for the structures is `well width / barrier width (percentage` x `of aluminium) / well width` .

Dingle *et al* (1975) measured the zero field optical density at 2K on a 50 / 15 (19%) / 50 structure (see figure 3.5). Kawai *et al* (1985) observed the e_1hh_1 photoluminescence peak at room temperature for 30/BW(50%)/30 structures with barrier widths in the range 12Å to 40Å. Le *et al* (1987) took 2K photoluminescence spectra on a 105/20/85 structure. Chen *et al* (1987) published 5K photoluminescence excitation spectra for a 75/18(27%)/75 configuration. Andrews *et al* (1988) published PLE spectra on a 48/16(30%)/48 structure at 5K and various biases. Debbar *et al* (1989)

measured absorption coefficients at 10K on a 35/30(20%)/35 structure (see figure 3.6). Onose *et al* (1989) observed photoconductivity at 77K on a 54/5.7(100%)/54 structure. Onose *et al*'s spectra agree qualitatively with those in this chapter in the rapid movement and fall of the e_1hh_1 peak and the growth of e_1hh_2 . The authors describe this as a 'blue shift' .Blue shifts can result in bias transmitting operation which is one of the criteria for SEED operation and consequently there has been some interest in this effect. In July 1989 Campi *et al* published calculations of energy levels and overlaps for a 31/35(30%)/31 arrangement at 0 and 50kV/cm and pointed out that one can consider the growth of the e_1hh_2 peak as a blue shift. This group published electroreflectance spectra consistent with their earlier calculations [Cacciatore *et al* (1989)]. Tokuda *et al* (1989) measured 77K photocurrent on the asymmetric structure 80/8(100%)/100. Lee *et al* (1989) calculated absorption coefficients at low temperature for various structures of the type - $75+\delta/18/75-\delta$ where δ= 0, 10Å, .., 60Å at zero field and for $\delta = 0, \pm 10$Å with field applied, and, both PLE spectra and calculated absorption for a 64/15(29%)/64 structure.

All the above measurements are at low temperatures (77K or below) except the electroreflectance of Cacciatore *et al* (1989) and the photoluminescence of Kawai *et al* (1985). For these and many of the others the link with absorption coefficient is not as direct as the measurement of photocurrent in this thesis. However, Islam *et al* (1987) had previously measured electroabsorption from a 46/11.5(30%)/46 structure in a waveguide configuration, presumeably at room temperature. They have two pairs of CDQWs compared with the five in this thesis (50/15(30%)/15) and as such my work is more likely to reveal problems due to growth fluctuations from one CDQW to the next. More importantly, they do not observe the growth of the e_1hh_2 peak with increasing reverse bias, at variance with my and their own modelling. The authors suggest this may be due to mixing between the valence band states (lh_1 and hh_2). The modelling and photocurrent work in this chapter does show a separation between the e_1lh_1 and e_1hh_2 peaks and demonstrates the growth of the e_1hh_2 peak. Furthermore, between fields of $\approx$3 and 22kV/cm Islam *et al* record a ratio of absorption change of about 0.8 (measured from +1V and +0.75V biases in their three dimensional figure), this value is considerably less than the ratio of $\approx$2 seen in photocurrent measurements here between similar electric fields. Whilst Islam *et al*'s data is useful, particularly for the perpendicular polarization, and forms one of the 'founding' coupled well papers, my work has shown better agreement between modelled and experimental data.

In summary, the computer model was used to predict a structure giving good optical modulation at low electric fields and room temperature. The discussion of the choice of barrier width for bias transmitting operation between coupled wells had not previously been published, nor had fluctuations in barrier width due to growth been considered [Atkinson *et al* (1990)]. The only other calculated absorption spectra for coupled well pairs that include field effects, excitonic effects and forbidden transistions were published independently by Lee *et al* in 1989. Their work differs from that in this

thesis in the calculation technique used, the temperatures considered and in emphasis (my work being on room temperature optical modulation).

Many authors have reported experimental measurements upon structures similar to the one I concluded would give good bias transmitting modulation. However, the room temperature photocurrent work in this chapter provides probably the best indication of the performance of a room temperature, electroabsorption based, optical modulator.

From the results in this chapter it is highly likely that coupled wells can function in a practical optical modulator and this forms the basis of the next chapter.

Chapter 5
Coupled Wells in Asymmetric Fabry Perot Reflection Modulators

§5.1 Introduction

In chapter 4 it was demonstrated theoretically how one can choose a coupled double quantum well structure to give reasonable modulation at low electric fields. It was shown from photocurrent measurements that this interpretation was very probably correct. As a consequence attention now focuses upon trying to fabricate a working optical modulator.

In 1989 Whitehead *et al* (July 1989) and Yan *et al* independently demonstrated an asymmetric Fabry Perot reflection modulator exhibiting a large contrast ratio, greater than 100:1 in Whitehead's case. This modulator used MQWs (uncoupled) and operated with an applied bias of 9V. Coupled wells operate at lower electric fields than comparable MQWs so there was the prospect of making a high contrast, low operating voltage device. A study of coupled wells in AFPMs forms the basis of this chapter.

At the time (October 1989) no work existed in the literature on the subject of coupled wells in AFPMs, now (September 1990) there are two papers, a theoretical one published by myself and co-workers (Atkinson *et al* 1990) and one by Law *et al* (May 1990) who achieve greater than 60:1 contrast ratio for an 8V operating swing, this device has been mentioned previously in §4.2 and is based on Wannier-Stark localisation in a superlattice.

§5.2 Synopsis of AFPM operation.

§5.2.1 Explanation

Figure 5.1 demonstrates the physics of the AFPM.

The optical beam has been drawn off normal for clarity, in practice normal incidence is used. An optical beam incident upon the front mirror is partly reflected as beam 1 and partly transmitted. The transmitted ray may experience multiple partial reflections with some rays exiting the cavity and some making multiple traverses. With the correct cavity dimension all the rays exiting from the front surface are in phase with each other and can be summed to form a single beam, beam 2. This beam is π out of phase with beam 1. Hence it is possible to achieve complete destructive interference, in other words zero reflection, when the amplitude of beam 1 is the same as beam 2. The absorption in the cavity may be varied by biasing quantum wells, hence the amplitude of beam 2 can be altered, specifically it can be varied such that there is either complete destructive interference or incomplete destructive interference - a high contrast reflection modulator.

To a first approximation there is no change in refractive index of the cavity, the relative phases of beams 1 and 2 remain unchanged and the device is *based entirely upon absorption changes.* The front mirror is just the air-semiconductor interface and the back mirror is formed from a multilayer stack (MLS) composed of materials with

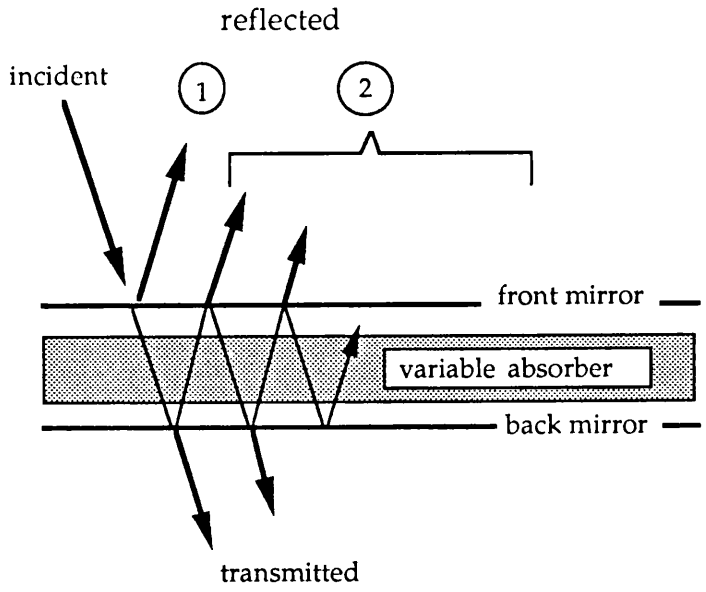

Figure 5.1 Operation of the asymmetric Fabry Perot reflection modulator. Rays have been drawn off normal for clarity only.

different refractive indices. Quantum wells form the absorbing material in a p-i-n diode arrangement as before.

§5.2.2 Formulae

A more detailed discussion of the AFPM may be found in Whitehead *et al* (Feb. 1989) from which some equations are reproduced below. Derivation of the equations is closely analagous to that found in text books for the spectroscopic Fabry Perot etalon [eg Fowles, Hecht and Zajac] but more general in that different front and back reflectivities and absorption in the cavity are considered. Changes in refractive index due to changes in absorption have been ignored here because previous calculations that neglect this effect for low finesse type cavities, like those used here, have been successful [Whitehead private communication]. In the 'normally-off' device (minimum reflection at zero bias) the omission of index changes could lead to an understating of device performance provided the operating wavelength matches the Fabry Perot reflectivity minimum at zero field (as it should).

The general equations for reflectivity, R and transmission, T, are;

$$R = \frac{B + F\sin^2\delta}{1 + F\sin^2\delta/2} \tag{5.1}$$

$$T = \frac{A}{1 + F\sin^2\delta/2} \tag{5.2}$$

where R and T refer to intensity (not amplitude) reflection and transmission, and

$$A = \frac{(1 - R_f)(1 - R_b)e^{-\alpha d}}{(1 - R_\alpha)^2} \tag{5.3}$$

$$B = \frac{R_f[1 - R_\alpha/R_f]^2}{(1 - R_\alpha)^2} \tag{5.4}$$

$$F = \frac{4R_\alpha}{(1 - R_\alpha)^2} \tag{5.5}$$

$$R_\alpha = \sqrt{R_f R_b} e^{-\alpha d} \tag{5.6}$$

and δ is the total optical phase shift difference between successive output beams. It is dependent upon cavity length L_c, wavelength, λ, the cavity refractive index n_c and any phase change upon reflection. (In the usual spectroscopic Fabry Perot all Rs are equal and $\alpha \equiv 0$ leading to $A \equiv 1$ and $B \equiv 0$). With the cavity 'on resonance ' ie,

$$\sin \delta = 0 \tag{5.7}$$

a reflection of zero can be achieved if,

$$B = 0 \ . \tag{5.8}$$

The necessary condition for B to be zero is that

$$\alpha d = -\ln\left(\frac{R_f}{\sqrt{R_f R_b}}\right) \ . \tag{5.9}$$

For the AFPMs in this thesis $\alpha d \approx 0.58$ to give B=0 .

In general for a cavity on resonance the reflectivity is given by,

$$R = \frac{R_f[1 - (R_\alpha/R_f)]^2}{(1 - R_\alpha)^2} \tag{5.10}$$

At wavelengths above the quantum well absorption edge $\alpha \approx 0$ and equations 5.1 and 5.2 reduce to the following,

$$T_{MAX} = \frac{(1 - R_f)(1 - R_b)}{(1 - \sqrt{R_f R_b})^2} \tag{5.11}$$

$$T_{MIN} = \frac{(1 - R_f)(1 - R_b)}{(1 + \sqrt{R_f R_b})^2} \tag{5.12}$$

$$R_{MAX} = \frac{(\sqrt{R_f} + \sqrt{R_b})^2}{(1 + \sqrt{R_f R_b})^2} \tag{5.13}$$

$$R_{MIN} = \frac{(\sqrt{R_f} - \sqrt{R_b})^2}{(1 - \sqrt{R_f R_b})^2} \tag{5.14}$$

T_{MAX} coincides in wavelength with R_{MIN} when

$$\delta = m\pi \tag{5.15}$$

where $m = 0, \pm 1, \pm 2, \ldots\ldots$. R_{MAX} coincides with T_{MIN} when

$$\delta = \frac{(2m+1)}{2}\pi \tag{5.16}$$

Important equations for calculating reflectivities are:

For a multilayer stack composed of $\lambda/4$ layers of material A and B, with indices n_A and n_B respectively, its reflectivity at the centre wavelength is given by,

$$R_{centre} = \left[\frac{x - y^{2N}}{x + y^{2N}}\right]^2 \tag{5.17}$$

where

$$x = \frac{\text{ref. index of medium from which light is incident}}{\text{ref. index of exit medium}}$$

and

$$y = \frac{n_A}{n_B}$$

and N is the number of layer pairs.

For a simple interface in which light is incident from material A into material B,

$$R_{int} = \left[\frac{n_A - n_B}{n_A + n_B}\right]^2 \tag{5.18}$$

from Fresnel's equations.

The multilayer stack bandwidth is,

$$\frac{\Delta\lambda}{\lambda_{\text{centre}}} = \frac{4}{\pi}\sin^{-1}\left(\frac{|n_B - n_A|}{n_B + n_A}\right) \tag{5.19}$$

[Macleod]

§5.2.3 The cavity length

In calculating the cavity length, L_c, required, phase changes upon reflection must be accounted for. When light travelling through a medium is reflected from a higher refractive index medium its phase is changed by π (from equation 5.18). For the AFPMs studied here there is a phase change of π for beam 1 (see figure 5.1) with respect to the incident beam and a change of π upon reflection within the cavity from the back mirror if it is a multilayer stack. (It is assumed that there are no phase changes upon transmission). The optical phase shift after one return traverse of the cavity is,

$$\delta = \frac{4\pi n_c L_c}{\lambda} + \pi \tag{5.20}$$

In order that all the constituents of beam 2 are in phase it must be that

$$\delta = 2\pi p \tag{5.21}$$

where p is an integer. By equating δs the cavity length L_c must be an odd number of quarter wavelengths long;

$$L_c = \frac{(2p-1)\lambda}{4n_c} \tag{5.22}$$

Consequently all constituents of beam 2 are in phase (modulo 2π) with the incident beam and thus beam 1 is π out of phase with respect to beam 2.

In a later Fabry-Perot structure with no multilayer stack there is no π phase change upon reflection at the back mirror so the condition for the constituents of beam 2 to be in phase is that the cavity length is an integer multiple of a half wavelength in the cavity. This will also give destructive interference between beams 1 and 2.

§5.3 Fitting the absorption coefficient

As mentioned in chapter 2 the model produces absorption coefficients proportional to their absolute values in cm^{-1} . It is necessary to fit one constant of proportionality by using experimental data. There are no published spectra for this or similar structures that give absorption coefficients in absolute units except for Islam *et al* (1987). Their data is for a waveguide device in which the CDQWs form less than 1% of the guiding core, it is not possible to compare their absorption coefficient with that for transverse modulators without a knowledge of the optical field strengths within their waveguide.

At the time I could not make an experimental measurement of α on coupled wells because the only reasonably working device had only 5 pairs of wells. Consequently I made a determination of α by assuming the scale from 115Å of CDQWs is the same as that for a 115Å of SQW because both contain a similar amount of absorbing material. Masumoto *et al* (1985) showed that the absorption coefficient at the continuum (ie at ≈832nm in figure 4.7) varies to a good approximation as $1/L_z$ where L_z is the well width. The modelled absorption at the continuum varies little with the FWHM chosen for the Lorentzian broadening, in contrast to the absorption close to the exciton peaks, hence I fixed the absorption scale to the continuum absorption. From transmission data [Whitehead *et al* (Sep 1988)] for a MQW sample with 145Å wide wells, 30% Al barriers and an antireflection coating I obtained a continuum absorption coefficient of $7470cm^{-1}$ (this refers to well material only). Using the $1/L_z$ dependence, the continuum absorption of 115Å wide wells is $7470 \times 145/115 = 9420cm^{-1}$. This technique predicts a continuum absorption of $7470 \times 145/105 = 10300cm^{-1}$ for 105Å wide wells, very close to that measured by Lengyel *et al* more recently (see figure 3.3). So, the α scale for the 15Å barrier CDQWs has been fitted, the e_1hh_1 zero field exciton peak in figure 4.9 has a value of $\approx 13000cm^{-1}$.

§5.4 Design of an asymmetric Fabry Perot reflection modulator

§5.4.1 The Mirrors

In the work of Whitehead *et al* (July 1989) the front mirror was formed by the air-semiconductor interface, the high refractive index mismatch of ≈2.5 resulting in a mirror reflectivity of ≈30%. The back mirror was formed from a multilayer stack of 12 periods of AlAs and $Al_{0.1}Ga_{0.9}As$ giving a reflectivity of ≈95% at the centre wavelength and a bandwidth of 95nm over which the reflectivity is at least 91% (section 5.2.2). Their modulator operated at ≈860nm.

To employ CDQWs the operating wavelength is lower (eg 822nm in device QT67)

Material	Wavelength (nm) 775	800	814	820	822	860	900	917	950	991
GaAs undoped		3.652	3.644	3.6415	3.640	3.632		3.573	3.547	3.515
$Al_{0.10}Ga_{0.90}As$					3.615	3.5547				
$Al_{0.12}Ga_{0.88}As$					3.591					
$Al_{0.15}Ga_{0.85}As$					3.549					
$Al_{0.30}Ga_{0.70}As$	3.4736	3.450	3.438	3.4321	3.427	3.4038	3.3811	3.3726	3.358	3.340
$Al_{0.50}Ga_{0.50}As$		3.285	3.280	3.276		3.250		3.262	3.213	3.193
AlAs				2.991	2.995	2.9767				
Sapphire	1.7609			1.7597		1.7587	1.7577	1.7574	1.7566	1.7558
CB345 average			3.4929		3.4857	3.4679		3.4327		3.3847

Refractive index data for GaAs to $Al_{0.3}Ga_{0.7}As$ from Casey *et al*, $Al_{0.5}Ga_{0.5}As$ and AlAs from Pikhtin *et al* and sapphire from Melles Griot.

Table 5.1 Refractive indices used in calculations

and all the cavity dimensions had to be redesigned because the semiconductor refractive indices are wavelength dependent (see table 5.1). Furthermore, I decided to use $Al_{0.12}Ga_{0.88}As$ instead of $Al_{0.1}Ga_{0.9}As$ in the MLS because at room temperature $Al_{0.1}Ga_{0.9}As$ has a band gap corresponding to 801nm, fairly close to the operating wavelength, but $Al_{0.12}Ga_{0.88}As$'s band gap is at 788nm.

Thus using $Al_{0.12}Ga_{0.88}As$ ensures that the AlGaAs absorption will be low in the MLS at 822nm. From these parameters the MLS reflectivity is 95% and at the centre wavelength of 822nm, the bandwidth is 95nm, data calculated from equations 5.17 and 5.19 in section 5.2.2. The front mirror remains the air-semiconductor interface.

§5.4.2 The number of coupled wells to include in the AFPM.

After having fixed the absorption scale for the 15Å barrier CDQW in section 5.3 the absorption coefficient at the zero field exciton peak and at 25kV/cm was determined from figure 4.9 (demonstrated in figure 4.17 to be correct). Using equation 5.10 the asymmetric Fabry Perot reflectivities were calculated for devices with varying numbers of coupled well units. The thickness of absorbing material d is the number of coupled well units n_p multiplied by their length (115Å). Operating voltages were calculated by assuming that each coupled well pair was separated from its adjacent pair by a barrier of thickness 85Å, the total length of the intrinsic region then being $n_p \times 200$Å, hence the operating voltage is the product of this length and the applied field (25kV/cm). Table 5.2 shows calculations based on the absorption changes in figure 4.9.

A previously reported AFPM device [Whitehead *et al* (July 1989)] employing uncoupled multiple quantum wells was observed to give a very high contrast with 9V bias and ≈3.5dB insertion loss. Table 5.2 shows a considerably lower operating voltage (2.2V), but the insertion loss is worse (9.4dB) in the coupled well case. Recently Yan *et al* (Feb 1990) have demonstrated an AFPM with an operating voltage swing of

No. of pairs of wells	Nominal Voltage	Insertion Loss	Contrast Ratio	Off-state reflection	On-state reflection
14	0.7V	3.3dB	2.1 : 1	22.6%	46.8%
32	1.6V	6.8dB	10.1 : 1	2.1%	21.0%
44	2.2V	9.4dB	$\approx\infty$: 1	0 %	11.5%

Table 5.2 Predicted performance of an AFPM with coupled quantum wells in the intrinsic region. In each case the electric field change is from 0 to 25kV/cm and the 'Nominal Voltage' is the product of the applied field and the length of the wells and barriers. Calculation asssumes a cavity with reflectivities at the front of 30% and 95% at the back, operating at its resonant wavelength.

only 2V achieving a change in reflection of 47 percentage points, however, the contrast ratio is low ($\approx$4). These results were obtained by using a high finesse cavity with a front mirror reflectivity of 80% rather than the 30% used here. They used essentially uncoupled wells and if this type of structure is desirable from a systems aspect the use of coupled wells could further reduce the operating voltage (high finesse cavities generally suffer from poor optical bandwidths and can be sensitive to temperature fluctuations which may not be acceptable in some systems). I shall concentrate on the lower finesse cavity.

The data in table 5.2 were calculated using figure 4.9 representing a one monolayer fluctuation in the barrier width as a guide to possible performance. Sample QT67 demonstrated that this was a good estimate, at least for the five barriers in that sample. If a 6Å total fluctuation in barrier width is assumed then in order to achieve a contrast ratio of 10.4:1 the device needs 40 pairs of wells (an operating voltage of 2.0V) and the insertion loss is 11.6dB. To obtain a very large contrast ratio the operating voltage required is 2.4V and the insertion loss is 14.7dB.

§5.4.3 Background doping and built in voltages.

The voltages in table 5.2 assume a p-i-n diode with an intrinsic region composed only of coupled well units and 85Å separating barriers, consequently the intrinsic region is short (in the case of 14 pairs of CDQWs it is 0.28μm long). Across a 0.28μm intrinsic region a built in voltage of 1.2V represents a field of $\approx$40kV/cm. Hence the wells would already experience a field beyond their designed operating field before reverse bias is applied. Various methods of overcoming this are discussed below.

The constraints on the system are that 1) the wells/barriers must be fabricated from GaAs and AlGaAs, 2) it must be possible to control the electric field by applying a voltage and the voltage should appear across the wells - necessitating an intrinsic region with high resistance, 3) the wells/ barriers must be capable of experiencing zero field or 'flat band'.

a) Alternatives to the p-i-n diode . There is no fundamental reason why p-i-n

diodes should be used to apply field, other methods have been used, Andrews *et al* used indium tin oxide (ITO) to provide one contact to the wells and an n^+ substrate to provide the other. ITO is transparent (commonly used in liquid crystal displays). However, this arrangement produces a Schottky barrier configuration with barrier heights of the order 0.9V in a similar fashion to pn diodes - see Parker for fuller discussion.

Similarly, Cacciatore *et al* (1989) evaporated a semi-transparent electrode of Cu_2S onto the surface of the undoped material - this formed a Schottky barrier according to the authors that required a forward bias of 0.7V to achieve flat band. Both these approaches suffer the same fundamental problem as p-i-n diodes, a potential barrier is formed that drops a voltage across the i region.

b) Dead space in the intrinsic region. The intrinsic region may be lengthened by inserting extra material that does not contain wells. Because of the background doping the built in voltage can be dropped in this 'dead space'. This was used in QT67 in §4.6.4

c) Extra Doping Layer. An extra layer may be inserted at the i-n boundary if the i region has p-type doping. This extra layer is p doped and the built in voltage is dropped in this layer, see figure 5.2 .

The thickness of the layer should be just sufficient to drop all the built in voltage within this layer. One has to be careful not to use too high a doping as the peak field may then exceed the breakdown field of the semiconductor which is about 300kV/cm [Craig Tombling private communication]. A doping concentration of $10^{17}cm^{-3}$ gives the most freedom in the control of dopants [John Roberts private communication] and it is this order of magnitude of doping that is considered later.

d) Forward biasing. The built in voltage can be at least partly offset by forward biasing the diode. At room temperature the built in voltage is thought to be approximately 1.2V in these samples (§4.6.4). In practice we find that the phase-locked photocurrent becomes unstable for forward biases greater than $\approx$0.7V although this value depends upon the sample. The instability in the phase locked signal is assumed to be due to the diode starting to pass a high forward current that the lock-in amplifier finds difficult to distinguish from the chopped photocurrent. Many authors publish spectra with small forward biases but do not discuss the current being driven and some state that they believe they have achieved 'flat band' ie zero net electric field across the wells [For example some of these authors are listed below, the structures of the first three appearing in section 4.7. Andrews *et al* reached this condition for +1.05V for their sample which has an ITO contact, Islam *et al* appear to have gone +0.5V beyond the forward bias needed achieve flat band, Chen *et al* applied +1.6V to their sample at 1.8K and Whitehead *et al* (1990) applied +1.0V to a room temperature device (p-i-n diode with 30% aluminium in the barriers) fabricated in a similar way to those in this thesis]. Hence it would appear to be possible to considerably offset the built in voltage although in my samples this leads to problems with photocurrent.

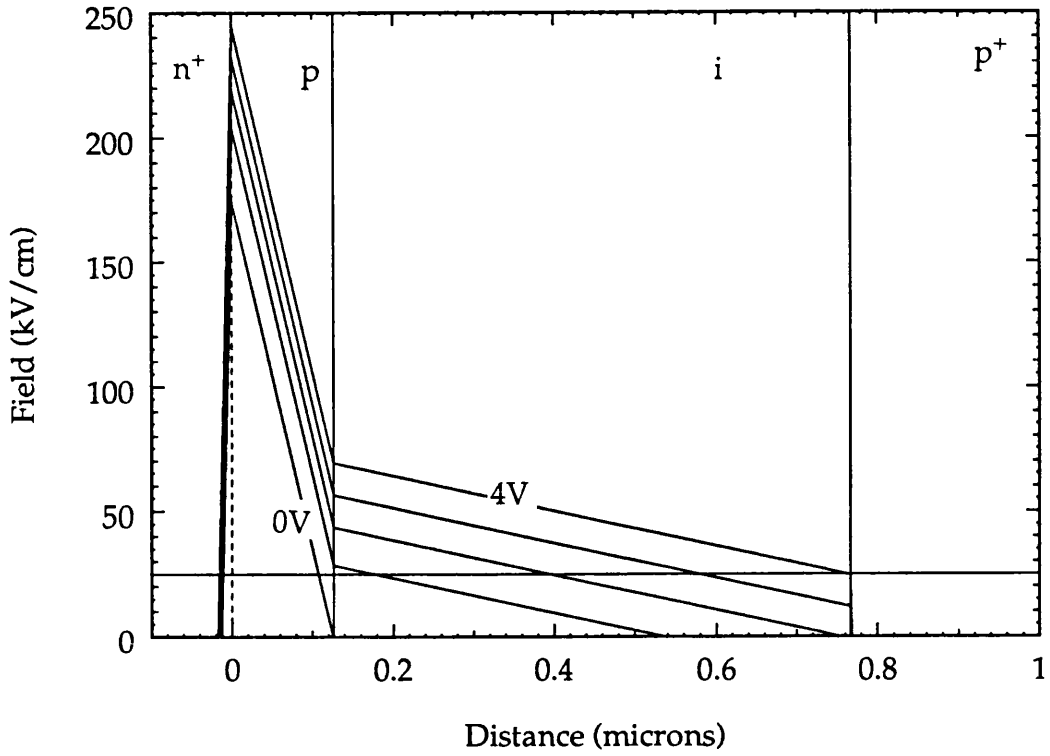

Figure 5.2 Calculated electric fields in a device with an extra doping layer. Figure plots the variation of electric field at reverse biases of 0,1,2,3 and 4V across a p-i-n diode containing an extra p^+ layer with a doping density of $10^{17}cm^{-3}$. The intrinsic region boundaries are denoted by the solid vertical lines, the assumed doping concentration is $5 \times 10^{15}cm^{-3}$. Solid horizontal line shows a field of 25kV/cm. 'Flat band' at 0V bias and fields greater than 25kV/cm at 4V bias.

The Choice made. ITO or Cu_2S electrodes would require development of processing techniques and appear to offer only a small benefit in terms of the built in voltage. Forward biasing is possible although it would require an investigation of the forward bias I-V characteristics and their relation to the built in voltage and to the type and quality of material and contacts. This would have been too time consuming. One option would be to forward bias the device to, say, 0.5V and drop the remaining voltage across a dead space or extra doping layer (hereafter these are called the 'extra layer'). The extra layer, when forward bias is used, need not be as long as if forward bias had not been used and the operating voltage swing could be reduced. However, calculation of the length of the extra layer required depends upon the background intrinsic doping concentration, if the doping concentration is lower than expected the depletion region will extend further into the portion of the intrinsic region containing the wells and barriers. It seems sensible not to aim at using both forward bias and an extra layer but to use an extra layer alone, if the doping turns out to be less than expected a forward bias could then be used to keep the depletion region out of the wells and barriers. (If the doping is higher than expected more bias is needed to achieve a given field across the wells.)

The relative merits of a dead space and doping layer were investigated. I decided to include 32 CDQW pairs in the intrinsic region, this uses 0.64μm of intrinsic material. The two electric field requirements are that the field must be a) zero across the wells at one bias and b) 25kV/cm or more at another bias. Fortunately the value of the field in the second condition is not critical so long as it is over 25kV/cm, see figure 4.6, also by reverse biasing QT67 up to 10V I confirmed that the modulation remains good up to a corresponding field of $\approx$100kV/cm (see figure 4.16).

For a background doping of $5 \times 10^{15}\text{cm}^{-3}$, a dead space of 0.6$\mu$m is required to drop 1.2V (see figure 5.3). To achieve a minimum field of 25kV/cm over the wells and barriers about 7V bias must be applied. Alternatively, if an extra doped layer of concentration 10^{17}cm^{-3} with width 0.126μm is used, flat band can be achieved and 4V reverse bias is required to give a minimum field of 25kV/cm (see figure 5.2), in each case the maximum field across the wells is less than 80kV/cm. Hence both conditions a) and b) are fulfilled.

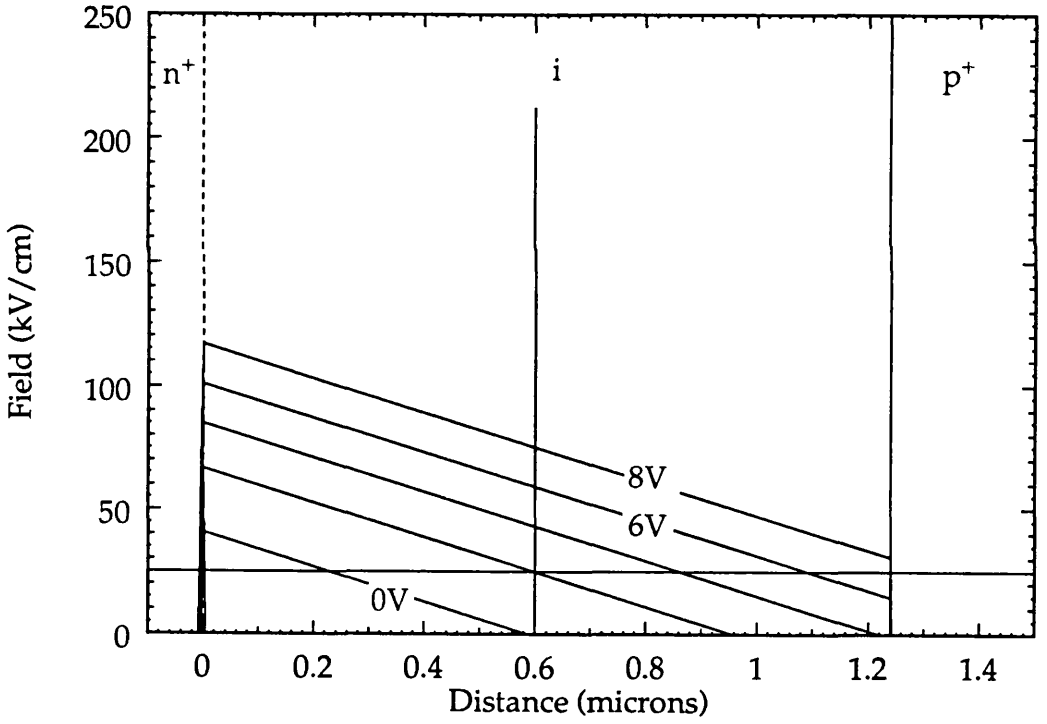

Figure 5.3 Calculated electric fields across a p-i-n diode with 'dead space' . Reverse bias voltages are 0,2,4,6 and 8V. Intrinsic region extends from 0 to 1.24μm, doping density assumed is $5 \times 10^{15}\text{cm}^{-3}$. The quantum wells are located between the solid vertical lines.

I decided to try inserting the extra doping layer to obtain 4V operation. I was told [John Roberts private communication 6 April 1990] that Sheffield had a calibration for a doping concentration of $4.8 \times 10^{16}\text{cm}^{-3}$ so I specified this thickness concentration and a thickness of 1821Å. If the grown doping is too high more bias will be needed to apply a field to the wells, if the doping is too low the devices will not experience flat

band although a forward bias can be used to offset this. The thickness of the layer should not present any problems in growth.

§5.4.4 Structure Requested

The MLS is naturally p-doped and for this reason previous AFPM devices had been grown n-i-p-MLS-substrate with the substrate being semi-insulating (no p-type substrate is available). Sheffield wanted to try heavily doping the MLS with donor impurities to make it n-type and then grow the device p-i-n-MLS-substrate with an n-type substrate. The layer structure requested is shown in figure 5.4 and was grown as CB294.

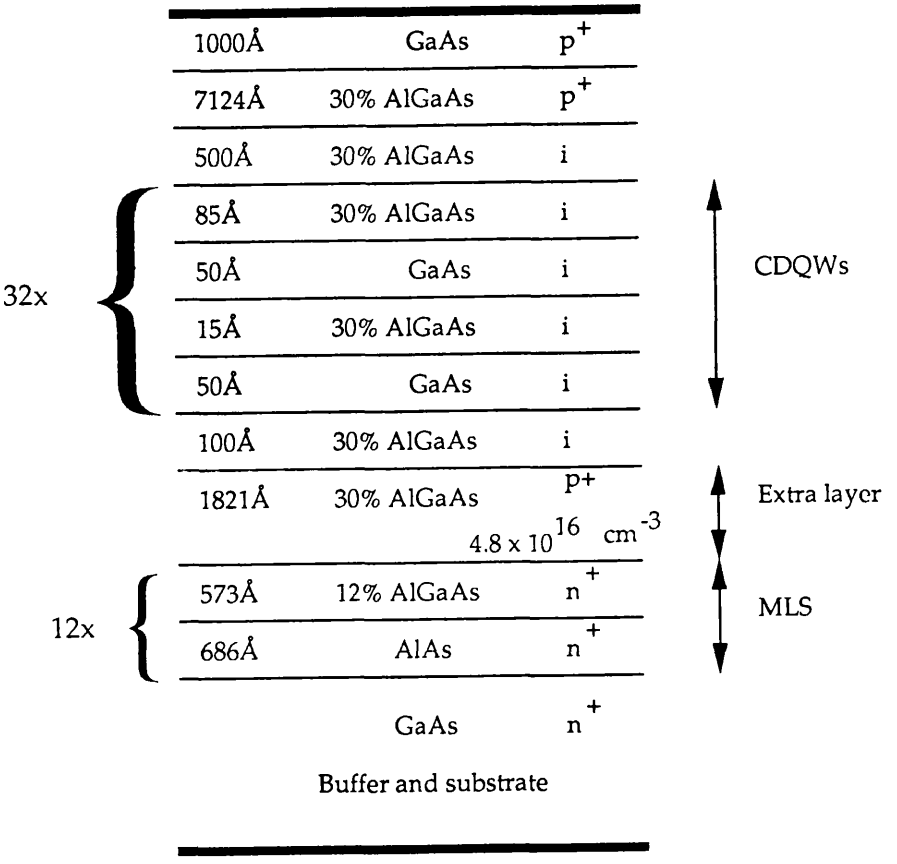

Figure 5.4 Schematic of the requested layer structure of CB294.

§5.5 Experimental Results for CB294

Reflectivity and photocurrent measurements were taken. The reflectivity was determined using an optical multichannel analyser.

The Optical Multi Channel Analyser : White light from a tungsten lamp is collimated, reflected through 90° by a beam splitter and is focussed onto the device. The reflected light passes back without deflection through the beam splitter and is focussed onto a fibre bundle. The fibre bundle transmits the light to a spectrometer consisting of a grating and an array of photodetectors. Reflection spectra, corrected for background electrical noise are available in 'real time'. These can be normalised

to the reflectivity from a freshly deposited gold film assumed to have a constant 95% reflectivity at these wavelengths.

Photocurrent data is shown in figure 5.5. The large peaks are due to Fabry Perot effects. At 0V and 2V reverse bias no photocurrent was observed on this photocurrent scale. Exciton peaks can be seen at around 820nm, their behaviour appears similar to QT67 although comparison is difficult due to the Fabry Perot effects. The biases required are above the 4V predicted in §5.4.3. A simple interpretation of CV measurements to give doping profile is not valid because of the extra p doping layer. Reflectivity measurements were taken on the optical multi channel analyser (OMA) and are shown in figure 5.6.

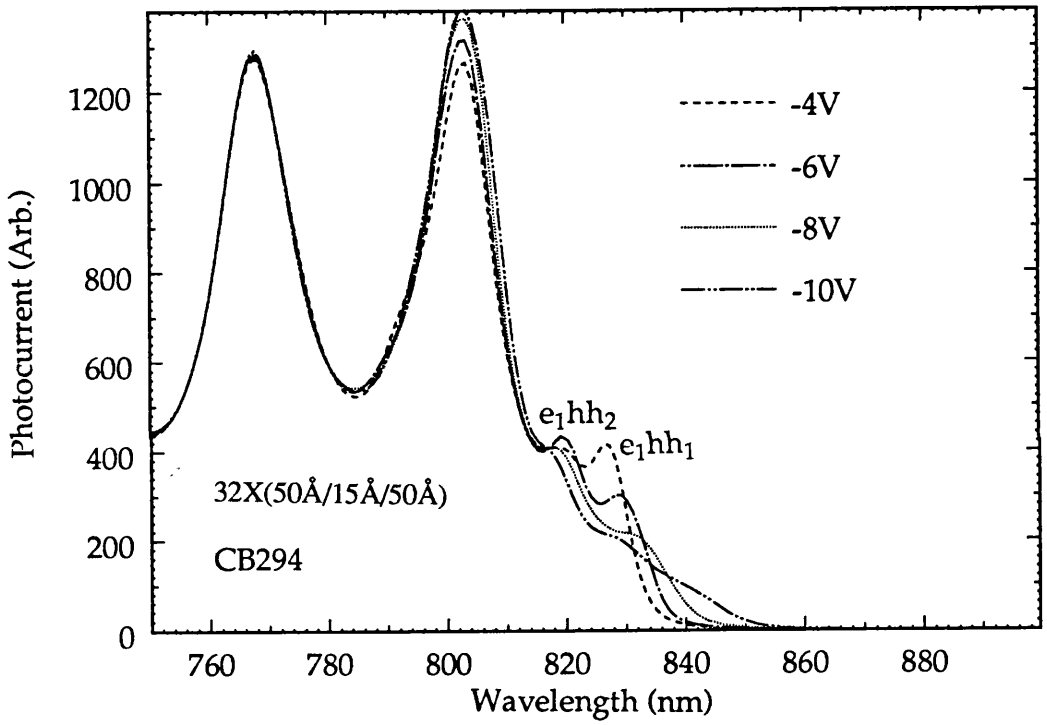

Figure 5.5 Raw photocurrent data from CB294. The two large peaks at ≈770nm and ≈804nm are due to Fabry Perot effects.

Very little change in reflectivity with bias was observed, by plotting the difference in reflectivity between the biased and unbiased cases small changes in reflection could be discerned from the background noise, for example at 10V reverse bias the largest change in reflection is 10 percentage points at ≈808nm.

It is commonly the case that variations in growth result in the thickness of a wafer varying across its area. Consequently the length of the Fabry Perot cavity changes and the wavelength of the Fabry Perot peaks vary. The thickness changes affect the wavelengths of the Fabry Perot peaks more than the excitonic peaks. A 5% increase in well and barrier width across the wafer represents a calculated shift of the exciton peak at zero field by 1.8nm. For a cavity that is 19 quarter wavelengths long a 5% increase is sufficient to change the interference from constructive to destructive at a

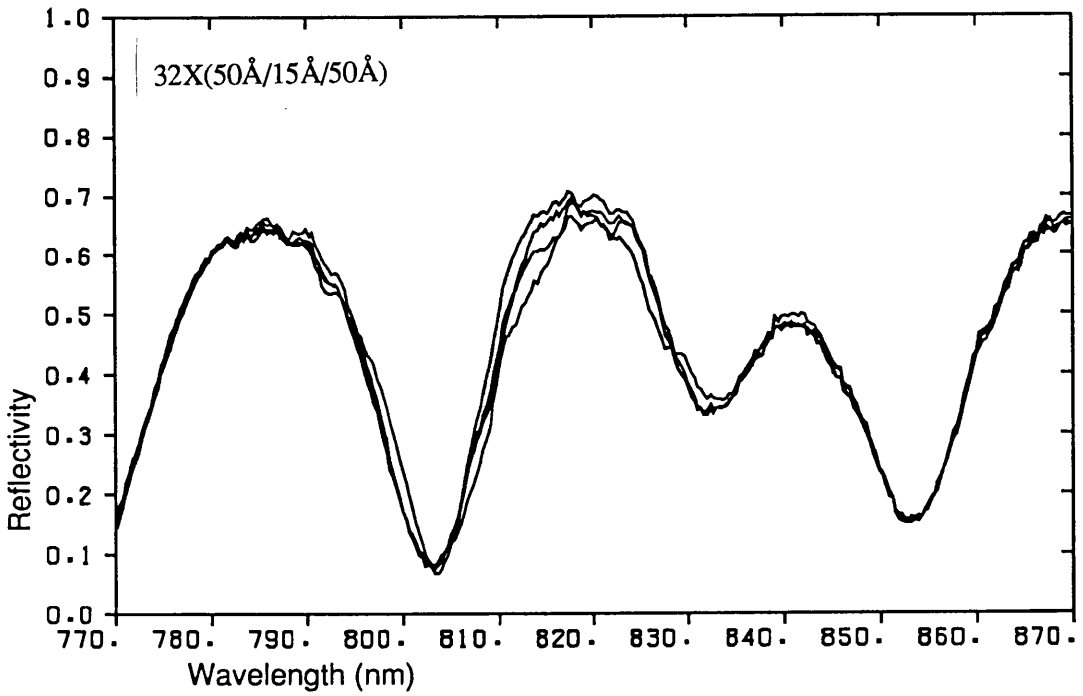

Figure 5.6 Reflectivity from CB294 at reverse biases of 0,10,15 and 20V. The 4V reflectivity shows no change from the 0V reflectivity.

given wavelength, this is much more significant than the 1.8nm shift. It is usual to 'map' the 0V reflectivity of a 2 inch wafer prior to the processing into mesas in order to determine the portion of wafer with the correct cavity length. This process usually reveals exciton peaks distinctly but figure 5.7 shows 0V reflection spectra at 3 places on the wafer, exciton peaks are barely discernable at ≈828nm.

The problem of device yield from such wafers is one that may have to be addressed in the future, particularly for arrays of devices. However at present these fluctuations are somewhat fortuitous as they make it more likely that some part of the wafer will have the correct cavity length. Furthermore, because the operating wavelength is sample dependent (table 4.1) these fluctuations again help to ensure that a portion of the wafer will have a cavity resonance at the correct wavelength.

§5.5.1 Interpretation of experimental results

The device is not exhibiting the predicted voltage performance or giving the predicted modulator reflectivities. There are 4 explanations.

1) The heavily doped n-type MLS could be causing problems as it is the first time this has been grown. Fabry Perot resonances are clearly seen, so a cavity exists, however, they should be more distinct over only ≈95nm, the bandwidth of the MLS. The implication is that there is something wrong with the reflectivity of the MLS, I believe a full investigation would not be worthwhile bearing in mind the other problems below and that other devices have worked previously.

2) The fitted absorption in section 5.3 could be too high. In this situation the

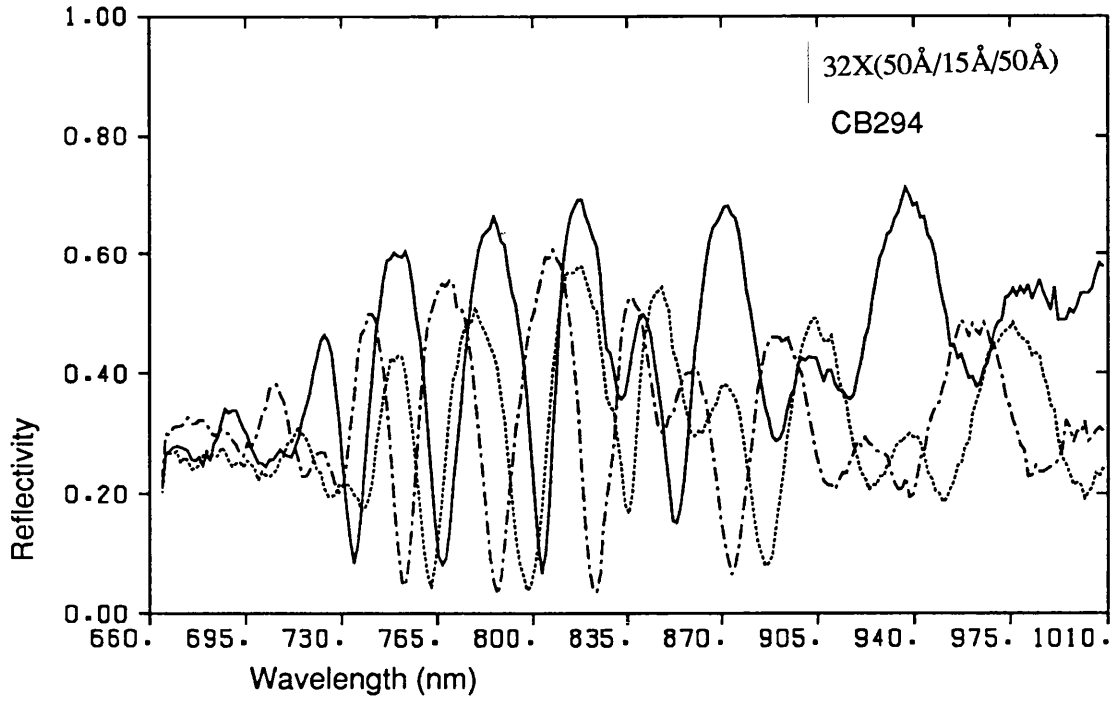

Figure 5.7 Zero bias reflectivities from CB294 at three different positions on the wafer.

actual absorption in the cavity would be too low, this could be the explanation for the lack of exciton features observed and prompted the work of section 5.6

3) The 1000Å GaAs cap did not have a window etched in it. At 830nm bulk GaAs has an absorption coefficient of $1.2 \times 10^{-4}\text{cm}^{-1}$ (Sturge 1962). This corresponds to an αd of 0.12 compared with the expected 0.42 from the 32 CDQWs at 0kV/cm. This extra 0.12, whilst not in the design of table 5.1 should not prevent a change in reflection from being observed if field could be applied to the wells.

4) These measurements were taken in May 1990 but in July 1990 we learnt that the p-doped layer had an acceptor concentration of $3.75 \times 10^{17}\text{cm}^{-3}$. This is 8 times that requested and used in the model. I believe this is the reason why the electrical performance is poor.

§5.6 Measuring the absorption coefficient of CDQWs.

The work above on CB294 implied that the absorption coefficient fitted in section 5.3 may be too low. I could not previously measure absorption coefficients as all samples with more than 10 pairs of wells had a high background doping problem. The structure in figure 5.8 was requested (CB345), this is entirely undoped to avoid the pn junction voltage.

The sample was mounted on a sapphire disc and the substrate thinned and then etched away to the etch stop layer [by A. Stride, University College London]. Transmission and reflection measurements were taken using the OMA and are shown in figure 5.9. Transmission was normalised to no device present, ie it is the ratio of device in to device out, reflection was normalised to the reflection of a freshly deposited gold film.

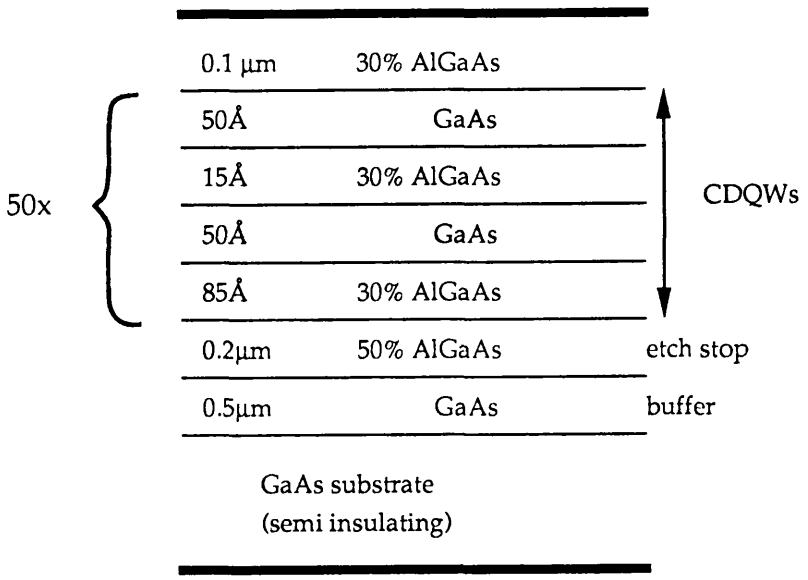

Figure 5.8 Schematic of the layer structure CB345 used for absorption measurements.

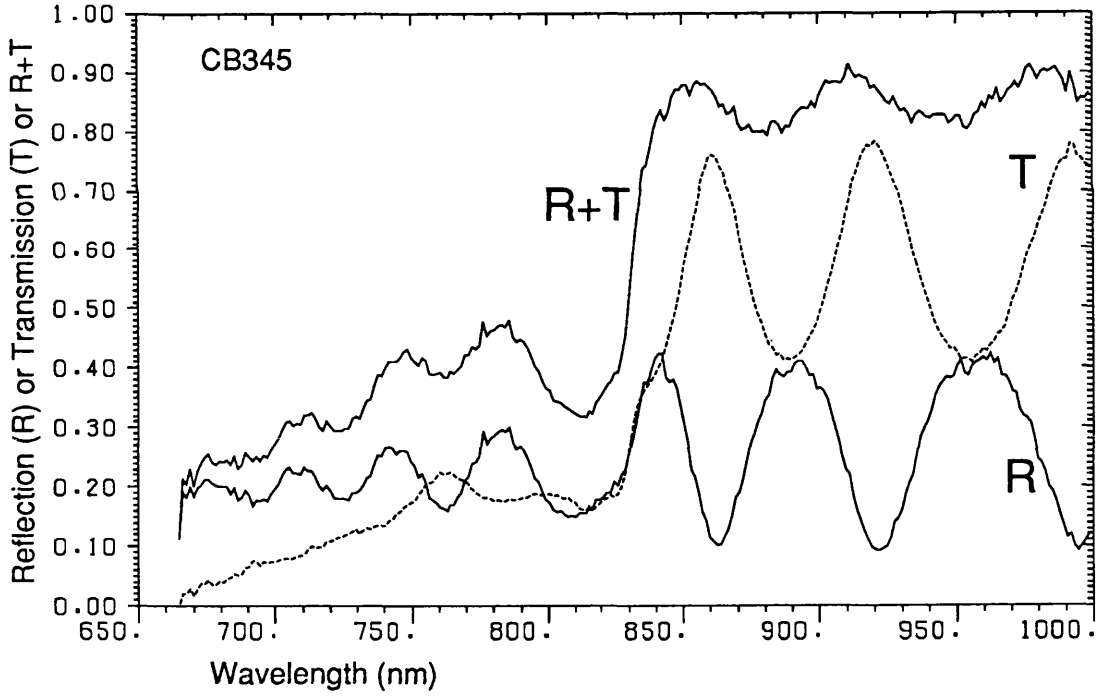

Figure 5.9 Normalised reflection and transmission and their sum for CB345, measured using the OMA.

These results demonstrate qualitatively the physics of asymmetric Fabry Perot cavities. In this case the air-semiconductor interface forms one mirror and the semiconductor to sapphire interface forms the other mirror (the mounting glue is assumed to be either negligibly thin or have the same refractive index as sapphire).

The cavity formed by the sapphire disc is ≈0.5mm thick, this would give Fabry Perot oscillations with a period of 0.5nm - much less than that from the semiconductor

cavity. Figure 5.9 nicely demonstrates the following points:

1) For wavelengths greater than 860nm where absorption is approximately zero the maximum and minimum reflection and transmission are each constant.

2) R_{MAX} and T_{MIN} occur at the same wavelengths, R_{MIN} and T_{MAX} occur at the same wavelengths (but different from R_{MAX} and T_{MIN}).

3) Absorption in the cavity causes the reflectivity to fall.

This data is not very accurate, if it were, the sum of R and T should be 1 for wavelengths where $\alpha = 0$. The transmission data were retaken using the monochromator and lock-in amplifier. A standard BPX 65 photodiode was used as the detector. Measurements were taken with the sample out of the beam (for normalisation purposes) and with the sample in the beam. When in the beam, the sample was placed close to the exit slit from the monochromator ensuring no light strayed around the sample. The normalised data is shown as a dashed line in figure 5.10.

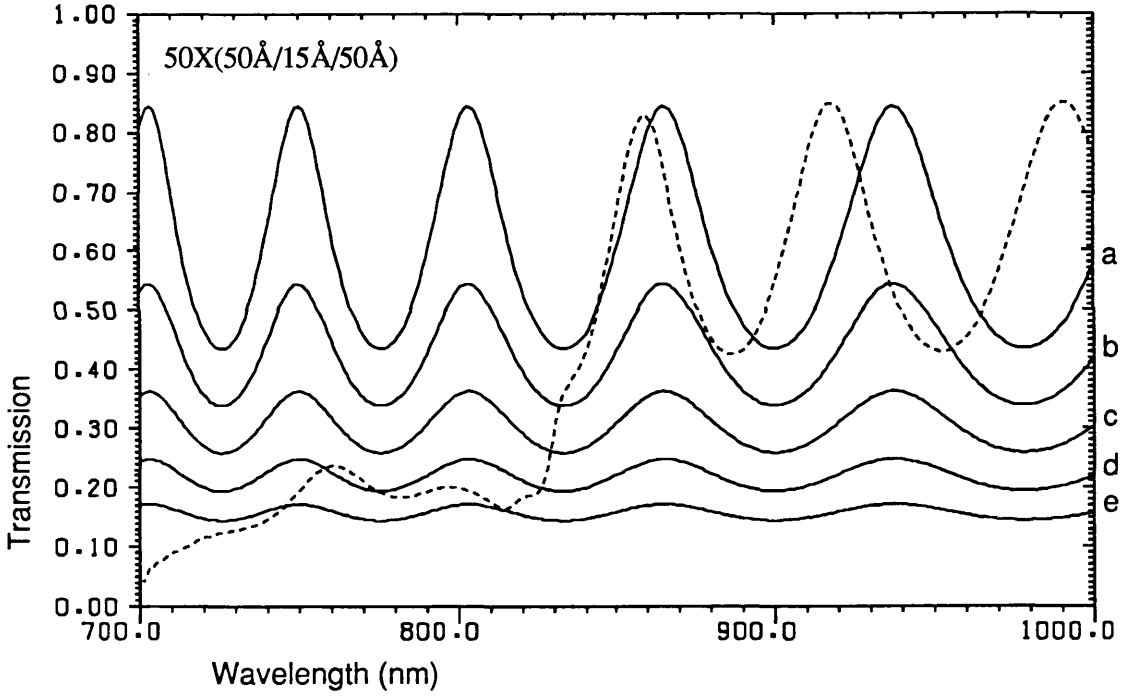

Figure 5.10 Normalised transmission of CB345 mounted on a sapphire disc (dashed) and the calculated transmission for this configuration for different values of absorption coefficient (solid curves). Calculation uses a fixed cavity refractive index of 3.4929 valid only at 814nm, an absorber length d of 0.575μm, a cavity length of 1.61μm and absorption coefficient values of a) 0cm^{-1}, b) 5750cm^{-1}, c) 11500cm^{-1}, d) 17250cm^{-1} and e) 23000cm^{-1}. Note that the calculated curve e) and the measured data agree at 814nm, also the maximum and minimum reflectivities in the low absorption region (high wavelengths) agree.

To gain a better understanding of the spectrum it is instructive to look at the solid curves which plot transmission spectra for different constant absorption coefficients from equation 5.2. Note that wavelengths are NOT DIRECTLY COMPARABLE

with the experimental dashed curve away from 814nm because the calculations do not include the variations of refractive index with wavelength (n_c at 814nm is used).

The front and back reflectivities of the cavity mirrors used are 30% and 9% and the loss at the air sapphire interface is 7.5%, calculated from equation 5.18 and using the relevant indices in table 5.1. Putting the front and back reflectivties into equations 5.11 and 5.12 gives T_{MIN} and T_{MAX} of 47% and 91% respectively and taking into account the loss at the air sapphire interface gives T_{MAX} and T_{MIN} of 43% and 84% - very close to that observed.

At wavelengths above 860nm the oscillations seen are those for $\alpha = 0$ in figure 5.10. At wavelengths below 850nm absorption starts to increase and the observed transmission comes from successively lower solid curves as absorption increases. The spectral feature seen at 831nm is due to a combination of the increase of transmission due to Fabry Perot effects and decrease of transmission due to increased absorption.

At 814nm the exciton peak can be seen as a trough in transmission. This is the wavelength at which the exciton peak was observed in a photo voltage spectrum [Sheffield University]. In order to determine α, equation 5.2 must be used for which it is necessary to know $\sin\delta/2$. δ is determined from the condition upon T_{MAX} ie that $\sin\delta_i/2 = 0$ where i denotes the i^{th} T_{MAX}. The notation here is such that as wavelength is increased, successive T_{MAX} are observed at the wavelengths $\lambda_{(i-1)}$, $\lambda_{(i)}$ etc, the cavity has average refractive indices $n_{c(i-1)}$, $n_{c(i)}$ at these wavelengths. To obtain T_{MAX} it must be that $\delta_i = m_i 2\pi$ and we know that $\delta_i = 4\pi n_{c(i)} L_c/\lambda_i$ from §5.2.3, consequently the product $m_{(i)}\lambda_{(i}/n_{c(i)}$ should be constant at $2L_c$ and equal to $(m_{(i)} + 1)\lambda_{(i-1)}/n_{c(i-1)}$ from which $m_{(i)}$ can be determined, Just using the relation above involves dividing by the difference of similar wavelengths (991-917) and it is more accurate to find the value of $m_{(i)}$ that gives a constant product $2L_c$ for the T_{MAX} peaks (i), $(i-1)$ *and* $(i-2)$. This gives $m_{(i)} = 11$ for λ_i=991nm and a cavity length of 1.61μm. From this α at 814nm is calculated to be 23000cm^{-1} using equation (5.2).

Inaccuracies in $m_{(i)}$ and the cavity length affect the calculation of δ. However at high absorptions the transmisssion as a function of wavelength or δ is almost flat (curve e in figure 5.10). Consequently the calculated value of 23000cm^{-1} for α should be reasonably correct, α is certainly greater than 17250cm^{-1} (curve d). Clearly an anti reflection coating would have aided these measurements.

The main points here are a)the absorption is higher than forecast in §5.3 b) inherently poor absorption cannot be the explanation for lack of exciton features observed in CB294.

§5.7 Redesigned AFPM

With the increased absorption coefficient the figures in table 5.2 no longer hold. The difference is that fewer pairs of CDQWs will be needed to achieve a given value of αd. This has two benefits, 1) a shorter intrinsic region length therefore a lower operating voltage 2) the device is less susceptible to electric field changes. For a peak

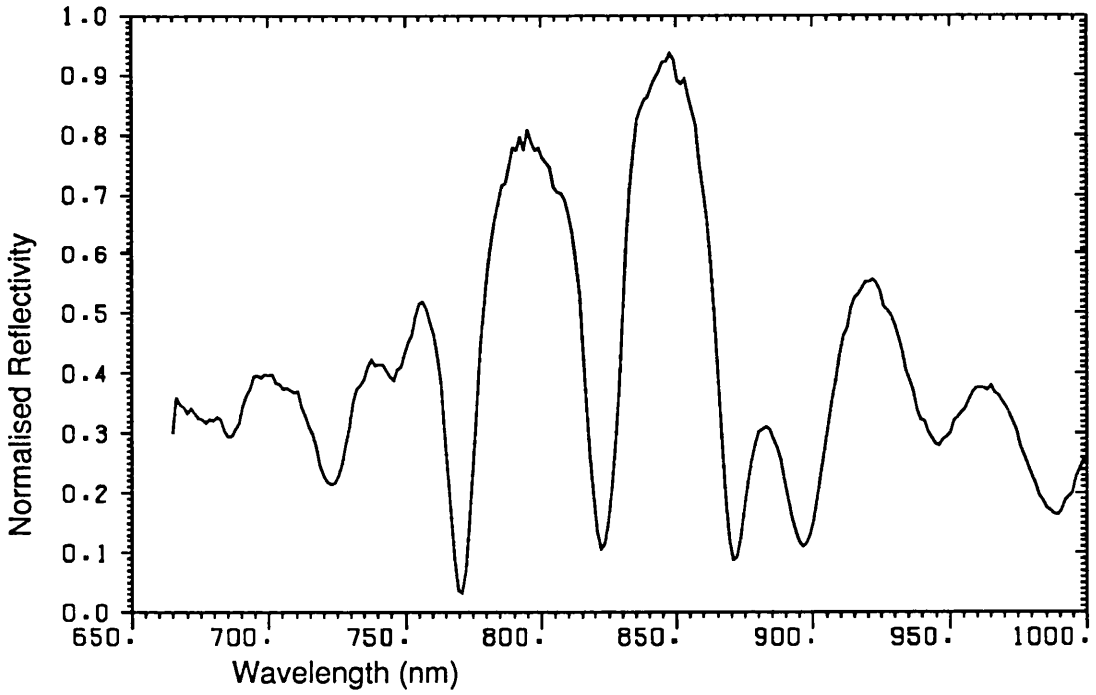

Figure 5.11 Normalised reflectivity from QT133, an AFPM structure containing 14 pairs of coupled quantum wells. Zero field only. The dip in reflection at 822nm is due to the coincidence in wavelength of the excitonic absorption and the Fabry Perot resonance.

absorption coefficient of 23000cm^{-1} the change in reflectivity of the 14 pair CDQW device is now expected to be 4% to 23% (from equation 5.10).

The AFPM was redesigned, this time 14 pairs of CDQWs were specified, the extra doping layer was omitted in favour of a dead space because this technique had worked before (QT67), for this number of wells the predicted operating voltages for an extra doped layer or a dead space are 1.75V and 3.75V respectively. The GaAs cap thickness was reduced to 100Å and the structure grown with a p-type MLS as is more usual for these devices. The layers were grown as QT133, mapping of this wafer clearly showed an excitonic peak. The normalised reflectivity of a device taken from a 'correct' part of the wafer is shown in figure 5.11, the data being measured on the OMA.

The dip in reflectivity at 822nm to $\approx$10% is the off state reflectivity and in consistent with an off state value of αd of $\approx$0.3 , corresponding to an absorption coefficient of 19000 cm^{-1} , whilst the OMA data is not very accurate it is consistent with the findings in §5.6 that the absorption coefficient is greater than 17250 cm^{-1}. Unfortunately application of a reverse bias to the device made no measurable change to the reflectivity. A number of other devices from the wafer were bonded but exhibited similar behaviour. The photocurrent spectra show no shift of peaks with bias, just an increase in photocurrent with reverse bias, the currents were low compared with those from other devices and noisy.

Sadly there has not been time to find the cause of this problem or repeat the growth and processing. It seems highly likely that the device will work as predicted because all aspects have been tested before; the modelling was verified from photocurrent measurements (chapter 4), a 'dead space' has been used previously (QT67), the absorption coefficient is high and the 0V reflectivity is as expected.

In summary, the use of CDQWs in an AFPM was predicted for the first time [Atkinson *et al* (1990)] based upon an estimate of the absorption coefficient. When a device failed to work the absorption coefficient at room temperature was determined experimentally to be greater than 17250cm^{-1}. There have been no previous measurements of the value of the absorption coefficient for a similar device at room temperature and in a non-waveguide configuration. The AFPM was redesigned and regrown, the new AFPM exhibited the expected zero field reflectivity. Although I have not succeeded in observing any change in reflectivity with applied bias, all the component mechanisms have been checked previously.

Chapter 6 Further Device Improvements

This chapter considers various ways of improving the performance of quantum well modulators. The first section uses the model developed in chapters 2 and 3 to investigate the barrier between wells in 'uncoupled' multiple quantum wells. The second section models the absorption spectra from an asymmetric well potential, its application to optical modulators is discussed.

§6.1 Thin barriers in multiple quantum wells.

§6.1.1 Introduction

The great majority of published modulator results involve structures containing multiple quantum wells. It has become standard to use barriers with widths of typically 60Å or greater. This barrier width is assumed to be sufficient to prevent significant coupling between carriers localised in different wells. There has not been a study of how narrow the barrier can be made without coupling effects changing the performance of these devices. It is generally desirable to have this barrier width as thin as possible, this permits the intrinsic region to be shorter for a given number of wells enabling lower operating voltages to be used for the same absorption change and resulting in a smaller field change across the wells due to background doping. Given that the work on coupling in chapters 4 and 5 revolved around barriers with widths of only 15Å it appeared plausible that one might be able to use barriers in multiple quantum wells with widths less than 60Å.

§6.1.2 Model Results.

All finite width barriers will cause some coupling in multiple quantum well structures. The series of wells should be thought of as one whole structure. In this structure there are many more levels than in one of the individual, isolated wells (in fact the number of levels is approximately the product of the number of wells and the number of energy levels in an isolated well). In the limit of very wide barriers the multiple quantum well levels are degenerate about isolated well levels, just as in figure 4.2 where the coupled well levels tended to those of the narrower single well. To investigate just how wide the barriers need to be one should ideally model electroabsorption spectra from the whole multiple quantum well structure. The large number of energy levels make computer modelling difficult because all these energy levels must be found as well as their corresponding wavefunctions. Furthermore, at large distances from the centre of the structure the argument of the Airy function (equation 2.14) becomes too large for the computer program. The latter point might be circumvented by a transformation of the distance variable z because no physical parameter (eg energy or wavefunction) goes to infinity. However, the problem of many levels is a property of the system.

I decided to model one, two, three and four wells, if there was no significant difference between the spectra as more wells were added then I felt I could assume the spectra were valid for a larger number of wells. Some justification for this assump-

tion comes from Kolbas *et al* who showed that as more wells are coupled together the width of the 'band' formed at zero field rapidly approaches the superlattice energy band width. In other words, if a single well has an energy level E_1, then two of these wells coupled will have two energy levels separated by an energy ΔE_2 and centred approximately on E_1; three wells coupled will have three energy levels with total separation ΔE_3 centred approximately on E_1 etc. For n wells the width of the 'band' is ΔE_n. As n is increased from 2, ΔE_n increases most at low n before rapidly approaching the superlattice limit ΔE_∞, hence by modelling one, two and three wells one should be able to spot significant coupling effects.

The well widths used in this modelling were 95Å because a) this is the same as that used in the successful AFPM work of Whitehead *et al* (Jul 1989) and close to that of Yan *et al* (1989), and b) for some time an ordinary p-i-n sample had been ordered from Sheffield by Mark Whitehead with fifty 95Å GaAs wells and 40Å $Al_{0.3}Ga_{0.7}As$ barriers. Some of the wavefunctions from a single 95Å well are plotted in figure 6.1 for zero electric field. The two vertical lines denote the edges of the well. All the depicted wavefunctions except the lh_2 decay quite rapidly in the barrier, for example at 40Å from the well/barrier interface the e_1 wavefunction has 2.5% of its maximum value. The implication of this figure is that by placing another well at about 50Å or more away from this well, the interaction between wavefunctions will be weak, at least for the lower energy levels.

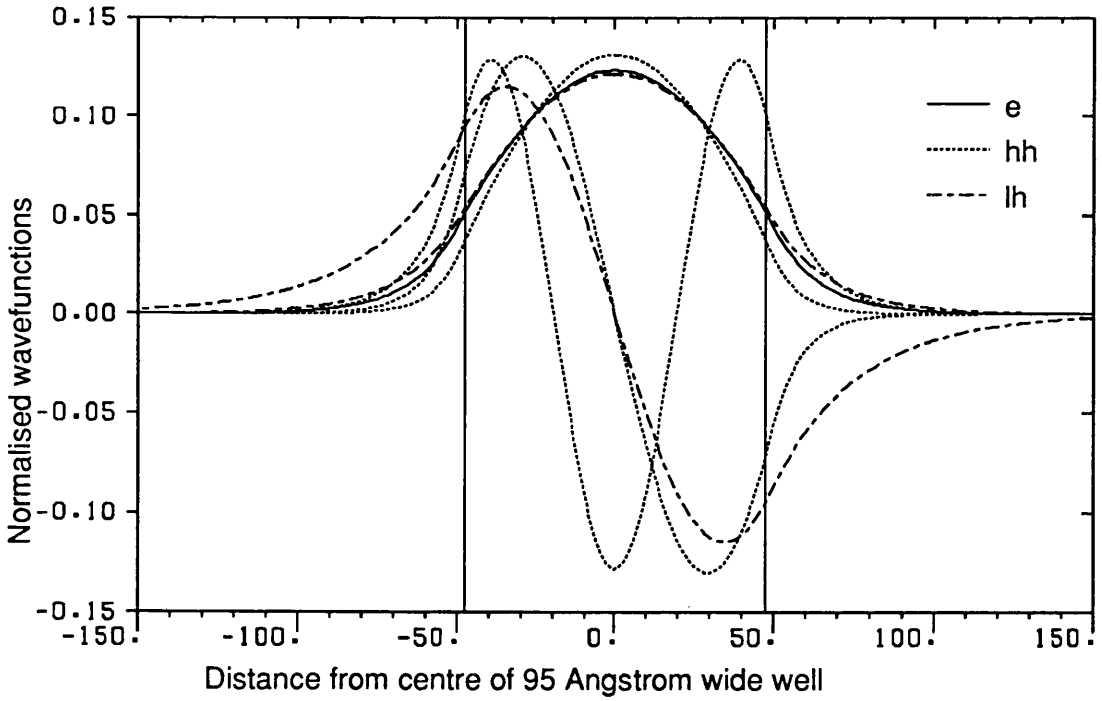

Figure 6.1 showing the normalised wavefunctions for all energy levels less than 100meV from the bottom of a 95Å wide well. Vertical lines denote the well walls.

In figure 6.2 the energy levels for two 95Å wells separated by a variable width

barrier are plotted. As the barrier width is reduced from a large value the separation of the almost degenerate energy levels increases. The barrier width at which the splitting is observed depends upon the carrier due to the different confinements of the different carriers and is related to the spread of the wavefunction into the barrier material shown in figure 6.1. For a 40Å barrier width the splittings (ΔE_2) of the lowest state are 1.84 meV for electrons, 0.04 meV for heavy holes and 2.27 meV for the light holes. The exciton FWHM used in the modelling is 8.5meV implying that for 40Å barriers the coupling induced broadening is acceptable. (By comparison ΔE_3 is 2.59 meV for electrons, 0.06 meV for heavy holes and 3.2meV for light holes and ΔE_4 is 2.96 meV for electrons, 0.07 meV for heavy holes and 3.67meV for light holes.)

The results presented so far have all been for zero field. Next the results of calculations of absorption spectra on various structures are presented at fields of both zero and 77kV/cm. (This field was chosen to correspond to the 9V operating voltage in Whitehead *et al* (Jul 1989) .) Figure 6.3 illustrates spectra for a single 95Å well, two 95Å wells coupled with a 40Å barrier, and three and four wells coupled with 40Å barriers.

The calculations show little difference in the absorption spectra at the operating wavelength (859nm in the modelled data). If coupling between the wells were important then I would expect to observe the rapid movement of the e_1hh_1 peak and see absorption features at wavelengths other than those seen in the single quantum well case. There is not perfect agreement between spectra largely because of errors in the modelling. In the 77kV/cm spectra, not all the energy levels that contribute to the lower wavelength peaks have been found to save time. As a result there is some discrepancy in the spectra at lower wavelengths. (This short cut was not used in the modelling of chapter 4.) For zero field no energy levels are neglected, the discrepancies between the single and coupled well spectra are due to genuine coupling and to modelling errors. The extent to which coupling is causing the observed effect was determined from modelling the 95Å/40Å/95Ådouble well structure and a 95Å/70Å/95Å structure where coupling effects should certainly be negligible. The result of this is that there is closer agreement at the e_1hh_1 exciton peak but there is still the discrepancy at 800-850nm, this discrepancy is worse in the 70Å barrier case. The cause of this was eventually traced to the computer routine that generates absorption spectra from the calculated overlaps. In order to calculate the Rydberg (equation 2.48) weighted averages were used for ϵ_r and for the effective masses perpendicular to the well plane used in the calculation of the reduced mass μ. This is assumed to be valid for narrow barriers where there is a considerable portion of the wavefunctions in the barrier, furthermore the effect of a weighted average will be small when the barrier width is small. When the system is essentially uncoupled the barrier material should not be included in the averaging.

In conclusion, this theoretical investigation of the coupling due to 40Å barriers between 95Å wells shows that one should not expect the bias absorbing modulation,

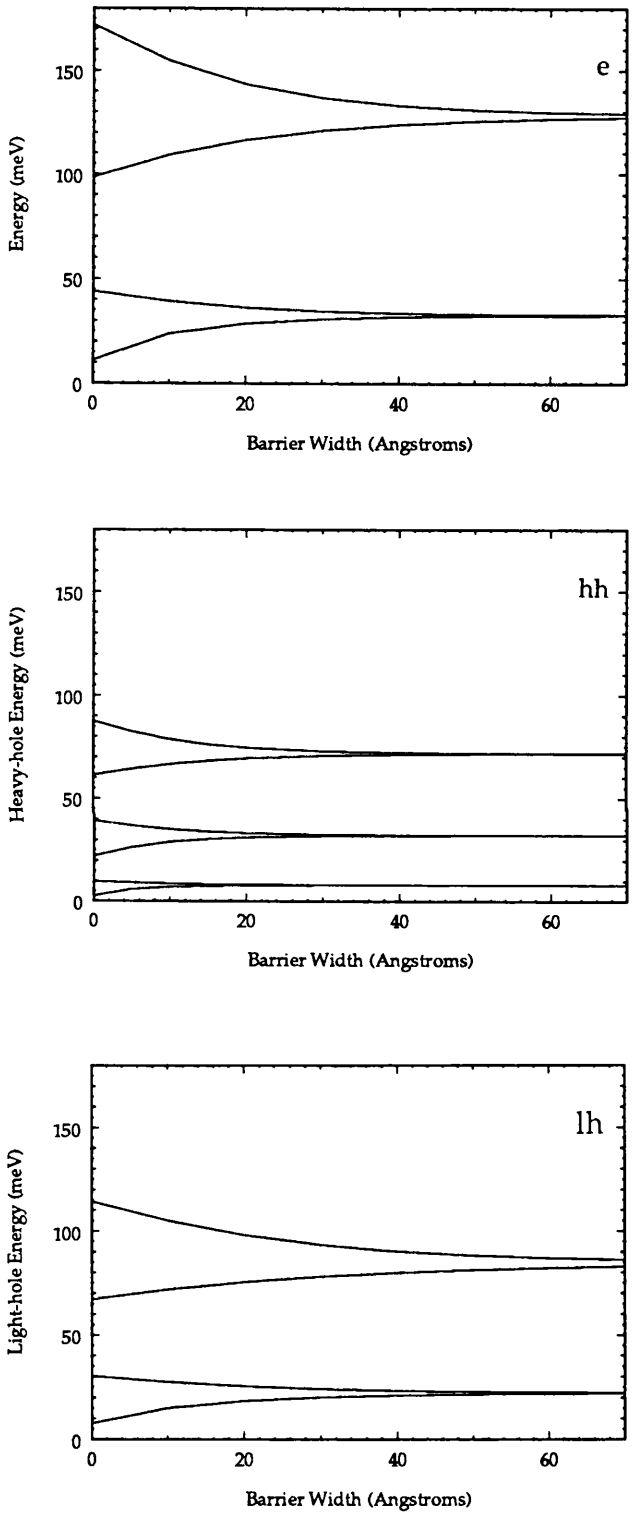

Figure 6.2 Plot of energy levels for two 95Å wide GaAs wells coupled by an $Al_{0.3}Ga_{0.7}As$ barrier of variable width. All energy levels for zero electric field.

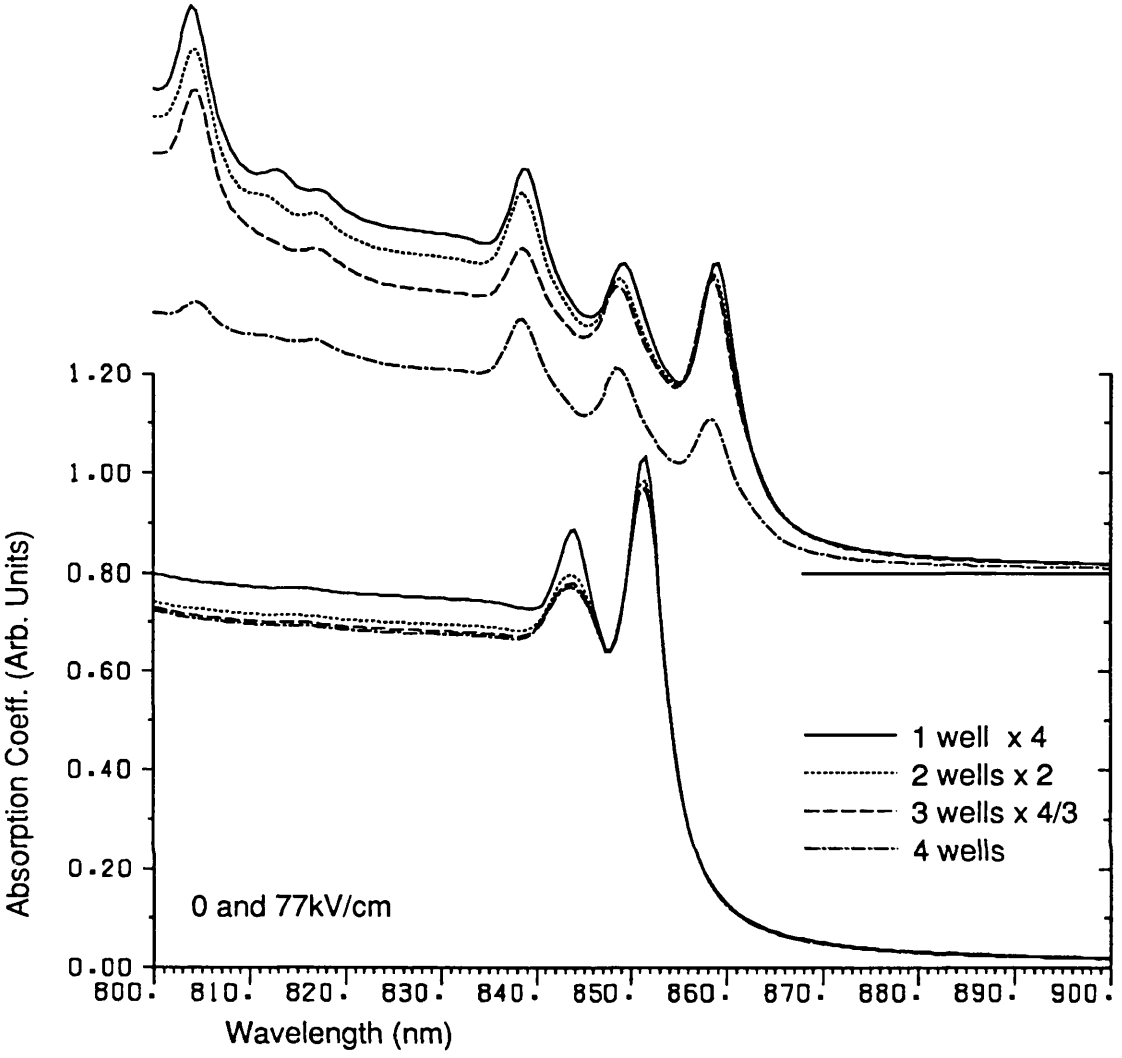

Figure 6.3 Calculated room temperature 0kV/cm and 77kV/cm spectra for different numbers of 95Å GaAs wells separated by 40Å $Al_{0.3}Ga_{0.7}As$ barriers. Erroneous missing of energy levels results in poorer agreement of the 77kV/cm spectra.

at 859nm, to be significantly affected by coupling between wells.

The modelling is not exhaustive in that the spectra for other barrier widths have not been modelled, also only two electric fields are considered here.

§6.1.3 Experimental Results

The MQW structure with fifty 95Å GaAs wells and 40Å $Al_{0.3}Ga_{0.7}As$ barriers was grown as CB190, CB233 and CB288. The repeats were due to the problem of high background doping (see chapter 4). Photocurrent from CB288 is shown in figure 6.4. Photocurrent from CB190 is similar to CB288 and CB233 is similar to both of them except that the features are less distinct. It is not clear whether coupling is occurring with bias at wavelengths of 860nm or greater, or whether background doping is causing

the broadening. In a similar fashion to QT67 a sample was grown with only 10 wells located centrally in a total of 1.135μm of intrinsic material, this has the code name CB308. Photocurrent results are presented in figure 6.5 along with the calculated absorption spectra for a single 95Å wide quantum well. Coupling is not occurring to a significant extent, the peaks are observed at the expected wavelengths and shift as expected for a series of uncoupled 95Å wide wells.

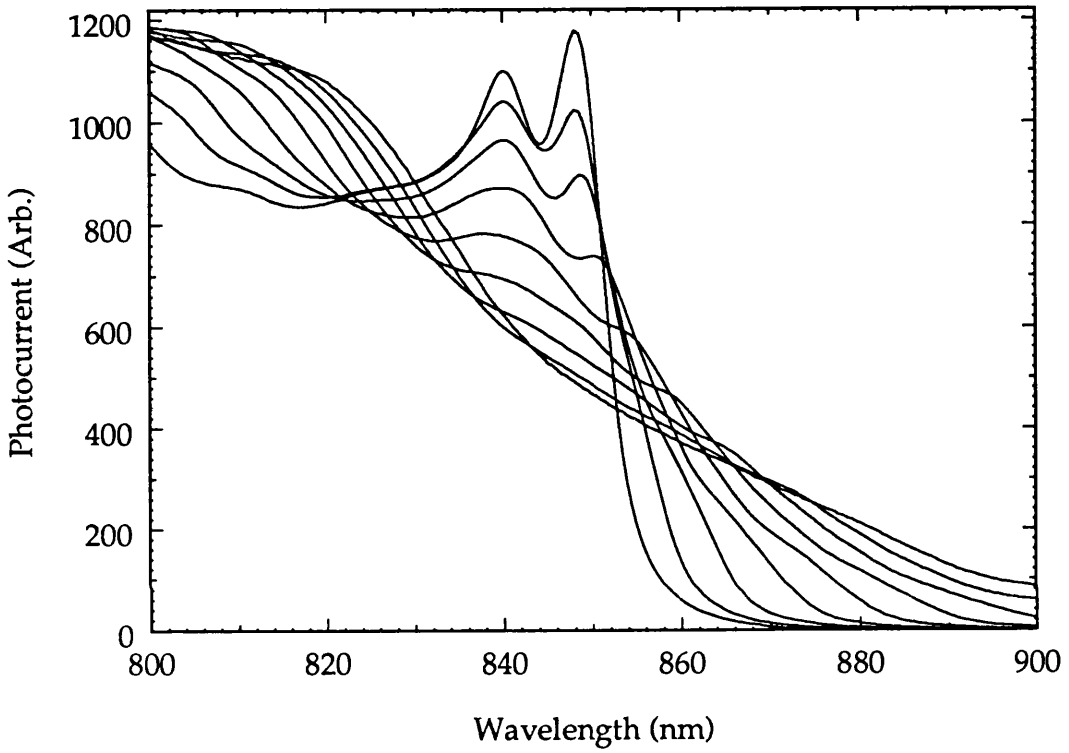

Figure 6.4 Photocurrent data (raw) from CB288 for reverse biases from 0V to 16V in steps of 2V. The intrinsic region is 50 × (95Å GaAs + 40Å $Al_{0.3}Ga_{0.7}As$) and 400Å of undoped $Al_{0.3}Ga_{0.7}As$ buffer next to the p region. Approximate background doping $10^{16}cm^{-3}$.

§6.1.4 Future work

This type of analysis could be applied to multiple quantum wells with other well widths, indeed the study for the 95Å well has not been exhaustive. The benefits of reducing the barrier width are more fruitful when the barrier material occupies a larger proportion of the intrinsic region, ie in the narrow well case.

The work of chapters 4 and 5 used 85Å barriers between the coupled double well pairs, this barrier width was assumed to prevent coupling between the CDQW pairs and it is likely in view of the work in this chapter that this width could be reduced.

The analysis in this section required a considerable amount of computer time because of the large number of energy levels and wavefunctions that have to be found, for example in the four wells modelling the zero field spectrum is the sum of 192

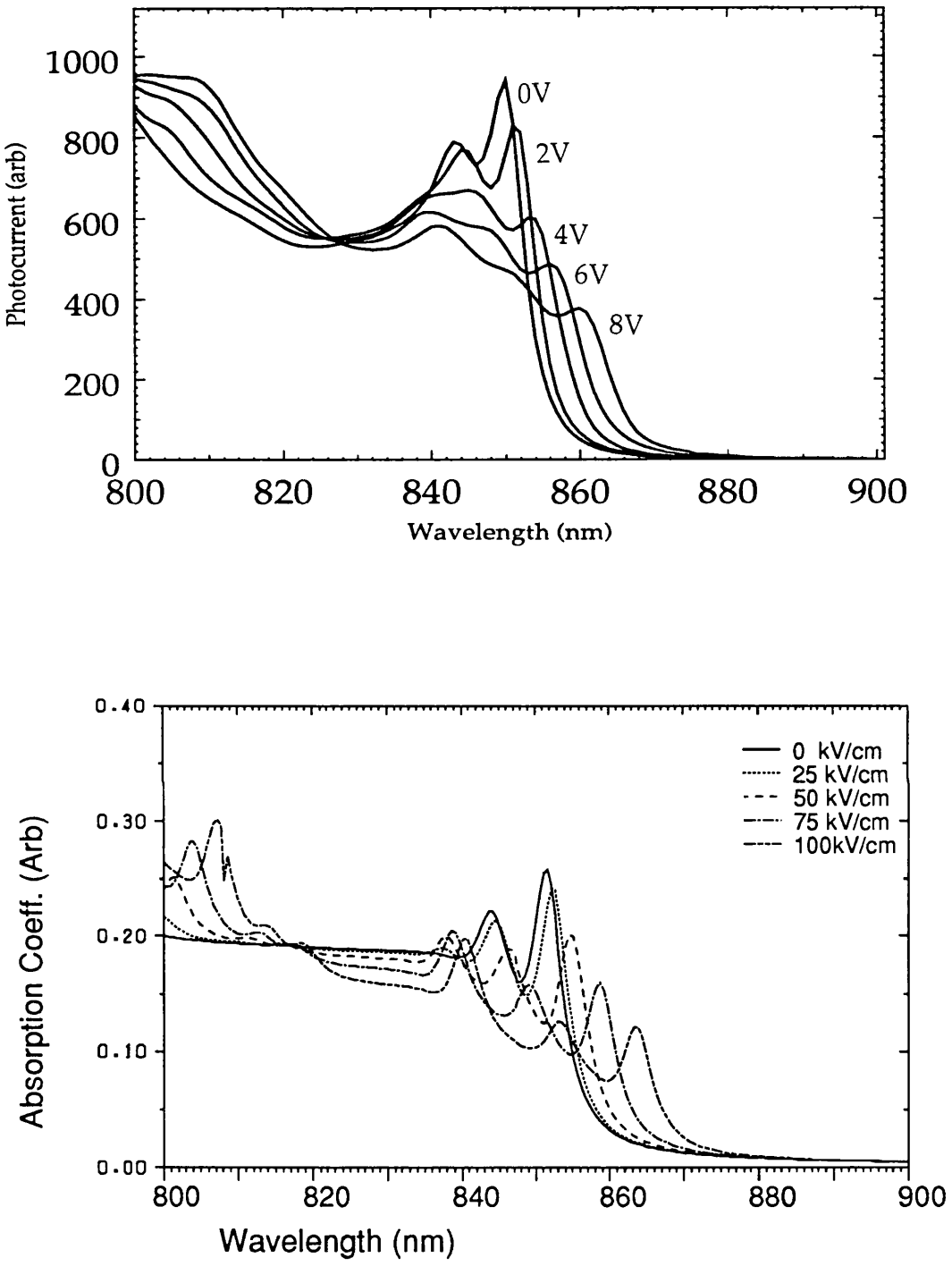

Figure 6.5 Raw photocurrent data from CB308 (upper graph) and calculated absorption spectra for a single 95Å wide well (lower graph). CB308's intrinsic region is 0.5μm of $Al_{0.32}Ga_{0.68}As$, $10 \times$ (95Å GaAs + 40Å $Al_{0.32}Ga_{0.68}As$) followed by a further 0.5μm of undoped $Al_{0.32}Ga_{0.68}As$. All the photocurrent data has been scaled by the same amount in the vertical direction in order that the experimental and theoretical spectra at the 'continua' (826nm for photocurrent, 820nm in the calculated data) have the same physical height in this diagram.

absorption peaks and although most of the peaks have zero height, each energy level contributes to the spectrum at least once.

As a short cut to determining the minimum barrier width in a multiple quantum well I believe it may be sufficient just to find the barrier width that gives no significant difference between the single and double well zero field spectra. The reasons for this are that a) at zero field coupling effects are most noticeable in going from one to two wells (previous discussion) and b) with field applied Wannier-Stark localisation rapidly takes place in these structures compared to normal superlattices which have wider energy bands and narrower barriers. From Bleuse *et al* (Jan 1988) the condition for Wannier Stark localisation is $F > \Delta E_n/ep$ where F is the electric field after bias is applied, e is the electronic charge and p is the multiple quantum well period. If the zero field spectra from one and two wells are similar ΔE_n should be less than about 8meV (the exciton FWHM), the shortest period one might reasonably envisage is $\approx$60Å hence localisation should occur so long as the field is greater than 15kV/cm, which is usually the case.

There has been a general reluctance to use narrow wells (less than 60Å) in multiple quantum wells partly because the electric fields required to cause a given shift of the exciton peak are large (see figure 3.9). If, between different biases the absorption coefficient α varies between α_{MAX} and α_{MIN} then Jelley *et al* (1989) showed experimentally that large changes in absorption coefficient $(\alpha_{MAX} - \alpha_{MIN})$ and large values of the ratio $\alpha_{MAX}/\alpha_{MIN}$ can be achieved with 35Å to 50Å wide wells at bias absorbing wavelengths (see figure 3.4 which reproduces Jelley *et al*'s 35Å absorption spectrum). * The trade off between improved absorption and increased electric fields has generally favoured larger well widths, however Pezeshki *et al* have recently demonstrated an AFPM operating with 50Å multiple quantum wells, they obtained an insertion loss of only 1.2dB, a modulation ratio of 7.5:1 with a 5V operating bias. This low insertion loss is largely achieved because they have used a narrow well with a large value of the ratio $\alpha_{MAX}/\alpha_{MIN}$. The well/barrier structure is nineteen 50Å GaAs wells and 75Å $Al_{0.33}Ga_{0.67}As$ barriers. Application of the ideas mentioned above to 50Å wells could yield thinner barriers and lower operating voltages, the benefits being greater for narrow wells where the barrier material occupies a larger proportion of the intrinsic region.

Figure 6.6 plots the calculated room temperature spectra for 50Å wells separated by various barrier widths. To prevent the errors in §6.1.2 the averaging of ϵ_r and effective masses in the Rydberg calculation has been suspended here and just the

* Much larger ratios can be obtained by working at low temperatures because the broadening of the absorption peak is small. Bailey *et al* (1989) demonstrated a transmission device with one hundred 100Å GaAs wells showing a ratio of biased to unbiased transmission of 1000:1 at 1.3K, this compares with a best value of 5.4:1 at room temperature for the same device. I shall only be concerned here with room temperature operation.

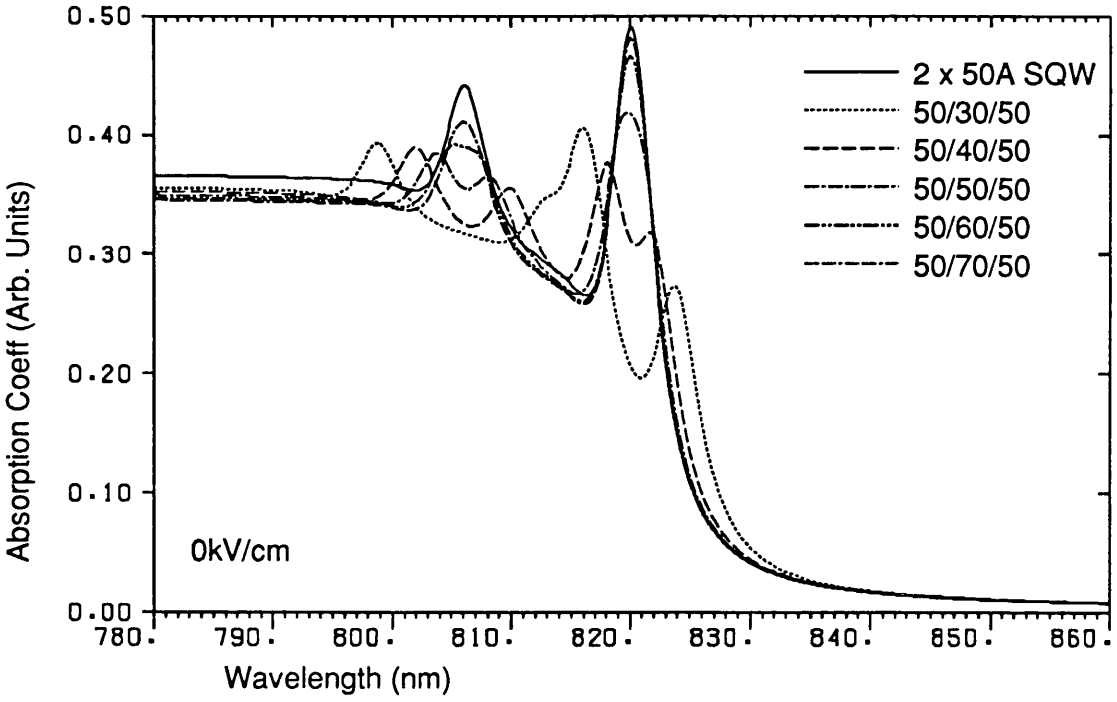

Figure 6.6. Calculated room temperature zero field absorption spectra for six structures. The 50Å single quantum well spectrum has been doubled to compare with the five double well structures. All wells are 50Å GaAs, barrier widths vary from 30Å to 70Å and are composed of $Al_{0.3}Ga_{0.7}As$.

GaAs values used. A 30Å barrier clearly results in coupling and there is little evidence of coupling at 60Å . By the arguments in the previous part of this section, 60Å should be acceptable as a barrier between 50Å wells.

It may be possible to use even thinner barriers if the operating wavelength is in the tail of the zero field e_1hh_1 peak ie. $\lambda \geq$830nm. This is often the case in narrow wells because the e_1hh_1 exciton maintains its height well with field yielding the large values of $\alpha_{MAX} - \alpha_{MIN}$ and $\alpha_{MAX}/\alpha_{MIN}$ mentioned earlier.

The single 50Å well and 50Å/40Å/50Å CDQW spectra in figure 6.6 have the same absorption coefficient at 830nm. When field is applied Wannier-Stark localisation will occur and the absorption coefficients should be the same. This idea should be qualified by noting that there is a significant difference in the spectra at lower wavelengths. The 50Å/40Å/50Å spectrum clearly shows two peaks (e_1hh_1 and e_2hh_2 at 822nm and 818nm respectively), for many wells one can expect a superlattice band width with a wider separation than this. The result could be increased α_{MIN} at ≈835nm. However, to counter this it could be the case that the built in field causes localisation due to the Wannier-Stark effect even at zero bias and all behaviour at wavelengths greater than 830nm is multiple quantum well like.

§6.1.5 Conclusion

The theoretical modelling and experimental photocurrent results have demon-

strated that 40Å $Al_{0.3}Ga_{0.7}As$ barriers between 95Å GaAs wells do not affect the optical modulation. A reduction of barrier width from 60Å to 40Å yields a 13% decrease in the length of the intrinsic region. This should yield a reduction in operating voltage of a similar percentage, a 9V operating voltage would become 7.8V.

Modelling of coupled 50Å GaAs wells implies that 60Å $Al_{0.3}Ga_{0.7}As$ barriers could be used. It is possible that even narrower barriers would be acceptable for bias absorbing operation.

[Note added after completion of this work. McIlvaney *et al* have published the transmission spectra from a device composed of 200 50Å GaAs wells and 200 50Å $Al_{0.3}Ga_{0.7}As$ barriers for use in a 2x2 array. The spectral features are clearly visible, a comparison with a wider barrier sample and with an antireflection coating to remove Fabry Perot effects would be useful.]

§6.2 Asymmetric Coupled Wells

The work so far in this thesis has concentrated upon symmetric coupled wells. In this section an asymmetric coupled well structure is considered ie pairs of wells of different width and/or depth coupled together. To facilitate this work the computer programs had to be generalised to allow for wells with different aluminium concentrations (ie different depths), the mathematics of chapter 2 is unchanged.

§6.2.1 The Structure of Golub *et al.*

In December 1988 Golub *et al* published the calculated 'electron-hole overlap' [ie e_1hh_1 overlap integral] as a function of field for the asymmetric structure of figure 6.7a. The overlap remains close to its maximum value of 1 for fields from 0 to 30kV/cm whereupon it falls very sharply to zero for all higher fields, depicted schematically in figure 6.7b. This calculation is supported by similar behaviour of the 10K "Photoluminescent yield for weak ($1W/cm^2$) excitation at 633nm".

This behaviour has the potential to be very useful for low voltage optical modulators where there is a built in field present. It is possible to achieve background dopings of the order of $5 \times 10^{14}cm^{-3}$ (eg Lengyel *et al*) for which the slope of field with distance across the intrinsic region of a p-i-n diode is fairly small (7kV/cm across one micron). The built in field, however, is fundamental to the device. The attraction of the Golub results is that the peak height, which is directly related to the overlap integral (equation 2.47), maintains a high value up to a certain transition field strength (F_T) after which it falls rapidly. The transition field is largely determined by the well/barrier structure and can be adjusted by design. If application of a reverse bias increases the field experienced by the wells through F_T (see figure 6.7c) then a rapid change in height of the e_1hh_1 peak could be achieved for a small change in voltage. Hence I believed this would be manifested by a large change in absorption for a small change in voltage.

I modelled the electroabsorption for this structure and the result is shown in figure 6.8. This shows no useful electroabsorption changes.

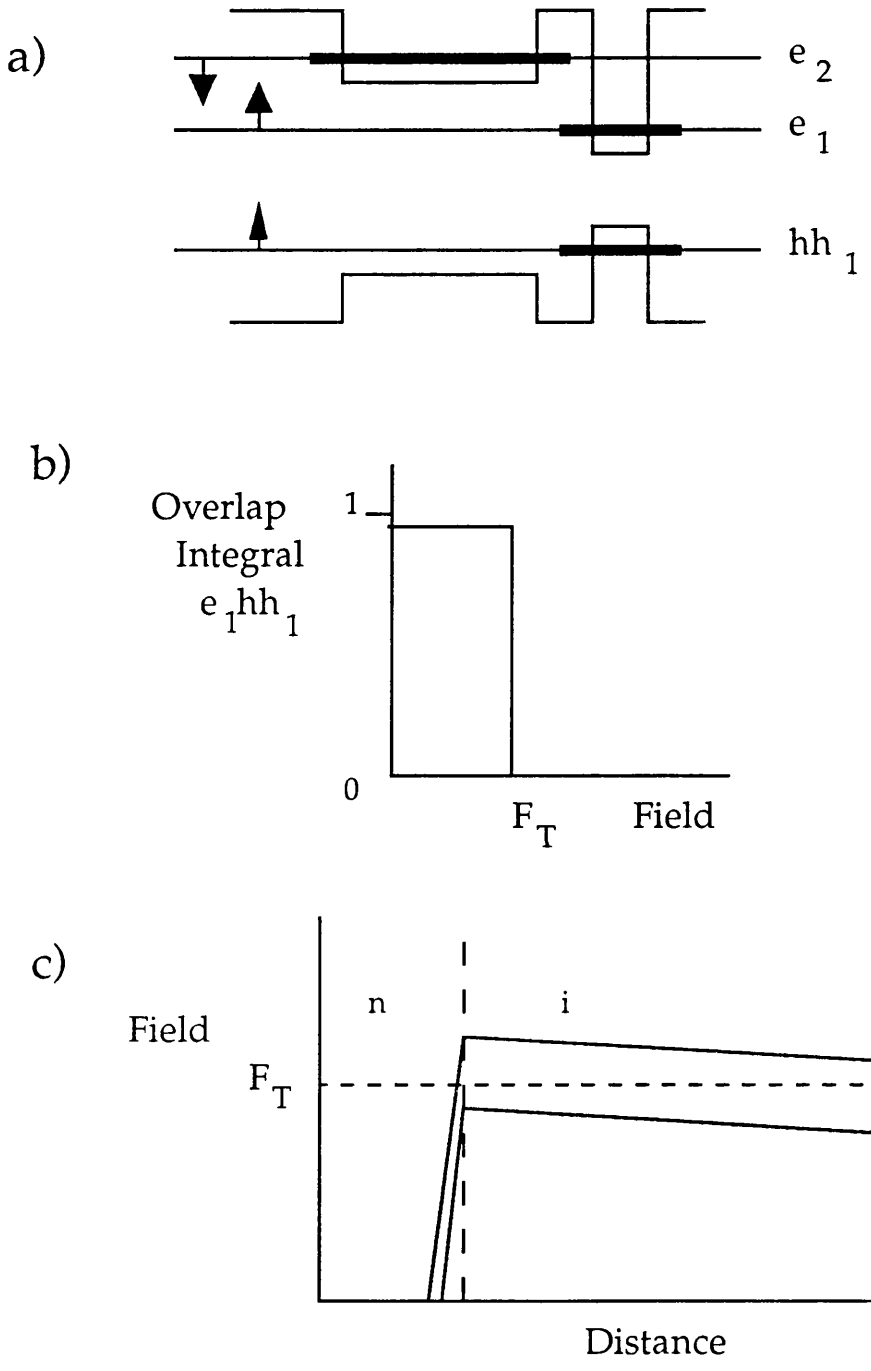

Figure 6.7 Schematic representations of
a) The well/barrier potential, e_1, e_2 and hh_1 energy levels at zero field. Thick portion of energy level denotes wavefunction localisation. Arrows show direction of movement of energy levels in a positive electric field.
b) Behaviour of the $e_1 hh_1$ overlap integral showing rapid fall at field F_T.
c) Field profile of a good p-i-n diode at 0V and a small reverse bias. With bias applied the field in the i region increases through F_T, hence the overlap will fall rapidly.

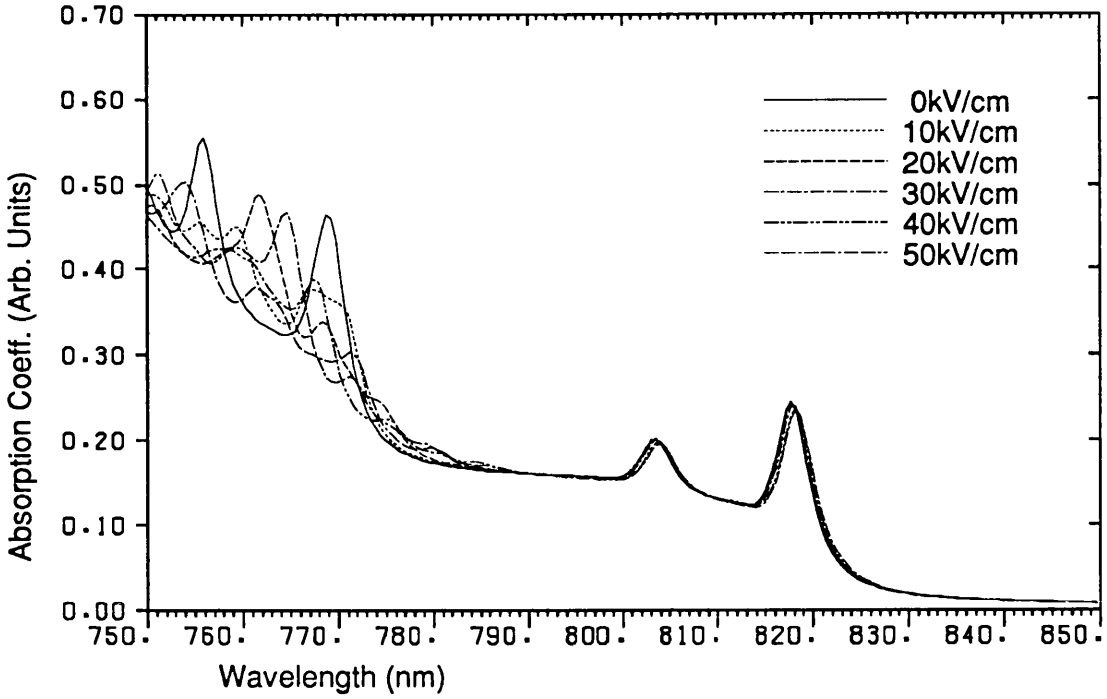

Figure 6.8 Calculated absorption coefficient for the structure in figure 6.7.

It is not that the model is in error, it predicts the rapid fall in e_1hh_1 overlap, at 20kV/cm the overlap is 0.96, at 30kV/cm it is 0.005. The fall of e_1hh_1 is almost exactly compensated by the rise of e_2hh_1 at an energy less than 1meV from the e_1hh_1 peak. This can be seen from the wavefunctions in figure 6.9.

In retrospect the absorption spectrum of figure 6.8 shows approximately the sum of the absorption spectra from the two wells isolated. The wide 36Å barrier leads to a close anticrossing of the e_1 and e_2 energy levels, hence the rapid fall in e_1hh_1, however, because the anticrossing is close, the 'repulsion' is small and e_2hh_1 grows at a similar wavelength. The photoluminescent yield fell in Golub's paper because at 10K where kT is 0.8meV the photoluminescent yield will show only the lowest energy transition and any within $\approx$0.8meV of this. For fields up to 20kV/cm the overlap is high and the radiative lifetime will be short, resulting in a high photoluminescent yield [P. Dawson private communication]. At fields just above the anticrossing (where separation of e_1 and e_2 is greater than $\approx$0.8meV) the e_1hh_1 overlap is small and the radiative lifetime is long giving a low photoluminescent yield. Hence there is a rapid fall in overlap but it is probably not a cure for the built in field problem.

For electroabsorption modulators this structure with a wide barrier does not appear to have much to offer, I shall now briefly consider narrowing the barrier. At this point an analogy with the discussion in section §4.3.1 can be drawn. A wide barrier gives rapid field movement but does not widely separate the lower energy levels in the resonant condition. (The 'resonant condition' here means the field at which two energy levels come close together, in the Golub structure this is at the transition field

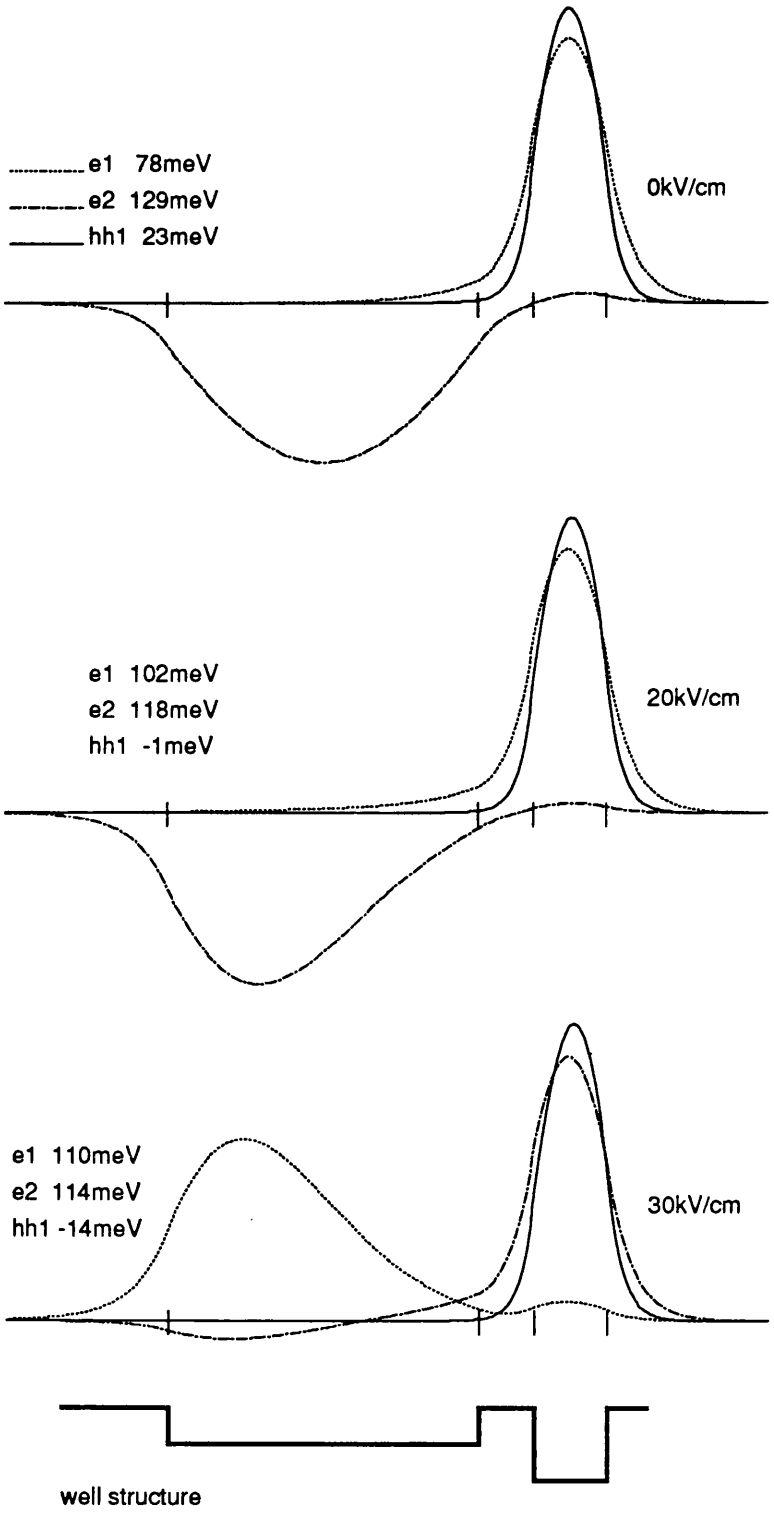

Figure 6.9 showing the normalized e_1, e_2 and hh_1 wavefunctions at three different positive electric fields as a function of distance, vertical bars show material interfaces. Note the switch in localisations of e_1 and e_2 between 20 and 30kV/cm while the transition energy remains approximately constant ($102 - 1 \approx 114 - 14$).

F_T, in the symmetric double well it is at zero field.) A narrow barrier gives poorer field performance but separates the resonant levels. In chapter 4 there existed an optimum width for modulation, in the asymmetric well case it is not clear without further modelling if an optimum exists or if it is useful. However, the symmetric pair is the only structure in which both electrons and holes can, in general, be at resonance at the same field (0kV/cm). As the rapid delocalisation of both electrons and holes plays a major part in the low field operation of the symmetric CDQW it seems likely that symmetric wells are preferable to asymmetric ones.

In conclusion, an asymmetric double well structure was studied because it was thought that the asymmetry might be used to offset the built in field in a p-i-n diode.(The asymmetry can in some ways be thought of as effectively a bias field.) For the structure studied no useful modulation was predicted although it is possible that with a narrower barrier more useful effects may be seen. Analogies with the study in chapter 4 of symmetric wells are made and further work is necessary but the general case of asymmetric quantum wells is fundamentally different in that one is not able to achieve resonance for all carriers at one value of field hence it is unlikely that there will be rapid changes in absorption with bias. It is unfortunate that in symmetric well devices this one field is zero, which presents some practical difficulties.

Chapter 7 Conclusions

The relatively simple quantum mechanics in this thesis and in other published works is adequate for calculating energy levels and wavefunctions. With some empirical data the most fundamental parameter, absorption coefficient, can be reliably calculated for wavelengths in the region of the absorption edge. A simple effective mass model appears to suffice, there is no need to consider energy dependent effective masses, strain, Sommerfeld factors, band mixing and more complex band structure parameters, at least not in GaAs wells with AlGaAs barriers where the concentration of aluminium is less than 45%.

This theory appears valid for a wide range of well and barrier structures and the model developed during the course of this thesis was used to handle single wells, pairs of both symmetric and asymmetric wells coupled together and 3 and 4 coupled wells. It is important when modelling coupled wells to include all transitions and not just the ground states. The theory was applied in detail to one particular coupled well structure in chapter 4 and the barrier width optimised for optical modulation. From photocurrent measurements, absorption measurements and the zero field AFPM reflectivity in chapters 4 and 5 there is little doubt that these devices will function as optical modulators at room temperature. Futhermore the modelling should be readily applicable to other coupled well structures and to non rectangular well shapes.

Growth by MOVPE produces devices with remarkably consistent well and barrier widths within one sample. However, the reproducibility from sample to sample for coupled well structures has shown variation in the work for this thesis (see table 4.1). One further problem was that of unintentional background doping caused by impurities in the intrinsic region of the device. This leads to broadening of the absorption spectrum due to variations of the electric field. The reproducibility problems and level of background doping require further investigation. The scope for reducing broadening mechanisms at room temperature through growth improvements is limited so long as low doping is achieved in growth because the dominant broadening mechanism is then thermal (phonon) broadening. It may be that MBE is a more reliable growth technique although the economic considerations of this and device mass production are a separate topic.

The yield of suitable devices from a wafer is excellent for non resonant devices and has not presented us with any problems. However, for an AFPM structure, the variation of layer thicknesses across a wafer sometimes results in only small areas of the wafer being usable. For arrays of devices that cover larger areas than single devices these fluctuations will in future need to be reduced.

Following the above comments on theory and growth some of the options available are discussed next. It should not be long before theoretical studies of GaAs based quantum wells will have looked comprehensively at the practical range of well widths, barrier widths, well and barrier material composition and number of wells for non resonant and AFPM devices. In the latter case the effects of different cavity lengths

and mirror reflectivities will additionally have been considered. Variations of all these parameters lead to trade offs between insertion loss, contrast ratio, operating voltage, intrinsic region length, capacitance, bandwidth and sensitivity to the built in voltage. The ideal compromise depends upon the system into which the device is to be applied. A study of the system requirements is beyond the scope of this thesis but if low voltage and a high contrast ratio at the expense of some insertion loss is desired the 50Å/15Å/50Å CDQW operating in bias transmitting mode ("normally-off" for an AFPM) may be used. This structure exhibits a ratio of maximum to minimum absorption coefficient of about 2:1 for a 25kV/cm electric field. It is generally true that the larger the value of the ratio mentioned above, the better both the insertion loss and contrast ratio that can be obtained. The value of 2:1 in this particular CDQW is lower than most MQW devices but on the other hand the operating field is considerably reduced. Coupled well pairs with well widths other than 50Å need to be studied to try to improve this ratio.

If low insertion loss, high contrast ratio applications that can support moderate drive voltages are required then such a situation lends itself towards MQW structures with narrower quantum wells. Here the ratio of maximum to minimum absorption is at its largest ($\approx$6.5:1 for 50Å wells [Jelley *et al* (1989)]), but, the electric fields required are higher. It is for these narrow well devices that reductions in the barrier width are likely to give the best improvements in operating voltage.

The use of narrow barriers between wells was shown theoretically and experimentally to be practical for 95Å wide wells (chapter 6). The result is that operating voltages can be reduced by narrowing the barriers at no expense to other performance (except perhaps capacitance). Because of the interest in narrower wells the reduction of barrier widths for MQWs with 50Å wide wells was briefly modelled in chapter 6 but more work should be undertaken in this direction. A careful consideration of the effects of coupling upon the absorption spectrum for a range of barrier widths should be studied. The barrier width might be narrowed such that coupling effects upon the whole e_1hh_1 exciton peak at zero field are just insignificant, or, for bias absorbing operation even narrower barriers might be used such that coupling does not affect the band tail of this peak.

Returning to coupled well pairs, I recommend that future work here should study symmetric coupled quantum wells with widths other than 50Å and investigate the asymmetric well structures in more detail. Both of these directions could yield low voltage devices with better performance than that demonstrated in this thesis.

The devices above incorporate narrow barriers and the consequences of these upon carrier transport and device capacitance and speed need to be studied. Also as operating voltages are reduced the built in voltage within a p-i- n diode arrangement becomes more significant. Forward bias may be used to offset this and an understanding of the exact values of the built in voltage and the forward bias at which the diode passes too high a current would be beneficial. The use of asymmetric coupled wells to offset the

built in field was studied in chapter 6, the particular structure proved not to be useful but more work is necessary although I am pessimistic as to its outcome.

To conclude, the impact of this thesis on future work upon quantum well optical modulators should be that the effects of coupling between quantum wells can be used to achieve lower operating voltages. A voltage reduction can be achieved in MQW structures through reductions in barrier width that permit only so much coupling as to not degrade performance. Alternatively devices may be fabricated that fully exploit the low electric field effects in truly coupled quantum wells.

References

Abramowitz, M and Stegun, IA. *Handbook of Mathematical Functions.* Dover publications **1964**

Adachi S. *GaAs,AlAs, and* $Al_xGa_{1-x}As$*: Material parameters for use in research and device applications.* Journal Of Applied Physics Vol 58 (3) R12 **(Aug 1985)**

Ahn D. *Enhancement of the Stark Effect in Coupled Quantum Wells for Optical Switching Devices.* IEEE Journal of Quantum Electronics Vol 25 (11) **(November 1989)**

Ajisawa A, Fujiwara M, Shimizu J, Sugimoto M, Uchida M and Ohta Y. *Monolithically integrated optical gate 2x2 matrix switch using GaAs/AlGaAs multiple quantum well structure.* Electronics Letters Vol. 23 (21) pp1121- 1122 **(October 1987)**

Andrews S.R , Murray C.M , Davies R.A and Kerr T.M. *Stark effect in strongly coupled quantum wells.* Physical Review B Vol 37 (14) pp.8198-8204 **(May 1988)**

Atkinson D, Parry G and Austin E J. *Modelling of electroabsorption in coupled quantum wells with applications to low-voltage optical modulation.* Semiconductor Science and Technology Vol. 5 pp516-524 **(1990)**

Austin E J and Jaros M. *Electronic structure of an isolated GaAs-GaAlAs quantum well in a strong electric field.* Physical Review B Vol 31 (8) pp 5569- 5572 **(April 1985)**

Austin E.J and Jaros M. *Carrier lifetimes and localisation in coupled GaAs- GaAlAs quantum wells in high electric fields.* Journal Of Physics C: Solid State Physics Vol 19 pp.533-541 **(1986)**

Austin E.J and Jaros M. *Electronic structure and transport properties of GaAs-GaAlAs superlattices in high perpendicular electric fields.* Journal Of Applied Physics Vol 62 (2) pp.558-64 **(July 1987)**

Bailey R B, Sahai R, Lastufka C and Vural K. *Temperature-dependent characteristics of GaAs/AlGaAs multiple quantum well optical modulators.* Journal of Applied Physics Vol 66 (8) pp3445-3452 **(October 1989)**

Barnes P, Zouganeli P, Rivers A, Whitehead M, Parry G, Woodbridge K and Roberts C. *GaAs/AlGaAs multiple quantum well optical modulator using multilayer reflector stacks grown on Si substrate.* Electronics Letters Vol. 25 pp995-996 **(1989)**

Bastard G. *Superlattice band structure in the envelope-function approximation.* Physical Review B Vol 24 (10) pp5693-7 **(1981)**

Bastard G, Mendez E E, Chang L L and Esaki L. *Variational calculations on a quantum well in an electric field.* Physical Review B Vol 28 (6) pp 3241-5 **(September 1983)**

Blakemore J. S. *Semiconducting and other major properties of gallium arsenide.* Journal of Applied Physics Vol 53 (10) pp. R123-R181 **(October 1982)**

Bleaney and Bleaney *Electricity and Magnetism* Oxford University Press **(1957)**

Bleuse J, Bastard G and Voisin P. *Electric-Field-Induced localization and oscillatory electro-optical properties of semiconductor superlattices.* Physical Review Letters Vol 60 (3) pp.220-3 **(January 1988)**

Bleuse J, Voisin P, Allovon M and Quillec M. *Blue shift of the absorption edge in AlGaInAs-GaInAs superlattices: Proposal for an original electro-optical modulator.* Applied Physics Letters Vol 53 (26) pp.2632-4 **(December 1988)**

Blood P and Orton J W. *The electrical characterisation of semiconductors.* Reports on Progress in Physics Vol 41 pp157-257 particularly section 4 **(1978)**

Blood P. *Capacitance-voltage profiling and the characterisation of III-V semiconductors using electrolyte barriers.* Semiconductor Science and Technology Vol 1 pp7-27 **(1986)**

Bloss W J. *Electric field dependence of quantum well eigenstates.* Journal of applied physics Vol 65 (12) pp4789-4794 **(June 1989)**

Bloss W L. *Electric field dependence of the eigenstates of coupled quantum wells* Journal of Applied Physics Vol 67 (3) pp1421-1424 **(February 1990)**

Boyd G D, Bowers J E, Soccolich C E, Miller D A B, Chemla D S, Chirovsky L M F, Gossard A C and English J H. *5.5 GHz Multiple quantum well reflection modulator.* Electronics Letters Vol 25 (9) pp558-9 **(April 1989)**

Brennan K F and Summers C J. *Theory of resonant tunnelling in a variably spaced multiquantum well structure: An Airy function approach.* Journal of Applied Physics Vol 61 (2) pp614-623 **(January 1987)**

Cacciatore C, Campi D, Coriasso C, Rigo C and Alibert C. *Blue shift of the absorption edge induced by electric field in a double quantum well demonstrated by electroreflectance.* Physical Review B Vol 40 (9) pp6446-9 **(September 1989)**

Callaway J. *Quantum theory of the solid state.* Academic Press New York **1976**

Campi D and Alibert C. *Optical blue shift in a double quantum well structure under an electric field.* Applied Physics Letters Vol 55 (5) pp454-456 **(July 1989)**

Capasso F, Mohammed K, Cho A Y, Hull R and Hutchinson A. *Effective mass filtering: Giant quantum amplification of the photocurrent in a semiconductor superlattice.* Applied Physics Letters Vol 47 (4) pp420-422 **(August 1985)**

Casey H C (Jr), Sell D D and Panish M B. *Refractive index of* $Al_xGa_{1-x}As$ *between 1.2 and 1.8eV.* Applied Physics Letters Vol 24 (2) pp63-65 **(1974)**

Charbonneau S, Thewalt M L W, Koteles E S and Elman B. *Transformation of spatially direct to spatially indirect excitons in coupled double quantum wells.* Physical Review B Vol 38 (9) pp 6287-6290 **(September 1988)**

Chemla D S, Miller D A B, Smith P W, Gossard A C and Wiegmann W. *Room temperature excitonic nonlinear absorption and refraction in GaAs/AlGaAs multiple quantum well structures.* IEEE Journal of Quantum Electronics Vol QE-20 (3) pp265-275 **(March 1984)**

Chen Y J, Koteles E S, Elman B S and Armiento C A. *Effect of electric fields on excitons in a coupled double-quantum-well structure.* Physical Review B Vol 36 (8) pp.4562-5 **(September 1987)**

Chiba Y and Ohnishi S. *Resonance-state calculation applying the Weyl-Titchmarsh theory: Application for the quantum-confined Stark effects on excitons in a GaAs-*$Al_xGa_{1-x}As$ *quantum well.* Physical Review B Vol 41 (9) pp6065-6068 **(March 1990)**

Cho H S and Prucnal P R. *Effect of paramaeter variartions on the performance of GaAs/AlGaAs multiple quantum well electroabsorption modulators.* IEEE Journal of Quantum Electronics Vol. 25 (7) pp1682-1690 **(July 1989)**

Chuang S L and Do B. *Electron states in two coupled quantum wells - A strong coupling-of-modes approach.* Journal of applied physics Vol 62 (4) pp1290-1297 **(August 1987)**

Cloonan T J, Herron M J, Tooley F A P, Richards G W, McCormick F B, Kerbis E, Brubaker J L and Lentine A L. *An all-optical implementation of a 3-D Crossover Switching Network.* IEEE Photonics Technology Letters Vol 2 (6) pp438-440 **(June 1990)**

Cochrane P. *The Future Symbiosis of Optical Fibre and Microwave Radio Systems.* 19th European Microwave conference, Wembley, London Paper Inv 7 pp72-86 **(Sept 1989)**

Crossland W A and Davey A B. *Liquid crystal spatial light modulators for optical interconnects and space switching.* IEE Colloquium "Optical Connection and Switching Networks for Communication and Computing" 16/1-4 Digest No. 1990/076 **(May 1990)**

Dawson P , Moore K.J , Duggan G , Ralph H.I and Foxon C.T.B. *Unambiguous observation of the 2s state of the light- and heavy-hole excitons in GaAs-(AlGa)As multiple-quantum-well structures.* Physical Review B Vol 34 (8) pp. 6007-6010 **(Oct. 1986)**

Debbar N , Hong S , Singh J , Bhattacharya P and Sahai R. *Coupled GaAs/AlGaAs quantum well electroabsorption modulators for low electric field optical modulation.* Journal of Applied Physics Vol 65 (1) pp.383-5 **(Jan. 1989)**

Dingle R , Gossard A.C , Wiegmann W. *Direct observation of superlattice formation in a semiconductor heterostructure.* Physical Review Letters Vol 34 pp.1327-30 **(May 1975)**

Dolfi D W, Nazarathy M and Jungerman R L. *40GHz Electro-optic modulator with 7.5V Drive voltage.* Electronics Letters Vol 24 (9) pp528-9 **(April 1988)**

Duggan G, Ralph H I and Moore K J. *Reappraisal of the band-edge discontinuities at the* $Al_xGa_{1-x}As$ *-GaAs heterojunction.* Physical Review B Vol 32 (12) pp8395-8397 **(December 1985)**

Fiorentini V. *Self-consistent DFT calculations of electronic states in superlattices and quantum wells with arbitrary compositional and doping profiles.* Semiconductor Science and Technology Vol 5 pp211-217 **(1990)**

Fowles G R. *Introduction to modern optics.* Holt, Rinehart and Winston Inc. **1968**

Fox A M, Miller D A B, Livescu G, Cunningham J E, Henry J E and Jan W Y. *Excitons in resonant coupling of quantum wells.* Physical Review B Vol 42 (3) pp1841-1844 **(July 1990)**

Galbraith I and Duggan G *Envelope-function matching conditions for GaAs / (Al, Ga) As heterojunctions* Physical Review B Vol 38 pp10057-9 **(1988)**

Galbraith I and Duggan G. *Exciton binding energy and external field induced blue shift in double quantum wells.* Physical Review B Vol 40 (8) pp5515-5521 **(Sept 1989)**

Ghatak A K, Thyagarajan K and Shenoy M R. *A novel numerical technique for solving the one-dimensional Schrödinger equation using matrix approach - application to quantum well structures.* IEEE Journal of quantum electronics Vol 24 (8) pp1524-1531 **(August 1988)**

Golub J E, Liao P F, Eilenberger D J, Harbison J P and Florez L T. *Type I-type II anticrossing and enhanced Stark effect in asymmetric coupled quantum wells.* Applied Physics Letters Vol 53 (26) pp 2584-6 **(December 1988)**

Goodhue W D, Burke B E, Nichols K B, Metze G M and Johnson G D. *Quantum well charge-coupled devices for charge-coupled device addressed multiple quantum well spatial light modulators.* Journal of Vacuum Science and Technology B4 (3) pp769-72 **(May/Jun 1986)**

Goossen K W, Boyd G D. Cunningham J E, Jan W Y, Miller D A B, Chemla D S and Lum R M. *GaAs-AlGaAs multiquantum well reflection modulators grown on GaAs and silicon substrates.* IEEE Photonics Technology Letters Vol 1 (10) pp304-306 **(October 1989)**

Gossard A C. *Growth of microstructures by molecular beam epitaxy.* IEEE Journal of Quantum Electronics Vol. QE-22 no. (9) pp1649-1655 **(Sept 1986)**

Harwit A, Harris J S Jr. and Kapitulnik A. *Calculated quasi-eigenstates and quasi-eigenenergies of quantum well superlattices in an applied electric field.* Journal of Applied Physics Vol 60 (9) pp3211-3213 **(November 1986)**

Harwit A and Harris J S Jr. *Observation of Stark shifts in quantum well intersubband transitions.* Applied Physics Letters Vol. 50 (11) pp685-687 **(March 1987)**

Hecht E and Zajac A. *Optics.* Addison-Wesley **1979**

Hiroshima T and Nishi K. *Quantum-confined Stark effect in graded-gap quantum wells.* Journal of Applied Physics Vol 62 (8) pp3360-3365 **(October 1987)**

Hong S and Singh J. *Study of excitons in an arbitrarily shaped* $GaAs/Al_{0.3}Ga_{0.7}As$ *single quantum well in the presence of static transverse electric field.* Journal of Applied Physics Vol. 61 (12) pp5346-5352 **(June 1987)**

Hong S C, Jaffe M and Singh J. *Theoretical studies of optical modulation in lattice matched and strained quantum wells due to transverse electric fields.* IEEE Journal of quantum electronics Vol QE-23 (12) pp2181-2195 **(December 1987)**

Hsu T -Y, Efron U, Wu W -Y, Schulman J N, D'Haenens I J and Chang Y-C. *Multiple quantum well spatial light modulators for optical processing applications.* Optical Engineering Vol 27 (5) pp372-384 **(May 1988)**

Hutcheson L D. *Optical Interconnects.* Special issue of Optical Engineering Vol 25 (10) p 1075 and subsequent articles. **(October 1986)**

Hutchings D C. *Transfer matrix approach to the analysis of an arbitrary quantum well structure in an electric field.* Applied Physics Letters Vol 55 (11) pp1082-1084 **(September 1989)**

Islam M N, Hillman R L, Miller D A B, Chemla D S, Gossard A C and English J H. *Electroabsorption in GaAs/AlGaAs coupled quantum well waveguides.* Applied Physics Letters Vol 50 (16) pp.1098-1100 **(April 1987)**

Jelley K W, Alavi K and Engelmann R W H. *Experimental Determination of electroabsorption in* $GaAs/Al_{0.32}Ga_{0.68}As$ *multiple quantum well structures as a function of well width.* Electronics Letters Vol 24 (25) pp1555-1557 **(December 1988)**

Jelley K W, Engelmann R W H, Alavi K and Lee H. *Well size related limitations on maximum electroabsorption in GaAs/AlGaAs multiple quantum well structures.* Applied Physics Letters Vol. 55 (1) pp70-72 **(July 1989)**

Kao C K. *Optical Fibre.* Peter Peregrinus Ltd. IEE Materials and devices series 6 **1988**

Kawai H, Kaneko J and Watanabe N. *Doublet state of resonantly coupled AlGaAs / GaAs quantum wells grown by metalorganic chemical vapor deposition.* Journal of Applied Physics Vol 58 (3) pp 1263-1269 **(August 1985)**

Khurgin J. *Novel configuration of self-electro-optic effect devices based on asymmetric quantum wells.* Applied Physics Letters Vol 53 (9) p779 **(August 1988)**

Kim I and Gustafson T K. *Analysis of quantum-confined structures using the beam propagation method.* Applied Physics Letters Vol 57 (3) pp285-287 **(July 1990)**

Klipstein P.C and Apsley N. *A theory for the electroreflectance spectra of quantum well structures.* J.Phys.C: Solid State Phys. Vol 19 pp.6461-6478 **(1986)**

Kojima K, Mitsunaga K and Kyuma K. *Calculation of two-dimensional quantum-confined structures using the finite element method.* Applied Physics Letters Vol 55 (9) pp882-4 **(August 1989)**

The above authors state that the reference [T.Miyoshi, H. Kimura, and M.Ogawa, Trans. Inst. Electron. Inf. Commun. Eng. Jpn. Vol E70, 297 (1987)] applied finite element calculations to a one dimensional quantum well with arbitrary potential profiles.

Kolbas R M and Holonyak N Jr. *Man made quantum wells: A new perspective on the finite square well problem* American Journal of Physics Vol 52 (5) pp431- 437 **(May 1984)**

Koyama F and Iga K. *Frequency chirping of external modulation and its reduction.* Electronics Letters Vol 21 (23) pp1065-6 **(November 1985)**

Lang D V, Sergent M B, Panish M B and Temkin H. *Direct observation of effective mass filtering in InGaAs/InP superlattices.* Applied Physics Letters Vol 49 (13) pp812-814 **(September 1986)**

Lang R and Nishi K. *Electronic state localization in semiconductor superlattices.* Applied Physics Letters Vol 45 (1) pp98-100 **(July 1984)**

Law K K, Yan R H, Merz J L and Coldren L A. *Normally-off high-contrast asymmetric Fabry-Perot reflection modulator using Wannier-Stark localization in a superlattice.* Applied Physics Letters Vol 56 (19) pp1886-1888 **(May 1990)**

Le H Q, Zayhowski J J and Goodhue W D. *Stark effect in* $Al_xGa_{1-x}As$*/GaAs coupled quantum wells* Applied Physics Letters Vol 50 (21) pp1518-1520 **(May 1987)**

Lee J, Vassell M O, Koteles E S and Elman B. *Excitonic spectra of asymmetric, coupled double quantum wells in electric fields.* Physical Review B Vol 39 (14) pp10133-10143 **(May 1989)**

Lengyel G, Jelley K W and Engelmann R W H. *A semi-empirical model for electroabsorption in GaAs/AlGaAs multiple quantum well structures.* IEEE Journal Of Quantum Electronics Vol 26 (2) pp296-304 **(February 1990)**

Lentine A L, Hinton H S, Miller D A B, Henry J E, Cunningham J E and Chirovsky L M F. *Symmetric self-electro-optic effect device: Optical set-reset latch.* Applied Physics Letters Vol. 52 (17) pp1419-1421 **(April 1988)**

Lentine A L, McCormick F B, Novotny R A, Chirovsky L M F, D'Asaro L A, Kopf R F, Kuo J M and Boyd G D. *A 2 kbit array of symmetric self-electrooptic effect devices.* IEEE Photonics Technology Letters Vol 2 (1) pp51-53 **(Jan 1990)**

Linke R A. *Transient chirping in single-frequency lasers: lightwave systems consequences.* Electronics Letters Vol 20 (11) pp472-4 **(May 1984)**

Little J W and Leavitt R P. *Low-temperature photocurrent studies of electron-state coupling in asymmetric coupled quantum wells.* Physical Review B Vol 39 (2) pp1365-1367 **(January 1989)**

Littleton R K and Camley R E. *Investigation of localization in a 10-well superlattice.* Journal of Applied Physics Vol 59 (8) pp 2817-2820 **(April 1986)**

Macleod H A. *Thin film optical filters* Adam Higler London **(1969)**

Marsh A C and Inkson J C. *Scattering matrix theory of transport in heterostructures.* Semiconductor Science and Technology Vol 1 pp285-290 **(1986)**

Masselink W.T , Pearah P.J , Klem J , Peng C.K , Morkoç H , Sanders G.D and Chang Yia-Chung. *Absorption coefficients and exciton oscillator strengths in AlGaAs-GaAs superlattices.* Physical Review B Vol 32 (12) pp.8027-34 **(December 1985)**

Masumoto Y, Matsuura M, Tarucha S and Okamoto H. *Direct experimental observation of two-dimensional shrinkage of the exciton wave function in quantum wells.* Physical Review B Vol 32 (6) pp4275-4278 **(September 1985)**

McAulay A. *Spatial-Light-Modulator Interconnected Computers.* Computer Vol. 20 (10) pp45-57 **(October 1987)**

McIlroy P.W.A. *Effect of an electric field on electron and hole wave functions in a multiquantum well structure.* Journal Of Applied Physics Vol 59 (10) pp.3532-6 **(May 1986)**

McIlvaney K, Marsh J H, Roberts J S and Button C. *Matrix-addressed 4x4 spatial light modulator using the quantum confined stark effect in GaAs/AlGaAs quantum wells.* Electronics Letters Vol. 26 (20) pp1691-1693 **(September 1990)**

Melles Griot *Optics Guide 4* product catalogue **1988**

Mendez E.E, Agulló-Rueda F and Hong J.M. *Stark localization in GaAs-GaAlAs superlattices under an electric field.* Physical Review Letters Vol 60 (23) pp. 2426-9 **(June 1988)**

Midwinter J E. *Novel approach to the design of optically activated wideband switching matrices.* IEE Proceedings Vol. 134 Pt J (5) pp261-268 **(October 1987)**

Miller D A B, Chemla D S, Damen T C, Gossard A C, Wiegmann W, Wood T H and Burrus C A. *Novel hybrid optically bistable switch: The quantum well self-electro-optic effect device.* Applied Physics Letters Vol. 45 (1) pp13-15 **(July 1984)**

Miller D A B, Chemla D S, Damen T C, Gossard A C, Wiegmann W, Wood T H and Burrus C A. *Band-Edge Electroabsorption in quantum well structures: The Quantum-Confined Stark Effect.* Physical Review Letters Vol 53 (22) pp2173-2176 **(November 1984)**

Miller D A B, Chemla D S, Damen T C, Gossard A C, Wiegmann W, Wood T H and Burrus C A. *Electric field dependence of optical absorption near the band gap of quantum well structures.* Physical Review B Vol 32 (2) pp 1043-1060 **(July 1985)**

Miller D A B, Chemla D S and Schmitt-Rink S. *Relation between electroabsorption in bulk semiconductors and in quantum wells: The quantum-confined Franz-Keldysh effect.* Physical Review B Vol 33 (10) pp6976-6982 **(May 1986)**

Miller D A B, Weiner J S and Chemla D S. *Electric-Field Dependence of Linear Optical Properties in Quantum Well Structures: Waveguide Electroabsorption and Sum Rules.* IEEE Journal of Quantum Electronics Vol QE-22 (9) pp1816-1830 **(September 1986)**

Miller D A B. *Optical bistability in self-electro-optic effect devices with asymmetric quantum wells.* Applied Physics Letters Vol 54 (3) pp202-204 **(January 1989a)**

Miller D A B. *Optics for low-energy communication inside digital processors: quantum detectors, sources, and modulators as efficient impedance converters.* Optics Letters Vol. 14 (2) pp146-148 **(January 1989b)**

Miller R C, Gossard A C, Kleinman D A and Munteanu O. *Parabolic quantum wells with the GaAs-*$Al_xGa_{1-x}As$ *system.* Physical Review B Vol 29 (6) pp3740-3743 **(March 1984)**

Miller R.C , Kleinman D.A and Gossard A.C. *Energy gap discontinuities and effective masses for GaAs-AlGaAs quantum wells.* Physical Review B Vol 29 (12) pp7085-7807 **(June 1984)**

Moore K J, Duggan G, Woodbridge K and Roberts C. *Exciton localization in* $In_xGa_{1-x}As$*-GaAs coupled quantum well structures.* Physical Review B Vol 41 (2) pp1095-1099 **(January 1990)**

Newson D J and Kurobe A. *Effect of residual doping on optimum structure of multi-quantum well optical modulators.* Electronics Letters Vol. 23 (9) pp439-440 **(April 1987)**

Newton R G. *Scattering theory of particles and waves* McGraw-Hill New York **1966**

Nichols K B, Burke B E, Aull B F, Goodhue W D, Gramstorff B F, Hoyt C D and Vera A. *Spatial light modulators using charge-coupled-device addressing and electroabsorption effects in GaAs/AlGaAs multiple quantum wells.* Applied Physics Letters Vol. 52 (14) pp1116-1118 **(April 1988)**

Nishi K and Hiroshima T *Enhancement of quantum confined Stark effect in a graded gap quantum well.* Applied Physics Letters Vol 51 (5) pp320-322 **(August 1987)**

Nojima S and Wakita K. *Optimization of quantum well materials and structures for excitonic electroabsorption effects.* Applied Physics Letters Vol 53 (20) pp1958-1960 **(November 1988)**

Okiyama T, Nishimoto H, Yokota I and Touge T. *Evaluation of 4-Gbit/s Optical Fiber Transmission Distance with Direct and External Modulation.* Journal of Lightwave Technology Vol 6 (11) pp1686-1691 **(November 1988)**

O'Mahony M J. *Future long line optical systems and networks.* Australian Conference on Optical Fibre Technology. Brisbane **(December 1989)**

Onose H , Yoshimura H and Sakaki H. *Field-induced decoupling of quantised levels and blue shift of absorption edge in a potential inserted quantum well structure.* Applied Physics Letters Vol 54 (22) pp.2221-2223 **(May 1989)**

Orton J W, Fewster P F, Gowers J P, Dawson P, Moore K J, Dobson P J, Curling C J, Foxon C T, Woodbridge K, Duggan G and Ralph H I. *Measurement of "material" parameters in multi-quantum-well structures.* Semiconductor Science and Technology Vol 2 pp597-606 **(1987)**

Pandey L N, Sahu D and George T F. *Density of electronic states in a biased resonant tunneling structure.* Applied Physics Letters Vol 56 (3) pp277-279 **(January 1990)**

Parker D G. *On the formation of near ideal quasi-Schottky barriers between indium tin oxide and gallium arsenide.* The GEC Journal of Research Vol 5 (2) pp116-123 **(1987)**

Pavesi L, Tuncel E, Zimmermann B and Reinhart F K. *Photoluminescence of disorder - induced localized states in GaAs/*$Al_xGa_{1-x}As$ *superlattices.* Physical Review B Vol. 39 pp7788-7795 **(April 1989)**

Pezeshki B, Thomas D and Harris J S Jr. *Optimization of modulation ratio and insertion loss in reflective electroabsorption modulators.* Applied Physics Letters Vol 57 (15) pp1491-1492 **(October 1990)**

Pikhtin A N and Yas'kov A D. *Dispersion of the refractive index of semiconducting solid solutions with the sphalerite structure.* Soviet Physics Semiconductors Vol 14 (4) pp389-392 **(April 1980)**

Rae A I M. *Quantum Mechanics.* UK:McGraw-Hill **1981**

Rejman-Greene M A Z and Scott E D. *Packaged 2x2 array of InGaAs/InP multiple quantum well modulators grown by double-sided epitaxy.* Electronics Letters Vol. 26 (13) pp946-948 **(June 1990)**

Roberts J S, Mason N J and Robinson M. *Factors influencing doping control and abrupt metallurgical transitions during atmospheric pressure MOVPE growth of AlGaAs.* Journal of crystal growth Vol 68 pp422-430 **(1984)**

Roberts J S, Pate M A, Mistry P, David J P R, Franks R B, Whitehead M and Parry G. *MOVPE grown MQW pin diodes for electro-optic modulators and photodiodes with enhanced electron ionisation coefficient.* Journal of Crystal Growth Vol 93 pp877-884 **(1988)**

Salvador A, Reed J, Kumar N S, Ünlü M S and Morkoç H. *Electroabsorption studies on GaAs asymmetric coupled quantum wells.* Surface Science Vol 228 pp188-191 **(1990)**

Sauer R, Thonke K and Tsang W T. *Photoinduced Space-Charge Buildup by Asymmetric Electron and Hole Tunneling in Coupled Quantum Wells.* Physical Review Letters Vol 61 (5) pp609-612 **(August 1988)**

Schiff L I. *Quantum Mechanics* Tokyo:McGraw-Hill **(1981)**

Sedra A S and Smith K C. *Microelectronic circuits.* Holt, Rinehart and Winston **1982**

Shields A J, Klipstein P C and Apsley N. *Lineshape Broadening and Polarisation Dependence of Electroreflectance Spectra of Single Quantum Wells.* unpublished **1988**

Shinada M and Sugano S. *Interband Optical Transitions in Extremely Anisotropic Semiconductors. I Bound and Unbound Exciton Absorption.* Journal Of The Physical Society Of Japan Vol 21 (10) pp.1936-1946 **(Oct 1966)**

Singh J. *A new method for solving the ground-state problem in arbitrary quantum wells:Application to electron-hole quasi-bound levels in quantum wells under high electric field.* Applied Physics Letters Vol 48 (6) pp434-6 **(February 1986)**

Singh J and Hong S. *Theory of electric field-induced optical modulation in single and multiquantum well structures using a Monte Carlo approach.* IEEE Journal of Quantum Electronics Vol QE-22 (10) pp2017-2021 **(October 1986)**

Singh J, Hong S, Battacharya P K, Sahai R, Lastufka C and Sobel H R. *System Requirements and Feasibility Studies for Optical Modulators Based on GaAs/AlGaAs Multiple Quantum Well structures for optical processing.* IEEE Journal of Lightwave Technology Vol. 6 (6) pp818-831 **(June 1988)**

Stevens P.J , Whitehead M , Parry G and Woodbridge K. *Computer modeling of the electric field dependent absorption spectrum of multiple quantum well material.* IEEE Journal Of Quantum Electronics Vol. 24 (10) pp.2007-16 **(Oct 1988)**

Stevens P J and Parry G. *Limits to Normal Incidence Electroabsorption Modulation in GaAs/(GaAl)As multiple quantum well diodes.* IEEE Journal of Lightwave Technology Vol 7 (7) pp1101-1108 **(July 1989)**

Stradling R A and Klipstein P C (editors) *Growth and Characterisation of Semiconductors.* Adam Higler : Bristol **1990**

Stringfellow G B. *Organometallic Vapor-Phase Epitaxial Growth of III-V Semiconductors.* Semiconductors and Semimetals Vol 22, Part A, Chapter 3 edited by Willardson R K and Beer A C **(1985)**

Sturge M D. *Optical Absorption of Gallium Arsenide between 0.6 and 2.75 eV.* Physical Review Vol 127 (3) pp768-773 **(August 1962)**

Tan C M, Xu J and Zukotynski S. *Study of resonant tunneling structures: A hybrid incremental Airy function plane-wave approach.* Journal of Applied Physics Vol 67 (6) pp3011-3017 **(March 1990)**

Tokuda Y, Kanamoto K, Tsukada N and Nakayama T. *Distinct observation of inter-well coupling effect on optical transitions in double quantum wells in an electric field.* Applied Physics Letters Vol 54 (13) pp1232-1234 **(March 1989)**

Trzeciakowski W, Sahu D and George T F. *Density of states in a resonant tunneling structure.* Physical Review B Vol 40 (9) pp6058-6062 **(September 1989)**

Wada O, Sakurai T and Nakagami T. *Recent progress in Optoelectronic Integrated Circuits (OEIC's).* IEEE Journal of Quantum Electronics Vol. QE22 (6) pp805-821 **(1986)**

Wada O, Furuya A and Makiuchi M. *Planar, Compitible OEIC's Based on Multi-quantum well structures.* IEEE Photonics Technology Letters Vol 1 (1) pp 16-18 **(January 1989)**

Watanabe N and Kawai H. *Single and coupled double-well GaAs/ALGaAs and energy-dependent light-hole mass.* Journal of Applied Physics Vol 60 (10) pp3696-3698 **(November 1986)**

Wheatley P, Bradley P J, Whitehead M, Parry G, Midwinter J E, Mistry P, Pate M A and Roberts J S. *Novel nonresonant optoelectronic logic device.* Electronics Letters Vol 23 (2) pp92-93 **(January 1987)**

Whitehead M, Parry G, Woodbridge K, Dobson P J and Duggan G. *Experimental confirmation of a sum rule for room-temperature electroabsorption in GaAs-AlGaAs multiple quantum well structures.* Applied Physics Letters Vol. 52 (5) pp345-347 **(February 1988)**

Whitehead M, Stevens P, Parry G, Roberts J S, Mistry P, Pate M and Hill G. *Effects of well width on the characteristics of GaAs/AlGaAs multiple quantum well electroabsorption modulators.* Applied Physics Letters Vol 53 (11) pp956-958 **(September 1988)**

Whitehead M, Parry G and Wheatley P. *Investigation of etalon effects in GaAs-AlGaAs multiple quantum well modulators.* IEE Proceeedings Vol. 136 Part J, No. 1. pp52-58 **(February 1989)**

Whitehead M, Rivers A, Parry G, Roberts J S and Button C. *Low-voltage multiple quantum well reflection modulator with on:off ratio > 100:1* Electronics Letters Vol 25 (15) pp984-985 **(July 1989)**

Whitehead M, Rivers A, Parry G and Roberts J S. *Very low-voltage, normally-off asymmetric Fabry-Perot reflection modulator.* Electronics Letters Vol 26 (19) **(September 1990)**

Wight D R, Allen P C Trussler J W A, Cooper D P, Esdale D J and Oliver P E. *Ultra high speed micro-optical modulators in GaAs: The TEAM and the LEAM.* Institute of Physics Conference Series No 79 : Chapter 12 pp667-72 **(1985)**

Wood T H, Burrus C A, Miller D A B, Chemla D S, Damen T C, Gossard A C and Weigmann W. *131ps Optical modulation in semiconductor multiple quantum wells.* IEEE Journal of Quantum Electronics QE21 (2) pp117-8 **(February 1985)**

Wood T H, Burrus C A, Tucker R S, Weiner J S, Miller D A B, Chemla D S, Damen T C, Gossard A C and Wiegmann W. *100ps waveguide multiple quantum well (MQW) optical modulator with 10:1 on/off ratio.* Electronics Letters Vol 21 (16) pp693-694 **(August 1985)**

Wood T H, Carr E C, Kasper B L, Linke R A and Burrus C A. *Bidirectional fibre-optical transmission using a multiple quantum well modulator/detector.* Electronics Letters Vol 22 (10) pp528-9 **(May 1986)**

Wood T H, Carr E C, Burrus C A, Henry J E, Gossard A C and English J H. *High speed 2x2 electrically driven spatial light modulator made with GaAs/AlGaAs multiple quantum wells.* Electronics Letters Vol. 23 (17) pp916-917 **(August 1987)**

Wood T H. *Multiple quantum well (MQW) waveguide modulators.* IEEE Journal of Lightwave Technology Vol 6 (6) pp743-757 **(June 1988)**

Woodgate G K. *Elementary Atomic Structure -second edition* Oxford:Clarendon Press. **1983**

Yamanishi M and Suemune T. *Comment on Polarization Dependent Momentum Matrix Elements In Quantum Well Lasers.* Japanese Journal Of Applied Physics Vol 23 (1) ppL35-L36 **(Jan 1984)**

Yamanishi M. and Kurosaki M. *Ultrafast optical nonlinearities by virtual charge polarisation in D.C biased quantum well structures.* IEEE Journal of Quantum Electronics Vol QE-24 (2) p.327 **(Feb 1988)**

Yan R H, Simes R J and Coldren L A. *Electroabsorptive Fabry-Perot Reflection Modulators with Asymmetric Mirrors.* IEEE Photonics Technology Letters Vol 1 (9) pp273-275 **(September 1989)**

Yan R H, Simes R J and Coldren L A. *Extremely Low-Voltage Fabry-Perot Reflection Modulators.* IEEE Photonics Technology Letters Vol 2 (2) pp118-9 **(February 1990)**

Yariv A. *The beginning of Integrated Optoelectronic Circuits.* IEEE Transactions on Electron Devices Vol ED-31 (11) pp1656-1661 **(November 1984)**

Yariv A, Lindsey C and Sivan U. *Approximate analytic solution for electronic wave functions and energies in coupled quantum wells.* Journal of applied physics Vol 58(9) pp3669-3672 **(November 1985)**

Yuh Perng-fei and Wang K.L. *Intersubband optical absorption in coupled quantum wells under an applied electric field.* Physical Review B Vol 38 (12) pp.8377-82 **(October 1988)**

Yuh P and Wang K L. *Formalism of the Kronig Penney model for superlattices of varible basis.* Physical Review B Vol 38 (18) pp13307-13315 **(December 1988)**

Acknowledgements

I would like to thank Dr.E Austin for starting the whole project at Imperial College and for her help before moving to Scotland. The facilities and advice at Imperial College computer centre have been very good and used extensively in the course of this work.

I am especially appreciative of Professor Gareth Parry for letting me join the group at University College London two years ago and his generous support, enthusiasm and encouragement over this time. Dr. John Roberts and Chris Button at Sheffield university have provided samples for experimental work very quickly. The device processing used the extensive experience of Tony Rivers and help from Fred Stride and others. When I arrived the experimental apparatus and control software had all been set up by the 'older' members of the group without whom I would not have been able to make so many measurements or obtain so much advice, three older members in particular are, Peter Stevens, Craig Tombling and Mark Whitehead. For all sorts of useful bits of software and the recovery of corrupted data I am grateful to Mark Abbott.

The whole three years have been made worthwhile by the present and recent members of the research groups both at UCL and Imperial College.

Finally I would like to acknowledge the UK SERC and British Telecom for funding this project.

List of publications

As First Author

Atkinson D, Parry G and Austin E J. *Modelling of electroabsorption in coupled quantum wells with applications to low-voltage optical modulation* Semiconductor Science and Technology Vol 5 pp516-524 **(1990)**

subsequently appearing in Engineering Optics **(August 1990)**

Atkinson D, Parry G, Rivers A and Roberts J S. *Modelling of low voltage electroabsorption modulators employing coupled quantum wells* Technical Digest no. 1990/ 103 from the Institute of Electrical Engineering Colloquium on 'Applications of Quantum Wells in Optoelectronics'. **(June 1990)**

As a Named Author

Parry G, Whitehead M, Stevens P, Rivers A, Barnes P, Atkinson D, Roberts J S, Button C, Woodbridge K and Roberts C. *The Design and Application of III-V Multiquantum Well Optical Modulators* Proceedins of the European Physical Society Meeting Lisbon. To appear in Physica Scripta **(1990)**